The Galaxy-Dark Matter Connection

Dissertation

zur

Erlangung der naturwissenschaftlichen Doktorwürde
(Dr. sc. nat.)

vorgelegt der

Mathematisch-naturwissenschaftlichen Fakultät

der

Universität Zürich

von

Simone M. Weinmann

von

Herrliberg ZH

Promotionskomitee

Prof. Dr. Ben Moore (Vorsitz)
Dr. Frank C. van den Bosch
Prof. Dr. Uros Seljak

Zürich, 2007

In the beginning the Universe was created. This has made a lot of people very angry and has been widely regarded as a bad move.

Douglas Adams

Contents

Zusammenfassung

Diese Doktorarbeit befasst sich mit der Verteilung und den Eigenschaften von Galaxien im Universum. Das All durchzieht ein kosmisches Netz aus unsichtbarer "dunkler" Materie, die nicht mit Licht wechselwirkt, wohl aber durch ihre Schwerkraft andere Materie beeinflusst. So sammelt sich die normale, baryonische Materie (aus der die Sterne und wir bestehen) im Laufe der Zeit entlang den Strängen und in den Knoten dieses Netzes an, wo sie sich abkühlt und sich teilweise zu Galaxien formt.

Dank enormen Fortschritten im letzten Jahrzehnt, hauptsächlich durch die Detektierung des kosmischen Mikrowellenhintergrunds, aber auch dank Messungen der Geschwindigkeiten von weit enfernten Supernovae, befinden wir uns heute im Zeitalter der sogenannten "Präzisionskosmologie". Kosmologie ist in die Nähe einer exakten Wissenschaft gerückt; es ist heute recht genau bekannt, zu welchen Anteilen das Universums aus dunkler Materie, Baryonen und dunkler Energie (welche die Beschleunigung der Expansion des Universums verursacht) besteht, auch wenn noch völlig unbekannt ist, was die dunkle Materie und dunkle Energie wirklich ist. Aufgrund der Kenntnisse des kosmischen Mikrowellenhintergrunds, welcher das Universum zu einer sehr frühen Zeit (d.h. einige 100'000 Jahre nach dem Urknall) abbildet, können wir heute die Entwicklung eines Universums, welches nur aus dunkler Energie und dunkler Materie — den beiden Hauptkomponenten — besteht, präzise am Rechner simulieren.

Allerdings ist das Verhalten der baryonischen Materie sehr viel komplizierter und sehr schwierig zu simulieren. In meiner Doktorarbeit befasse ich mich damit, wie baryonische Materie, beziehungsweise Galaxien, sich in einem Universum aus dunkler Materie verteilen. Nur so kann man eine Verbindung zwischen dem realen, beobachteten Universum und den Simulationen herstellen.

In einem ersten Teil meiner Doktorarbeit benütze ich einen statistischen Zugang zu diesem Problem. Da man weiss, dass sich alle Galaxien innerhalb von Halos aus dunkler Materie befinden, welche eine bis hunderte von Galaxien enthalten können, kann man mithilfe eines Gruppenfinder-Algorithmus, den man auf einen Galaxienkatalog anwendet, auf die dahinterliegenden Halos aus dunkler Materie schliessen. So konnten wir feststellen, welche Galaxien sich in einem gemeinsamen Halo befinden. Wir haben Zusammenhänge zwischen Galaxieneigenschaften und der Masse des Halos, in dem sie sich befinden, festgestellt und damit als eine der ersten eine neue Beschreibung der bekannten Beziehung zwischen Galaxieneigenschaften und ihrer Umgebung gefunden. Unser Hauptresultat ist, dass der Anteil rote Galaxien, die aufgehört haben, Sterne zu formen, mit zunehmender Halomasse kontinuierlich ansteigt. Dieser Trend beginnt schon in kleinen, mitgliederarmen Galaxiengruppen. Unsere neue Beschreibung hat vermutlich eine tiefere physikalische Bedeutung als jene zwischen Galaxieneigenschaften und der Galaxiendichte, die bis anhin benützt wurde.

In einem weiteren Projekt verglichen wir unsere Resultate mit denjenigen aus einem semi-analytischen Modell. Dieses Modell benützt empirische und/oder theoretisch plausible Rezepte, um eine Simulation eines Universums aus dunkler Materie mit Galaxien zu besiedeln. Obwohl dieses Modell bis anhin als sehr erfolgreich galt, konnten wir mit unseren Tests zeigen, dass es immer noch gewisse ernsthafte Probleme hat, die Beobachtungen zu reproduzieren. Zum Beispiel enthält das Universum im Modell viel zu viele rote Satellitengalaxien, die in der Realität nicht beobachtet werden.

Während der Arbeit an diesen beiden Projekten wurde klar, dass die meisten ungelösten Fragen bezüglich der Verteilung und Eigeschaften von Galaxien mit einem zentralen Problem zu tun haben; nämlich, wie Sternentstehung in Galaxien unterdrückt wird. Wieso geht die globale Sternentstehungsrate dramatisch zurück? Wieso wachsen zentrale Galaxien in grossen Galaxienhaufen nicht einfach immer weiter, wie von Simulationen vorausgesagt? Wieso formen kleine Subhalos aus dunkler Materie kaum Galaxien? Wieso gibt es zwei verschiedene Arten von Galaxien, von denen die einen aktiv Sterne formen, während die anderen vollkommen damit aufgehört haben? Wir können diese Fragen erst beantworten, wenn wir die Mechanismen verstanden haben, die die Neubildung von Sternen in Galaxien stoppt. Es gibt sehr viele verschiedene Prozesse, die dies verursachen können. Um diese im Detail zu studieren, kann man entweder präzise, detaillierte Beobachtungen einzelner Galaxien machen, oder die Prozesse simulieren.

In meinem dritten Projekt habe ich letzteren Zugang gewählt und die Reionisation des Universums genauer studiert. Die Strahlung der ersten Galaxien und Quasare ionisiert den neutralen Wasserstoff im Universum. Dieser Prozess hat wahrscheinlich deutliche Auswirkungen auf Galaxienenstehung, indem er den Wasserstoff aufheizt und so die Bildung von Galaxien in kleinen Halos verhindert. Die Reionisation ist daher ein vielversprechender Ansatz, um das Rätsel zu lösen, vor das uns die kleine Anzahl Satellitengalaxien in der Lokalen Gruppe stellt: Laut Simulationen sollte es viel mehr davon geben. Mithilfe einer grossen kosmologischen Simulation, bei der die Propagation von Strahlung genau verfolgt wird, haben wir untersucht, wie die Reionisation des Universums genau vor sich geht. In praktisch allen bisherigen Modellen wurde angenommen, dass die Reionisation instantan passiert; wir haben aber festgestellt, dass der Zeitpunkt der Reionisation stark von der Masse eines Halos abhängt. Grosse Halos werden sehr viel früher ionisiert, aber auch kleinere Halos werden signifikant früher ionisiert als das Universum als ganzes. Zudem haben wir auch untersucht, ob kleinere Galaxien manchmal von der Strahlung, die von grösseren Nachbarn ausgeht, ionisiert werden. Im Falle unserer eigenen Galaxie wäre es zum Beispiel möglich, dass sie vom benachbarten Virgo-Galaxienhaufen ionisiert wurde. Wir haben herausgefunden, dass eine solche “externe Reionisierung” tatschlich nicht unwahrscheinlich ist.

Summary

In this PhD thesis, I have investigated the distribution and the properties of galaxies within the dark matter large-scale structure. A pure dark matter universe is relatively easy to simulate today, thanks to the fact that we believe to have quite precise knowledge of the important cosmological parameters that have been measured from the Cosmic Microwave Background. However, the behaviour of baryons, i.e. gas and stars, is much more difficult to reproduce in simulations, due to the many complicated hydrodynamical processes that are occurring, such as cooling with many different cooling channels which depend on the metallicity of the gas, shocks, star formation, supernova feedback etc.

In my thesis, I used a large galaxy catalogue combined with a novel group finding algorithm to establish a connection between the distribution of galaxies and dark matter. We assumed that each galaxy lies in a dark matter halo containing one up to hundreds of galaxies, and used the total light emitted by galaxies per halo to obtain an estimate of the total halo mass. Thus, we were able to quantify the properties of galaxies as a function of total halo mass, thereby presenting a novel way to describe the relation between galaxy properties and their environment. We have found that the fraction of galaxies which have ceased to form stars and have become red gradually increases with halo mass. This effect is already visible in relatively low-mass groups, which indicates that the process truncating star formation is not only occurring in the most massive haloes. Thus, it is probable that processes like "strangulation", in which the hot gas halo surrounding a galaxy is removed, are the explanation of the well known relation between galaxy properties and environment.

In a follow-up project, we compared our results with model predictions from a very successful semi-analytical model that had been implemented on top of the "Millennium simulation". We found that the fraction of red satellite galaxies is strongly overpredicted in this model and thus we were able to show that the efficiency of "strangulation" in the model is much too high. This indicates that the implementation of this mechanism has to be revisited in new semi-analytical models. During the work on these projects, it became apparent that most of the unsolved questions regarding the properties and distributions of galaxies are closely connected to the way in which star formation is truncated in galaxies. Why is the global star formation rate declining dramatically? Why are there much more subhaloes in the Local Group than there are visible satellites? Why has a significant fraction of galaxies stopped forming stars altogether?

In a third project, we investigated one of the important mechanisms which is likely to strongly influence gas physics and star formation in galaxies in more detail. The UV light of the first stars and quasars in the universe ionized the previously neutral atoms of which the universe consisted, a process which is called "reionization". This had a major impact on gas cooling and inhibited the formation of the lowest mass galaxies. Using a large dark matter-only simulation combined with a very efficient radiative-transfer code, we have investigated when and how galaxies were reionized. We found that unlike it is assumed in many models, reionization did not happen at a fixed redshift in the entire universe. Instead, the reionization redshift is a strong function of halo mass, with today's most massive haloes having been reionized very early. Interestingly, we also found that a significant fraction of galaxies is not reionized by the light of their own stars, but by the radiation from nearby objects that collapsed before the galaxy itself was likely to have formed stars. Consequently it is conceivable that for example the Milky Way was reionized

by the progenitor of the nearby Virgo cluster.

Important Abbreviations and Symbols

Abbreviations

AGN	Active Galactic Nucleus
CDM	Cold Dark Matter
CMB	Cosmic Microwave Background
cD	Supergiant Elliptical Galaxy found in Cluster Centers
CLF	Conditional Luminosity Function
DM	Dark Matter
EW	Equivalent Width; measure of the strength of a spectral line
FoF	Friend-of-Friend
Gyr	Gigayear
H	Hydrogen
H II	ionized atomic hydrogen
Hα	emission line in H, traces ionization
ICM	Intra-Cluster Medium
IGM	Inter-Galactic Medium
ISM	Interstellar Medium
KS-test	Kolmogorov-Smirnov-test to compare 2 distributions
ΛCDM	Model of Universe including CDM and dark energy
LF	Luminosity Function; number density of galaxies per luminosity interval
LG	The Local Group of Galaxies
MGRS	Mock Galaxy Redshift Survey
Mpc	Megaparsec; corresponds to 3×10^{22} meters
MW	Milky Way
NFW-profile	Navarro, Frenk & White (1997) DM density distribution in a halo
NYU-VAGC	New York University Value Added Galaxy Catalogue, based on SDSS
RS	Redshift Survey
RT	Radiative Transfer
SAM	Semi-Analytic Model
SDSS	Sloan Digital Sky Survey; very large galaxy survey
SFR	Star Formation Rate
SSFR	Specific Star Formation Rate (SFR per stellar mass)
SPH	Smoothed Particle Hydrodynamics; Method used in Gas Simulations
ULIRG	Ultra-Luminous Infrared Galaxy
WMAP	Wilkinson Microwave Anisotropy Probe (measures CMB)
WMAP1	WMAP first year results (Spergel et al. 2003)
WMAP3	WMAP third year results (Spergel et al. 2007)
2dFGRS	2-degree Field Galaxy Redshift Survey; large galaxy survey

Symbols

h	Hubble constant in units of 100 km/s per Mpc
L	Luminosity
L_*	Characteristic Galaxy Luminosity; Parameter in the LF
M	Mass

$M_\odot$	Solar Mass, corresponds to $1.98 \cdot 10^{30}$ kg
$M_\mathrm{r}, M_\mathrm{g}$	absolute magnitude measured in r-band/g-band respectively
n	index of the primordial power spectrum of density fluctuations
R_vir	virial radius
σ_8	rms density fluctuations on scales of 8 Mpc h^{-1} today
σ	standard deviations; also used for velocity dispersion
Ω_b	baryon density in units of the critical density
Ω_m	matter density in units of the critical density
Ω_Λ	vacuum energy density in units of the critical density
z	redshift

Chapter 1

Introduction

Wo viel Licht ist, ist auch viel Schatten.

J.W. von Goethe

In this chapter, I will give an overview of the current scientific understanding of how the dark and the luminous universe are connected, and present some background information about the evolution of galaxies, and its potential drivers. As one of the essential prerequisites for a large part of my PhD research has been a galaxy group catalogue, I will also explain the basic ideas behind the construction of the catalogue.

1.1 The Dark and the Luminous Universe

1.1.1 Dark Matter and Cosmology

According to current knowledge, only a small fraction of the matter contained in the universe is emitting photons and thus can be detected by telescopes. From the motion of galaxies in large clusters, the Swiss astronomer Zwicky found the first evidence for the existence of "dark matter", which dominates the luminous matter by a factor of around 10, back in the year 1933. Today, the existence of dark matter is well established, thanks to rotation curves of spiral galaxies, galaxy lensing etc. Based on evidence from measurements of the cosmic microwave background, large galaxy surveys, and measurements of the recession velocity of distant supernovae, it seems today most likely that the universe has a flat geometry and a density equal to the critical density and will expand forever with increasing velocity due to the vacuum energy. Expressed in more detail, according to the most recent measurements of the cosmic microwave background by the WMAP 3-year result (WMAP3 hereafter), 24% of the total density of the universe is made up of dark matter, 4.2% consists of baryonic matter, and 76% of the mysterious dark energy, causing the expansion of the universe to accelerate (Spergel et al. 2007). Other important cosmological parameters measured by WMAP3 include σ_8, n and the Hubble parameter H, where σ_8 is the variance in the linear density perturbations measured in a sphere of $8h^{-1}$Mpc, n is the index of the primordial power spectrum of density fluctuations (see

1.1.2) and H quantifies the relation between the recession velocity and the distance of galaxies. According to WMAP3, $\sigma_8 \sim 0.74$, $n \sim 0.95$ and $H \sim 74$ km/s per Mpc.

From the primordial deuterium abundance, which traces nucleosynthesis, but also from measurements of the cosmic microwave background, it seems unlikely that the dark matter is solely made out of baryonic material, like dead stars or black holes. There is evidence that dark matter consists of some unknown form of matter, which is is only interacting by gravity (and maybe also by the weak force). In the current standard model of cosmology, dark matter is "cold", which means that it consists of relatively massive particles, for which random velocities are small (Blumenthal et al. 1984). However note that warm dark matter, which would consist of slightly lighter particles, has been suggested as a potential solution to some problems related to the inner density slopes of dark matter haloes and of the "missing satellite problem". The currently favoured dark matter particle is the so-called "neutralino", which emerges from the supersymmetric theory of particle physics. No such particle has been detected yet and the theory of supersymmetry has yet to be validated.

1.1.2 Structure Formation in a CDM Universe

In this chapter, I will give a short summary of how structure formation occurs in a standard CDM universe. Please refer to Peacock's "Cosmological Physics" (1999) for further details. According the the theory of inflation (Guth 1981), the universe underwent a phase of exponential growth after the Big Bang. Thereby, quantum fluctuations in spacetime were inflated to super-horizon scales and froze out as classical density fluctuations, which were the seeds of galaxies and clusters we see today. How did galaxies evolve out of these initially small perturbations in the density field? A structure can only grow if its size is above the Jeans length $\lambda_{\rm J}$, which is the scale below which pressure can oppose gravity efficiently. It corresponds roughly to the distance that sound can travel in the collapse time:

$$\lambda_{\rm J} = c_{\rm S}\sqrt{\frac{\pi}{G\rho}}, \tag{1.1}$$

where $c_{\rm S}$ is the sound speed, G the gravitational constant and ρ is the mean density of the universe. Dark Matter has a very small Jeans length. Thus, dark matter structures are free to start forming directly after inflation. However, their growth rate will be very small as long as the density of the universe is still radiation dominated. Between the time when the universe stops being radiation dominated, and the time of recombination (this is the time when the close coupling between matter and radiation ends and the universe becomes transparent), the dark matter fluctuations can grow effectively, while the baryonic material cannot, due to the large Jeans mass. Therefore, at recombination, the dark matter has larger variations in density than the baryonic material, thus supplying the "seeds" of structure formation. After recombination, the baryons quickly fall into the existing dark matter potential. To describe the fluctuations in the density field, one uses the dimensionless quantity $\delta(x)$:

$$\delta(x) = \frac{\rho(x) - \langle\rho\rangle}{\langle\rho\rangle} \tag{1.2}$$

It is useful to consider the Fourier transform of δ, $\delta_{\rm k}$. $P(k) = \langle|\delta_{\rm k}^2|\rangle$ is then the power spectrum as a function of wavenumber k. In order to determine the sequence of structure

formation, we need to know if the fluctuations in the initial power spectrum are higher at the low or at the high mass end. The first structures will collapse at the scale at which the fluctuations are strongest. $P(k)$ is usually taken to be a power law in wavenumber k:

$$P(k) \propto k^n \tag{1.3}$$

According to current understanding, n is expected to be close to 1 (0.95 according to the WMAP 3-year results). If we define $\Delta_{\rm M}$ as the mean fluctuations in a volume which on average contains a mass M, one obtains

$$\Delta_{\rm M} \propto M^{\frac{3+n}{6}} \tag{1.4}$$

This means that there will be more power on small scales, from which it can be inferred that structure formation will occur bottom-up. This means that small structures form first, gradually assembling into bigger haloes and clusters. The largest clusters in the universe today are the ones collapsing now, which means that the galaxies of which they consist are no longer recessing from each other with the Hubble flow, and experience "turn-around". The fact that collapse occurs "bottom-up" is of paramount importance to the way in which galaxies form and evolve.

1.1.3 The Biased Distribution of Galaxies

As outlined above, the growth of dark matter structures is fairly well known, given the cosmological parameters. Thus, as dark matter only interacts by gravity, a dark matter universe can be simulated relatively easily by N-body codes. What emerges is a complex picture, in which the universe consists of a web of filaments, sheets and knots made out of dark matter. Individual haloes are found, which sometimes contain a large number of gravitationally bound subhaloes around one central, very large object, likely corresponding to a central cD galaxy in a galaxy cluster. As stunning as this picture is, one would of course like to compare it to the observed distribution of baryonic material in the universe, which is what we can observe. Unfortunately, simulating the distribution of galaxies is a great deal more difficult than only the dark matter, since it involves complicated gas physics, different cooling processes, star formation, supernova feedback, AGN feedback etc. Therefore, it is not easy to verify if the simulated universe really corresponds to the universe we can observe.

In order to do a first attempt of such a comparison, the simplest possible approximation would be to assume that each dark matter halo contains the universal fraction of baryons, and that these baryons assemble into one galaxy per dark matter halo. This would mean that large clusters contain one single huge galaxy of luminosity $> 100\ L_*$ (Peacock, 1999) which is dramatically at odds with observations. First, only a relatively small fraction of all baryons in the universe is in the form of stars in galaxies. Second, large dark matter haloes normally do not contain only one galaxy, but several. As a first correction to this model, it is thus necessary to follow the detailed merger history of the dark matter haloes and subhaloes. The more massive a halo is, the later it has assembled. If small haloes become gravitationally bound to a bigger object, it does not necessarily mean that they will merge with the central object. Subhaloes survive and still contain distinct galaxies. And even if a subhalo is tidally disrupted by the potential of its massive parent halo, it is well possible that the galaxy it contained will survive and orbit the central potential for

a long time, before it may fall into the central object. In this way, groups and clusters of galaxies are formed, where one large gravitationally bound dark matter structure contains several up to hundreds of individual galaxies. Taking into account the detailed merger history, problems still remain. In particular, both at the massive and at the low mass end, too many and too massive galaxies are formed (see Fig. 1.1). To summarize, the following well-known problems are apparent:

- **The overcooling problem**
  What is described by the "overcooling problem" is the fact that model predictions for the brightness and star formation rate of central cluster galaxies disagree fundamentally with observations: In the models, cooling is dramatically over-efficient, leading to very bright, actively star-forming galaxies in the center of clusters, which are not observed in reality. This problem has already been noted by White & Rees (1978). But also for smaller mass galaxies, cooling is less efficient than one would expect from simple models (Navarro & Steinmetz 1997).

- **Overprediction of the faint end of the LF**
  At the faint end of the luminosity function, too many galaxies are formed in simple models (White & Frenk 1991; Benson et al 2003, see Fig. 1.1). This problem seems today more or less solved thanks to the inclusion of feedback from supernovae and stellar winds which heat up the gas at the low mass end (Larson 1974; White & Rees 1978 etc.), although this worsens the problem at the bright end.

- **The missing satellite problem**
  The "missing satellite problem" has been first described by Klypin et al. (1999) and Moore et al. (1999) and may be related to the overprediction of the faint end of the LF, although the "missing satellite problem" refers to galaxies with considerably lower mass. It was found in N-body simulations that the shape of the substructure mass function should be independent of the mass of the parent halo (Moore et al. 1999). Thus, in simulations, a large number of subhaloes are present in the Local Group, which in principle would be expected to host numerous satellite galaxies, similar to what is observed in massive galaxy clusters. However, the observed number of satellite galaxies in the Local Group is very low.

1.2 Galaxies and Their Evolution

1.2.1 Introduction

Galaxies belong to the most fascinating structures in nature. Dwarf galaxies typically contain $\sim 10^7$ individual stars, while the most massive galaxies can contain up to 10^{12} stars. The stars are following complex orbits within the gravitational potential of the galaxies. Many galaxies contain a central black hole, whose mass is closely related to the mass of the galaxy and may play an important role in their evolution. Galaxies seem to be isolated structures in the vast emptiness of space; however, in reality, they are continuously ejecting gas and metals[1] into the intergalactic medium, and in order to form stars they also have to accrete gas from outside. The light coming from their stars has reionized the entire

[1] In astrophysics, all elements heavier than Helium are termed "metals"

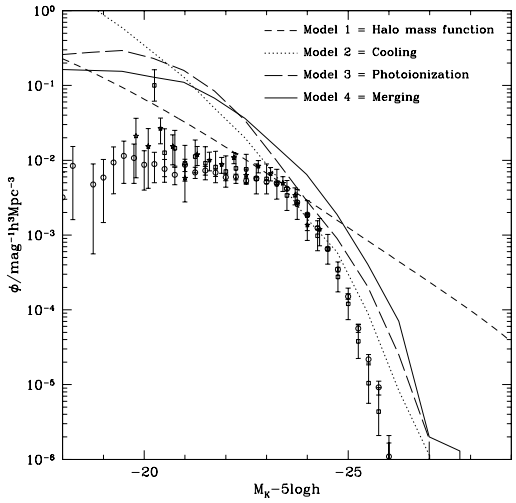

Figure 1.1: *In this figure from Benson et al. 2003, it is shown nicely that light does not trace mass at the faint and bright end of the LF and that feedback is needed. Points show observational results, lines denote model predictions. In Model 1 (dashed line), the halo mass function is directly converted into a LF assuming a fixed mass-to-light ratio. Models 2-4 correspond to simple semi-analytical models without feedback, which are far away from observations.*

intergalactic medium which was previously neutral. Moreover, all galaxies are embedded in dark matter haloes or subhaloes, and this dark matter is what shaped their evolution and structure. Galaxies on the other hand might influence the detailed distribution of the dark matter in the central regions of dark matter haloes.

1.2.2 Galaxy Formation and Star Formation

In an important early attempt to explain the formation of our Galaxy, Eggen, Lynden-Bell and Sandage (1962) suggested a "top-down" collapse, in which a proto-Galactic cloud collapsed inwards to form our Galaxy. However, this picture turned out to be at odds with observations. For example, it could not explain the fact that approximately one-half of all halo stars are in retrograde orbits. Today, a bottom-up picture including substantial dissipation is favoured, which has been outlined by White & Rees (1978). See Baugh (2006) for a recent review on galaxy formation. In this picture, a dark matter halo hosting a single galaxy today has formed from the merging of many smaller haloes, in part of which star formation had already begun. Once a given fluctuation in the dark matter separates from the Hubble expansion and turns around, gas will be heated to the virial temperature $T_{\rm vir}$ by shocks as it falls into the gravitational potential well of the dark halo:

$$T_{\rm vir} = \frac{1}{2}\frac{\mu m_{\rm H}}{k} V_{\rm H}^2 \tag{1.5}$$

where $\mu m_{\rm H}$ is the mean molecular weight of the gas, k is Boltzmann's constant, and $V_{\rm H}$ is an equivalent circular velocity of the dark matter halo at the virial radius, $V_H = \sqrt{GM/r_{\rm vir}}$.

Important timescales governing galaxy formation are the cooling timescale and the free-fall time scale:

$$t_{\rm cool} \propto \frac{1}{\rho_{\rm gas}} \tag{1.6}$$

$$t_{\rm ff} \propto \frac{1}{\sqrt{\rho_{\rm gas}}} \tag{1.7}$$

Only if the cooling timescale is below the freefall timescale, the gas can contract and form stars (Rees and Ostriker 1977, Silk 1977). Otherwise the gas will remain in hydrostatic equilibrium. If the angular momentum of the cooling gas is conserved, the cold gas settles into a rotationally supported disk. For the outer, low-density gas in large haloes, $t_{\rm cool}$ is larger than the Hubble time. Therefore, the baryonic mass of galaxies basically is constrained by an upper limit. However, even taking into account the long gas cooling time, galaxies in large haloes are too massive in models when compared to observations ("overcooling problem", White & Rees 1978). We will come back to this issue in section 1.2.5.

It is very important to note that only a relatively small fraction of the gas present in a typical dark matter halo has condensed into luminous galaxies, the rest is expected to still surround galaxies as hot haloes. It is not entirely clear what the origin of these hot haloes is; either a large fraction of the gas has never cooled onto the galaxies for unknown reasons (e.g. Navarro & Steinmetz 1997) or the gas has cooled but then was reheated by supernova feedback. With the exception of the hot gas halo found by Pederson et al. 2006 around a disk galaxy, there has been little success in detecting diffuse X-ray emitting haloes on larger scales around quiescent disk galaxies, which are expected to be present in the scenario outlined above. For example, Li et al. (2007) find a X-ray halo around a massive disk galaxy which is significantly less luminous than predicted by the simulations (like carried out by Toft et al. 2002). A popular explanation of the relatively low fraction of baryons that were able to cool down into galaxies is feedback by SN and stellar winds which may reduce the infall rate or cause outflows, although the details of this process are still relatively unclear. For more massive galaxies, on the other hand, AGN feedback and/or the fact that they are in the "hot accretion" regime apparently prevent the surrounding hot halo gas entirely from cooling, thus leading to the predominance of early types for galaxies with high stellar masses (see section 1.2.5 for more details). If no external or internal processes inhibit gas cooling in the surrounding hot halo, galaxy formation is still ongoing today, with gas constantly being accreted by the galaxy and condensing into stars. In order to form stars at a rate comparable to our own MW, a galaxy has to accrete $\sim 1 M_{\odot}$ per year in gas.

How does the hot extended halo cool onto a disk galaxy and form new stars? The cooling rates are strongly dependent on both the metallicity and the temperature of the gas and are thus expected to change dramatically (i) after reionization, especially for low-mass haloes, (ii) with time due to the increased pollution of the IGM with metals. Cooling in massive haloes mainly occurs via bremsstrahlung, as electrons are accelerated in an ionized plasma, or, at slightly lower temperatures, via the emission of photons from excited atomic states which are caused by collisions between partially ionized atoms and electrons. Once a small part of this hot plasma has cooled sufficiently, it can form a molecular cloud, whose composition is dependent on the metallicity of the gas: If the metallicity is high enough, dust particles are present, which lead to an enhanced production of H_2, a molecule which is particularly important for cooling. From these molecular clouds, stars can form.

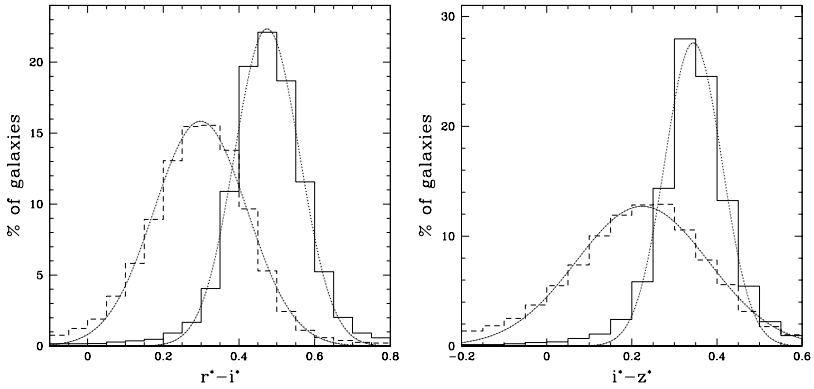

Figure 1.2: *The bimodal ($r^* - i^*$) and ($i^* - z^*$) colour distribution of galaxies in an early data release of the SDSS. The solid curves are Gaussian fits to the data. On the x-axis, going from left to right means that the galaxy colour becomes redder.(Figure from Strateva et al. 2000)*

How this exactly happens is still poorly known; both top-down processes, in which a gas cloud fragments into subclumps which form stars (Krumholz et al. 2005), and bottom-up processes, in which low mass stellar cores accrete gas from the cloud (Bonnell et al 1997), have been suggested. Once these stars terminate their lives, the gas may be recycled within the galaxy or ejected with the winds originating from SNe into the hot surrounding halo or beyond. Note that galaxy formation may proceed differently for elliptical and disk galaxies. It seems that ellipticals form the majority of the stars early in the galaxy-building process, while disk galaxies seem to form more stars at the time when they have already settled into a disk. Future simulations will hopefully reveal more about this potentially very important difference.

1.2.3 The Bimodality of the Galaxy Population

It has long been known that there are different types of galaxies in the universe, but only with large galaxy redshift surveys like the SDSS, it has become clear that the galaxy population in the local universe shows a striking bimodality in terms of colours (see Fig. 1.2 and Fig. 1.3), but also star formation rate and structural parameters (e.g. Strateva et al. 2001, Balogh et al. 2004, Baldry et al. 2004), with only few galaxies lying in between the two prominent peaks of the distribution. Nearly all galaxies can be categorized as being either “late type” or “early type”. According to current understanding, these terms might be a bit of a misnomer: Initially, it was thought that “early type” galaxies formed in a monolithic collapse early in the history of the universe (based on the Eggen, Lynden-Bell and Sandage 1962 scenario), while “late type” galaxies appear only at later times. This picture has undergone major revision today, mainly because the standard cosmological model dictates that structure formation occurs bottom-up, i.e. that large objects form latest, out of smaller components. Therefore, in the current paradigm which is employed in most semi-analytical models, it is assumed that galaxies form as disky “late types” and can be transformed into “early type” by different processes, like mergers etc. In what follows, I will describe typical properties of late and early type galaxies.

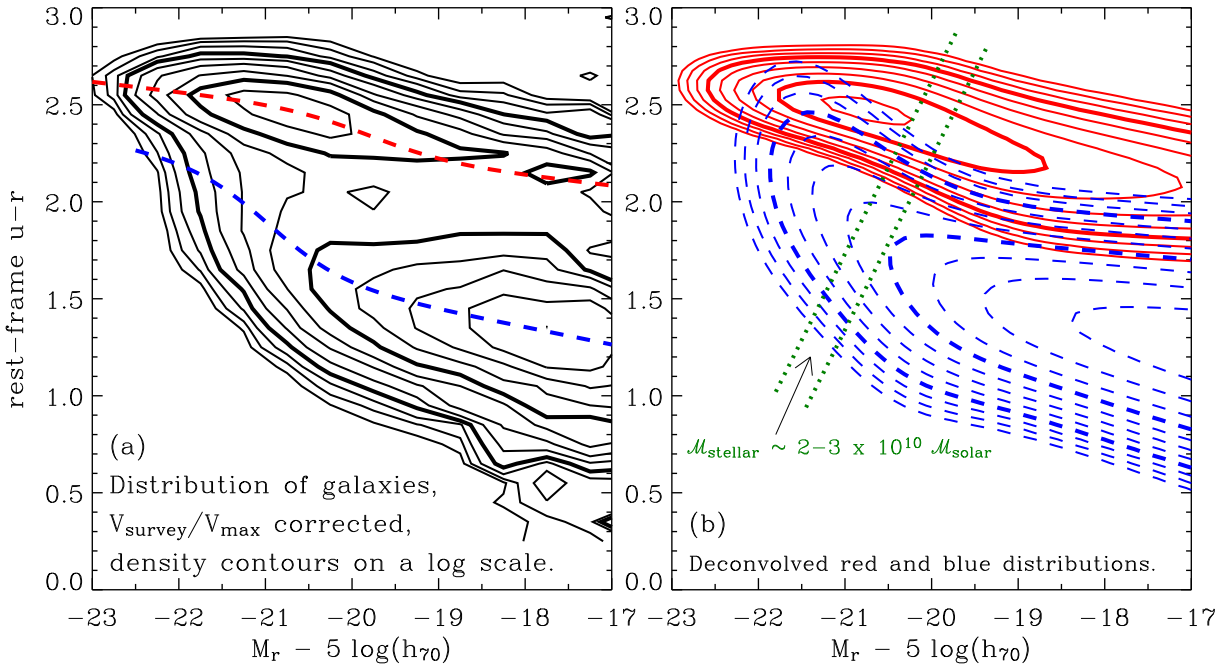

Figure 1.3: *Colour-magnitude distributions from Baldry et al. 2004, based on data from the SDSS. The left hand panel shows the observed bimodal distribution. The contours are on a logarithmic scale in number density, doubling every two levels. The dashed lines show the colour-magnitude relations of the red and blue sequences. Right hand panel: Deconvolved and parameterized distributions. The solid contours represent the red distribution and the dashed contours the blue distribution.*

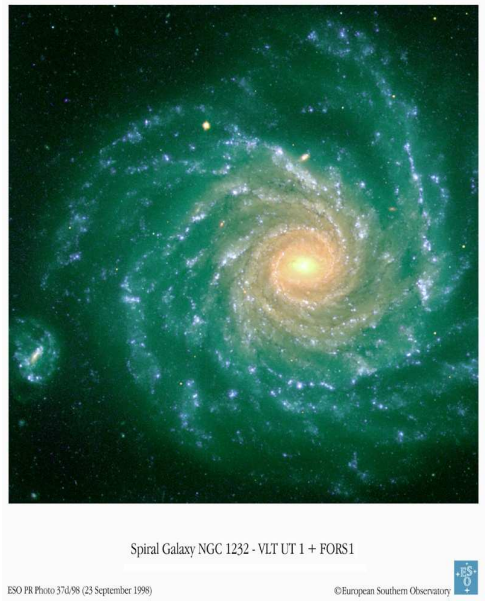

Figure 1.4: *A typical late type galaxy*

- **Late Type Galaxies**

  The most characteristic property of a late type galaxy is that it is actively forming stars, which often make it appear blue, since young stars have blue colours. Already quite low star formation rates are sufficient to maintain the blue colour of a galaxy. Late-type galaxies contain a relatively large mass in gas and dust. The latter is responsible for the fact that some late type galaxies also display red colours, especially when seen edge-on. In terms of structural properties, late type galaxies tend to have a relatively low central concentration. Spiral galaxies like the Milky Way or Andromeda are typical examples of a late type galaxy. They are supported by rotation and have the typical spiral arms, sometimes tightly wound, sometimes open. Spiral galaxies can also contain a central bulge (where "bulge" is simply defined as the excess light in the center of a disk galaxy, if one extrapolates the surface brightness profile of the outer disk), leading to enhanced central concentration.

- **Early Type Galaxies**

  The vast majority of early type galaxies appear red, because their star formation has practically ceased. Since the young, blue, luminous stars are missing, early type galaxies are less luminous than late type galaxies at a fixed stellar mass. Early type galaxies contain little or no gas and dust. Structurally, typical early type galaxies have a high central concentration. Most of them can be classified into "elliptical" and "lenticular" galaxies. Elliptical galaxies are smooth and featureless, while lenticular galaxies have a prominent disk without spiral arms. It has been claimed that lenticulars are galaxies at a stage in between spiral and elliptical galaxies, as they obey the exponential surface-brightness profile characteristic of spirals, but contain no dust, gas or young stars. Luminous ellipticals are supported by anisotropic pressure, while fainter ellipticals seem to be oblate, isotropic rotators (Davies et al. 1983). Early

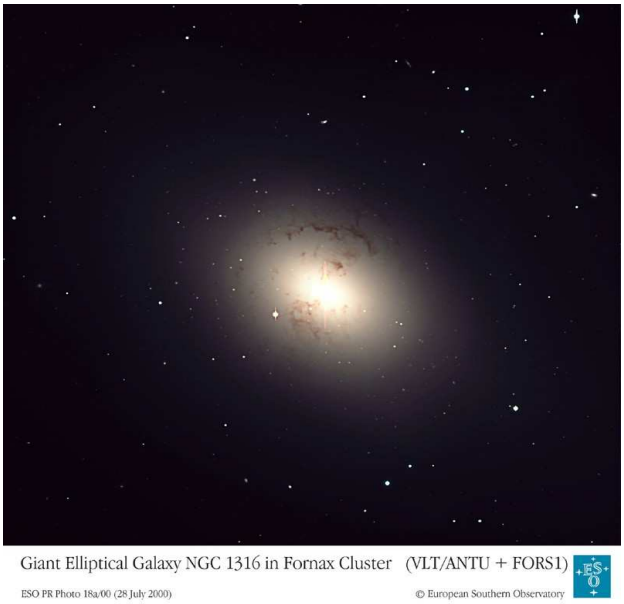

Figure 1.5: *A typical early type galaxy*

type galaxies are often found in denser regions of the universe. The most massive known galaxies, central cD galaxies in clusters, are practically always early type in the local universe. Note that there is also a subset of disk galaxies with red colours that should probably be classified as early types.

1.2.4 Galaxy Ecology

The abundance of early-type (or red) galaxies increases with galaxy density (Dressler 1980 and numerous follow-up studies, see Fig. 1.6) and towards the center of galaxy groups and clusters (Whitmore et al. 1993 etc.), while the opposite applies to late-type (or blue) galaxies. Many theoretical explanation for this fundamental observation have been suggested, however, up to now, no consensus has been reached. Thanks to the ever-increasing amount of both statistical data coming from large galaxy surveys at high and low redshift and detailed observations of galaxies in clusters and groups, there is hope that there will be much progress in the coming years on the question where the observed "galaxy ecology" originates.

It is often debated in the literature whether the observed correlation between galaxy properties and environment can be explained by "nature" or "nurture" or both, but it is not clear how these two basic theories, or maybe rather viewpoints, are defined. In principle, one would assume that "nature" processes are the processes which are determined to occur from the initial DM density field alone, i.e. are "genetically imprinted" already at high redshifts — however, this actually applies to all processes: whether a galaxy will be falling into a large cluster or not is completely determined by the initial density field. According to the "nature" viewpoint, on the other hand, each galaxy starts its life blue, disky and star-forming, and by some process (again, for example when falling into a large cluster) will be transformed into an early type, passive system. However, one could argue that

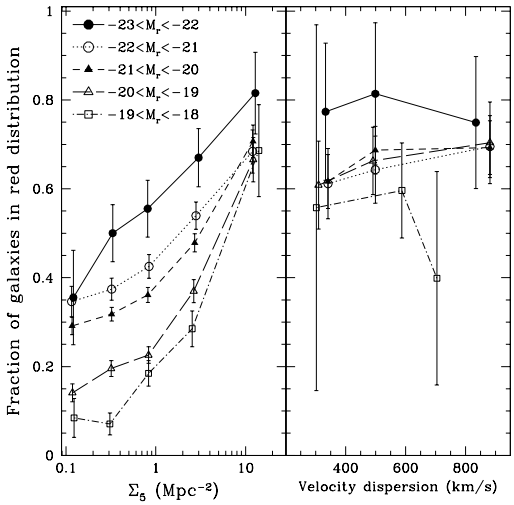

Figure 1.6: *The fraction of galaxies in the red distribution in the SDSS (Figure from Balogh et al. 2004). On the left hand panel, it can be seen nicely how the fraction of red galaxies strongly increases with local density to the 5th nearest neighbour. On the right hand panel, no trend with velocity dispersion is visible due to the large errorbars (see Chapter 2 for another method to estimate group masses).*

some process shutting down star formation has occurred for all red galaxies, since every galaxy has to have had star-forming (maybe not disky, though) progenitors at some point. Whether galaxy-galaxy mergers are to be counted as a "nature" or "nurture" process for example is unclear. Thus, I will not adopt this nomenclature here, and simply list a number of processes that could lead to the observed relation between galaxy properties and environment, no matter when they occur. The first two (or three) mechanisms are mostly counted as being "nature" processes in the literature, while the rest is regarded as being a "nurture" process. I will discuss how these mechanisms are supposed to operate, and what the current understanding of their significance is, both in groups and clusters. See also e.g. Boselli & Gavazzi (2006) or de Lucia (2006) for recent reviews on different mechanisms that could explain the relation between galaxy properties and their environment.

- **Different Galaxy Formation Processes**
  A region which has collapsed into a massive cluster today must have been a region of high overdensity already early on. In such regions, galaxy formation will clearly happen earlier than in other parts of the universe, and thus maybe also happen differently, in a way which favours early type galaxy formation. This explanation may well be partially valid for the central cD galaxies in massive clusters, which are clearly very different from the typical field galaxy. However, in the case of satellite galaxies in groups and clusters, it has been observed that the red fraction has been increasing since a redshift of ~ 1 (e.g. Cucciati et al. 2006, Cooper et al. 2007). This indicates that these galaxies have probably not been affected by their special location in a higher density region before the cluster or group collapsed.

- **Assembly Bias**
  According to the standard extended Press-Schechter formalism, the mass assembly

history of a given halo only depends on its final mass (Sheth, Mo & Tormen 2001). However, recent results from simulations indicate that the larger scale environment might significantly influence the mass accretion history of a given halo (e.g. Gao & White 2007, Maulbetsch et al. 2007). For example, low-mass old haloes are almost always located close to big structures and have their mass accretion suppressed at late times (Wang, Mo & Jing 2007), which possibly explains the age-dependent clustering of dark matter haloes as found by Gao, Springel & White (2005) and Wechsler et al. (2006). Wetzel et al. (2007) find that haloes which recently experienced a major merger are generally more strongly clustered. All these results indicate that galaxies with a given mass residing in low- and high-density environments may have a different formation redshift and mass assembly history, which could influence their properties significantly.

- **Mergers**
  Major mergers (i.e. mergers between galaxies of comparable mass) are violent, destroying the disks of the involved galaxies, possibly resulting in the creation of a spheroidal system and thus providing an important pathway leading from late to early type galaxies. Mergers are expected to trigger an initial starburst which use up the gas in the involved galaxies and thus lead to a termination of star formation in the long run (e.g. Mihos & Hernquist 1996). However, there are still some problems with this scenario (see e.g. Naab & Ostriker 2007), and either multiple mergers or binary mergers of spirals whose progenitors no longer exist need to be invoked to reproduce the properties of today's early type galaxies in detail. Also, mergers are most common in poor groups of galaxies and become less important in massive clusters, where the velocity dispersion of the satellites is too high. Thus, if mergers were the primary driver of galaxy transformation, one would expect that the fraction of early type galaxies would saturate above a certain halo mass, which is not observed. Additionally, since a population of heavily star-forming, massive blue disk galaxies has recently been discovered (e.g. Melbourne et al. 2005), widespread and frequent mergers, which were advocated by Bell et al. 2004 to explain the presence of massive red galaxies, do not seem to be necessary anymore since these could be formed by simple star formation truncation (Bell et al. 2007).

- **Tidal interactions**
  The interaction of a galaxy with the potential of the parent halo may cause stripping of gas, dark matter and stars, and could distort the morphology of a galaxy. Examples of structurally distorted galaxies have been observed in galaxy clusters, likely to correspond to systems influenced by tidal forces. Such effects have also been reproduced in hydrodynamical simulations (e.g. Mastropietro et al. 2005a). Especially low mass galaxies with low central concentration can easily be completely disrupted by tidal interactions, if they come close to the center of their parent halo potential.

- **Interactions between the interstellar medium and the intracluster medium**
  The most important interaction between the interstellar medium in galaxies and the hot cluster gas is probably ram pressure stripping. Ram pressure is a pressure exerted on a body which is moving through a fluid medium. If a galaxy is moving through the hot gaseous intracluster medium of a large galaxy cluster, its own inter-

stellar gas can be swept away by this pressure. According to Gunn & Gott (1972), ram-pressure stripping occurs only if the ram pressure, characterized by $\rho_{\rm ICM}v^2$, is greater than the gravitational restoring force of the satellite galaxy's disk. Thus, it should only be effective in the central regions of major galaxy clusters like Coma and Virgo. Also, the orientation of a galaxy with respect to its trajectory can reduce the effect of ram-pressure stripping considerably. In poorer environments, ram-pressure stripping may still affect dwarf galaxies, and may contribute to the stripping of the hot extended gas halo around normal spiral galaxies ("strangulation", see below) and the low-density part of the ISM (e.g. Levy et al. 2007). Several recent studies indicate that ram-pressure stripping of the interstellar medium may not be the dominant mechanism causing galaxy type transformations (e.g. Goto 2006,Chapter 2 of this thesis), although there is compelling observational evidence that it happens at least in some galaxies in massive clusters (e.g. Koopmann & Kenney 2004). Other suggested stripping mechanisms include thermal evaporation (Cowie & Songalia 1977) or viscous stripping (Nulsen 1982). Thermal evaporation describes the mechanism in which the cold gas within galaxies is heated by the contact with the hot ICM in the cluster and cannot be retained by the galaxy. It becomes important for clusters with a high ICM temperature and is more important for smaller galaxies, but can be suppressed by the presence of magnetic fields. Viscous stripping has a similar effect on the gas in a galaxy as ram-pressure stripping and is most important for large and fast galaxies (Boselli & Gavazzi 2006 and references therein) and galaxies on more circular orbits (Chung et al. 2007). It is also largely insensitive to the orientation of the galaxy (Nulsen 1982).

- **Strangulation**
  Strangulation (also called "starvation" or "suffocation") is the process of a galaxy losing its hot, extended gas halo, which serves as a supply for star formation. It has been first suggested by Larson et al. (1980) as a solution for the decline in star formation rate in galaxies becoming part of a bigger cluster. Since the hot halo gas is more loosely bound than the intragalactic gas, strangulation can also occur in relatively poor environments. It is expected to be caused by a combination of ram-pressure and tidal stripping and will affect the star-formation rate only after the galaxy has used up its own interstellar gas. In order to reproduce the observed fraction of red galaxies in clusters, Balogh, Navarro and Morris (2000) argue that the timescale for strangulation to inhibit star formation in a galaxy has to be of order 1-3 Gyr, which is in agreement with the numerical results by Bekki et al. (2002) and Kawata & Mulchaey (2007). The timescale with which strangulation operates depends on the efficiency with which cold disk gas is reheated by supernovae and thus added to the hot halo, where it can be stripped. This effect is likely to be more effective for low mass galaxies, which may make the timescale of strangulation increase with galaxy mass. In semi-analytical models, strangulation (together with mergers) is the only environmental effect that is included, but it likely truncates star formation on a too short timescale, which leads to the overprediction of red satellites which we have identified in Chapter 3. Nevertheless, strangulation is a promising candidate for explaining the difference in star formation rate between the field and denser regions. It does not directly affect the morphologies of galaxies, but once star formation has ceased, the fading of the disk may lead to an increased luminosity-

weighted bulge-to-total ratio, which may let the galaxy appear spheroidal.

- **Galaxy Harassment**
  Galaxy Harassment is a form of tidal interaction, caused by high speed encounters between different subhaloes and/or galaxies in groups and clusters. It can cause morphological transformation in galaxies (Moore et al. 1998). However, galaxy harassment is only efficient for low-luminosity galaxies with a low central density and thus might be important for the evolution of dwarf ellipticals and low-surface brightness galaxies in clusters, but not for the evolution of more luminous cluster galaxies.

How can we discriminate which of the mechanisms proposed above is actually occurring? First, it is important to find out in which environments exactly the red galaxy fraction is enhanced compared to the field. By now, it has become quite clear that this is not only the case in cluster environments, but also in poorer galaxy groups, which is an argument against the importance of ram-pressure stripping and galaxy harassment (see also Chapter 2). The second essential quantity which can help to find out which processes are dominant is the timescale over which star formation is suppressed. This transformation timescale is expected be short for processes like ram-pressure stripping, galaxy harassment, galaxy mergers etc., and long for processes like strangulation. Different studies have attempted to extract this timescale from observations, leading to widely differing results, some of which will be discussed in what follows.

Using population synthesis models (e.g. Bruzual & Charlot 2003), it is possible to predict the evolution of $D_n(4000)$ and H_δ, which are two stellar absorption line indicators, for different star formation quenching scenarios. Kauffmann et al. (2004) find in their analysis of galaxies in the SDSS that short timescales for quenching (< 1 Gyr) produce an evolutionary track of those two stellar absorption line indicators which is in disagreement with observations, and that longer timescales for star formation truncation need to be invoked. On the other hand, Tanaka et al. (2007) find their data (at slightly higher z) to be in better agreement with an evolution of $D_n(4000)$ and H_δ as predicted in a scenario where an initial starburst is followed by a sharp truncation, which they argue is evidence for the importance of galaxy-galaxy interactions.

Another method to estimate the timescale over which star formation truncation operates is by the fraction of blue galaxies in clusters. Based on observations of a sample of clusters at moderate redshifts, Kodama & Bower (2001) argue that an abrupt truncation of star formation is inconsistent with the observed colour distribution of galaxies. Similarly, Balogh et al. (2000) claim that a quick truncation of star formation would lead to too high fractions of red galaxies in clusters and a too high fraction of K+A galaxies[2], and thus argue in favour of the strangulation scenario. On the other hand Balogh et al. (2004) argue that since there are only very few galaxies observed with properties in between the typical properties of late and early type galaxies, it follows that the transformation should be occurring on a short timescale. It is thus far from clear what the timescale for galaxy transformation in high density environments really is, and further studies will be necessary.

[2]K+A galaxies are galaxies with strong Balmer lines but no nebular emission lines, which indicates that their SF was sharply truncated. They are very rare (< 1 % of the population in SDSS according to Quintero et al. 2004)

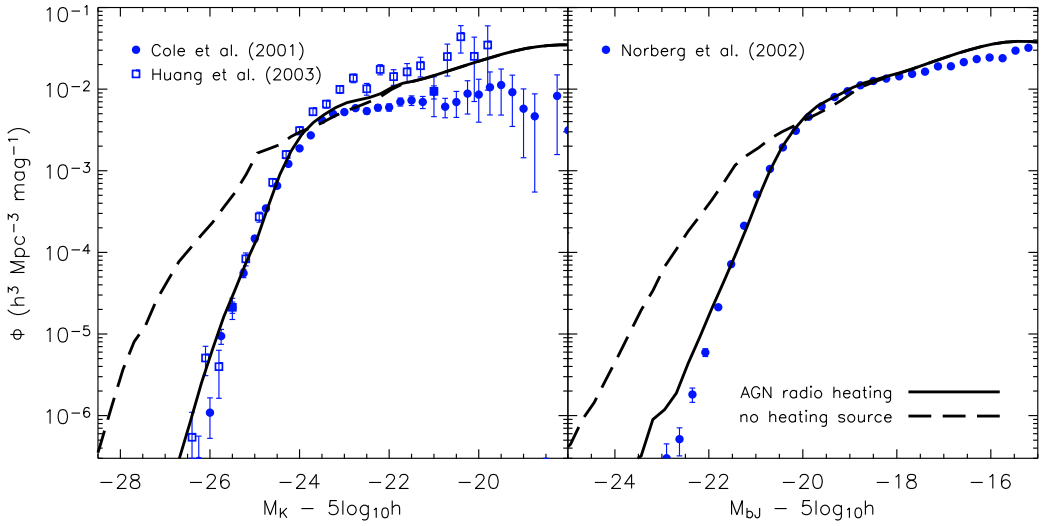

Figure 1.7: *Figure from Croton et al. 2006. The solid line show the model prediction for the LF from the semi-analytical model by Croton et al. which includes supernova-feedback, feedback by reionization and AGN-feedback. Comparison to the observational results shows good agreement both in the K (left) and* b_J *(right) band. Comparing this figure to Fig. 1.1 shows how important the inclusion of feedback in the models is.*

1.2.5 Dependence of Galaxy Type on Stellar Mass

Besides the relation between galaxy properties and environment that was discussed in the previous chapter, there is another, perhaps even more fundamental relation observed: The correlation between galaxy properties and stellar mass. Kauffmann et al. (2003) point out that there is a critical stellar mass for galaxies at $\sim 3 \cdot 10^{10} M_{\odot}$, above which galaxies tend to be early type much more often. This also corresponds to the cutoff in the stellar mass function of blue cloud galaxies found by Bell et al. (2007). Since more massive galaxies have been found to be more strongly clustered, and the fraction of massive galaxies increases towards the center of groups and clusters due to mass segregation (van den Bosch et al., in prep.), the relation between galaxy stellar mass and galaxy properties may even partially explain the environmental effects discussed above (but see also Skibba et al. 2007 who find that the average satellite mass is independent on host halo mass).

For central galaxies, stellar mass is directly related to the mass of the hosting dark matter halo. For satellite galaxies, on the other hand, stellar mass is supposed to be related to the mass of the dark matter halo in which the galaxy resided when it was last a central halo ($M_{\rm infall}$ see e.g. Conroy et al. 2006). Thus, the relation between galaxy properties and stellar mass may in fact be a relation between galaxy properties and halo mass or $M_{\rm infall}$ respectively. Additionally, as discussed in section 1.1.3, the difference in shape between the observed luminosity function and the halo mass function indicates that galaxy formation becomes inefficient both at the high and the low mass end, for reasons still not completely understood (these effects are related to the "overcooling problem" and the "missing satellite problem", see section 1.1.3). In what follows, I will present a list of mechanisms that have been proposed to explain the halo / stellar mass dependence of

galaxy properties and in particular to truncate galaxy formation at the low and high mass end of the halo mass function.

1. Mechanisms likely to suppress star formation at the high mass end:

   - **Hot vs. Cold Accretion**
     In the standard paradigm of galaxy formation (based on White and Rees 1978, see section 1.2.2), gas is accreted onto the galaxy in two stages. First, it is shock-heated to the virial temperature of the parent halo, and then, the shock-heated gas in the halo radiatively cools and collapses onto galaxies. However, recent simulation results indicate that there is also another mode of gas accretion, termed "cold" accretion, in which the gas never gets shock heated and enters galaxies in the form of cold clumps which fall in along filamentary structures. This "cold accretion" is especially important for low mass haloes, and appears to dominate at high redshift (Kereš et al. 2005, Dekel & Birnboim 2006). According to these results, it is only above a critical dark matter halo mass of about $\sim 10^{11.4} M_{\odot}$ that "hot accretion" is actually occurring. Intriguingly, the baryonic mass corresponding to this dark matter halo mass is very close to the mass at which Kauffmann et al. (2004) have observed the transition from predominantely late type galaxies at low masses to a dominance of early types at higher masses. This would indicate that there might be some mechanism at work which strongly suppresses hot accretion in the real universe, for example AGN feedback as described below. Dekel & Birnboim 2007 and Birnboim, Dekel & Neistein 2007 argue that AGN feedback is not needed and cooling is suppressed in the hot accretion mode naturally.
   - **AGN feedback**
     AGN ("Active Galactic Nucleus") feedback is a popular explanation for the change in galaxy formation efficiency at high masses and used by many models (e.g. Granato et al. 2004; Croton et al. 2006, Cattaneo et al. 2006a; Sijacki & Springel 2005). These models make use of the fact that the accretion of gas into a black hole in the center of a galaxy can release a large amount of energy that might heat up the surrounding gas halo. There are two different modes of AGN activity observed: the quasar mode, which seems to be important at high z, is shortlived, powerful and probably triggered by mergers; and the radio mode, which is longer-lived and supported by the continuous, quiescent accretion of gas into the black hole. In order to lead to the observed strong mass dependence of galaxy type, AGN feedback should only become efficient above a critical mass. Additionally, it should be very stable. It is not clear yet if and how AGN feedback can fulfill these two conditions. Croton et al. 2006 for example have suggested that AGN feedback might only be efficient above the critical mass for "hot" accretion. In Chapter 3, we test the semi-analytical model from Croton et al. against observations and will discuss the way in which this feedback mechanism operates in more detail.
   - **Gravitational heating**
     Gravitational heating and dynamical friction heating by satellites orbiting in the halo potential may transfer energy from the motion of galaxies into the ICM (e.g. Miller 1986, El-Zant et al. 2004, Khochfar & Ostriker 2007). However, it

seems that this effect alone is not sufficient to prevent the cooling catastrophe (e.g. Kim 2007).

2. Mechanisms likely to suppress star formation at the low mass end:

   - **Supernova Feedback**
     Gas ejection by stellar winds and supernovae can cause a galaxy to lose gas (Larson 1974; White & Rees 1978; Dekel & Silk 1986). This effect is not important for massive galaxies, but is expected to become dominant for low mass haloes with shallow gravitational potentials. Supernova feedback is included in practically all semi-analytical models and numerical simulations of galaxy formation used today, since it has proven to be extremely difficult to reproduce the luminosity function without it.
   - **Reionization**
     The radiation of the first galaxies, quasars and possibly also Pop III stars in the universe ionized the previously neutral hydrogen present both in and between galaxies. Reionization inhibits gas cooling in low mass haloes in two ways: First, it heats the intergalactic mediums to a temperature of $\sim 10^4$ K, which restricts the infall of baryons into haloes with virial temperatures below 10^4 K. Second, the radiation increases the ionization state of the hot gas, thereby removing certain channels for cooling. These effects have been described in detail by Efstathiou 1992, Babul & Rees 1992, Toul & Weinberg 1996, Nagashima et al. 1999, Gnedin et al. 2000.

In Fig. 1.7, it is shown that a model including feedback from supernovae, AGN and reionization can accurately match the observed LF. However, other models including completely different recipes to truncate cooling might be able to fit the data equally well, and so this result does not in fact prove that AGN feedback is what truncates star formation at the high mass end.

1.2.6 Downsizing

As outlined above, the current star formation rate in a galaxy is strongly dependent both on its environment and mass. It is obvious that also a massive galaxy in a dense environment which is not forming stars at present must have been heavily star forming at some point in time, to build up its present stellar mass, likely at a time when it still consisted of many smaller progenitor galaxies. It has been found that the global star formation rate per unit volume is strongly decreasing since z=1 where it had been roughly ten times larger (Madau et al. 1996). At the same time, the typical mass of galaxies hosting active star formation has been decreasing with time, as detected by several high-redshift surveys (Cowie et al. 1996, Kodama et al. 2004 etc.) Also, synthetic stellar evolution analysis has revealed that today's massive galaxies generally formed their stars earlier and over a shorter timescale than lower mass galaxies (Thomas et al. 2005). Note that the latter two phenomena are not caused by the same effects, as outlined by Neistein et al. 2006: While it is quite straightforward to understand that the most massive galaxies of today must have formed their first progenitors earliest due to their biased location in the density field and thus formed their star earlier than lower mass galaxies, it is less obvious why the characteristic mass of galaxies with the highest SSFR should be decreasing. Interestingly

though, Zheng et al. 2007 find that the star formation rate is declining with time both in high and low mass galaxies with nearly the same rate, suggesting that the notion of the star formation rate declining only in high mass galaxies is in fact not correct and influenced by observational bias.

Many mechanisms have been proposed to explain the decline in star formation rate since $z \sim 1$: The build-up of structure (and thus the increasing importance of effects taking place in groups and clusters, as outlined in section 1.2.4), a decline in the galaxy merger rate, the shift of the threshold mass for the "hot" accretion mode (and thus also AGN feedback) to lower masses with time, or the declining supply of new gas falling in from the cosmic web at $z < 1$ (Noeske et al. 2007). It could well be that downsizing, the dependence of galaxy properties on stellar mass and on environment might be all interconnected; how exactly is still not clear.

1.3 Constructing Galaxy Group Catalogues

1.3.1 Galaxy Group Catalogues: Overview

In large galaxy redshift catalogues one observes that galaxies are spatially highly clustered. There are huge regions, the so-called voids, which contain nearly no galaxies; in other regions, many galaxies are present in a relatively small volume. Already early on in the history of galaxy redshift catalogues, there have been attempts to assign galaxies to groups and/or clusters (hereafter, I use the term "groups" for massive clusters, single galaxies in their DM halo and everything in between). One can then relate the properties of the galaxies in the groups to the velocity dispersion or the richness of the groups, or their spatial clustering and distribution functions. Such group catalogues have been constructed using various galaxy surveys, for example the CfA redshift survey (e.g. Geller & Huchra 1983), the Las Campanas Redshift Survey (e.g. Tucker et al. 2000), the 2-degree redshift survey (Merchàn & Zandivarez 2002; Eke et al. 2004) and the SDSS (Bahcall et al. 2003; Lee et al. 2004; Berlind et al. 2006; Koester et al. 2007). The goal of such approaches should be to assign only galaxies to the same group which really reside in the same dark matter halo. Different types of group finders have been used in such analysis. The most simple, and most widely used algorithm is a friend-of-friend (FoF) algorithm. One defines a linking length along the line of sight (using the redshifts obtained for the galaxies) and in the transverse direction. One starts with one galaxy and looks for all neighbour galaxies within the linking length, which will be assigned to the group, then continues with the same procedure using each individual galaxy of the group, until no more galaxies can be added. If the linking length is too small, one will miss galaxies at the outskirts of groups, if it is too big, neighbouring galaxies or groups which do not share a common dark matter halo might be connected by accident. These two problems are quantified by the terms "completeness" and "contamination". The completeness F_t is the ratio between the number of true members identified by the group finder and the total number of true group members. The contamination F_i is the ratio between the number of false members (interlopers) selected by the group finder and the total number of true members. If one wants to give equal weight to those two criteria, an ideal group finder should maximize the parameter $\Psi = F_\mathrm{t} \times (1 - F_\mathrm{i})$. Galaxy group masses are commonly estimated using the velocity dispersion of the galaxies in the groups, using the virial theorem. However, this method is not very accurate, especially for groups with a small number of members, and

projection effects introduce relatively large errors.

1.3.2 The Group-Finding Algorithm of Yang et al.

Yang et al. 2005 present a novel group finding algorithm which has been used throughout this work. How this group finder works in detail is presented in the Appendix of this thesis. Here I will give just a brief overview. As a first step, the group finder uses the traditional FoF approach with a relatively small linking length to find the centers of potential groups. Using an estimate for the total luminosity of the galaxies in a group, which is extrapolated from the measured luminosity and the redshift of the group, one can obtain an estimate for the total group mass. For this, we use the mass-to-light ratio as a function of mass, given in van den Bosch, Yang & Mo (2003). Note that this function is cosmology dependent. From the mass, the velocity dispersion can be estimated. Using the sizes, masses, velocity dispersions and centers of the groups thus obtained, it is possible to assign group membership to a larger fraction of the galaxies in the survey. Using these new groups, one can calculate new group centers and reiterate the entire procedure, until there is no further change in the membership of galaxies in groups. One of the main advantages of this approach is that it is possible to get mass estimates also for groups with a very low number of members, even only one. This group finding algorithm has been extensively tested using mock galaxy redshift surveys and has been found to perform very well in terms of completeness and contamination. Applying this group finding algorithm to the 2dFGRS, Yang et al. (2005) have been able to predict that the first-year results of the WMAP satellite overestimated σ_8. Indeed, the third-year WMAP results corrected σ_8 down from ~ 0.9 to ~ 0.74. This prediction is a remarkable success and shows that the group finding algorithm is working very well.

1.3.3 The Sloan Digital Sky Survey (SDSS)

The SDSS (York et al. 2000) is one of the most ambitious astronomical surveys undertaken to the present day and is at the moment still ongoing. In the following chapters, I will frequently refer to this survey, on which our galaxy group catalogue is based. The SDSS is a joint, five passband (u, g, r, i, z) imaging and medium-resolution spectroscopic survey. Upon completion, it will provide a 3-dimensional map of about a million galaxies and quasars, covering more than a quarter of the sky. The SDSS has already led to many important discoveries. It provided measurements of the large-scale structure of the universe in a volume of unprecedented size which allowed to put important independent constraints on cosmological parameters, being orthogonal to the WMAP measurements. Also, the theoretically predicted baryonic acoustic oscillations were measured in the SDSS. These baryonic oscillations which are imprinted in the galaxy power spectrum provide a promising tool for probing the cosmological distance scale and dark energy. Also, several new dwarf galaxies in the Local Group have been detected thanks to the SDSS.

Chapter 2

Galaxy Groups in the SDSS: The Dependence of Galaxy Properties on the Host Halo Mass[1]

The Earth is geological, yes, but this geological entity grows people, and our existence on the Earth is a symptom of this other system, and its balances, as much as the solar system in turn is a symptom of our galaxy, and our galaxy in its turn is a symptom of a whole company of other galaxies.

Alan Watts

2.1 Abstract

Using a large galaxy group catalogue constructed from the Sloan Digital Sky Survey (SDSS DR2), we investigate the correlation between various galaxy properties and halo mass. We split the population of galaxies in early types, late types, and intermediate types, based on their colour and specific star formation rate (SSFR). At fixed luminosity, the late (early) type fraction of galaxies increases (decreases) with decreasing halo mass. Most importantly, this mass dependence is smooth and persists over the entire mass range probed, without any break or feature at any mass scale. We argue that the previous claim of a characteristic feature on galaxy group scales is an artefact of the environment estimators used. At fixed halo mass, the luminosity dependence of the type fractions is surprisingly weak, especially over the range $0.25 \lesssim L/L^* \lesssim 2.5$: galaxy type depends more strongly on halo mass than on luminosity. In agreement with previous studies, the late (early) type fraction increases (decreases) with increasing halo-centric radius. However, we find that this radial dependence is present in haloes of all masses probed (down to $10^{12}h^{-1}\,\mathrm{M}_\odot$), while previous studies did not find any radial dependence in haloes with $M \lesssim 10^{13.5}h^{-1}\mathrm{M}_\odot$. We argue that this discrepancy owes to the fact that we have excluded

[1]This chapter has been published in MNRAS (Weinmann et al., 2006a)

central galaxies from our analysis. We also find that the properties of satellite galaxies are strongly correlated with those of their central galaxy. In particular, the early type fraction of satellites is significantly higher in a halo with an early type central galaxy than in a halo *of the same mass* but with a late type central galaxy. This phenomenon, which we call 'galactic conformity', is present in haloes of all masses and for satellites of all luminosities. Finally, the fraction of intermediate type galaxies is always ~ 20 percent, independent of luminosity, independent of halo mass, independent of halo-centric radius, and independent of whether the galaxy is a central galaxy or a satellite galaxy. We discuss the implications of all these findings for galaxy formation and evolution.

2.2 Introduction

The local population of galaxies consists roughly of two types: red galaxies, which reveal an early type morphology and which have little or no ongoing star formation, and blue galaxies with active star formation and a late-type morphology. The case for two distinct classes of galaxies has recently been strengthened as the use of large galaxy redshift surveys has shown that the distributions of colour and star formation rate (SFR) of the galaxy population are bimodal (e.g., Strateva et al. 2001; Blanton et al. 2003b; Kauffmann et al. 2003, 2004; Baldry et al. 2004; Brinchmann et al. 2004; Balogh et al. 2004a,b). In addition, studies at intermediate redshifts have shown that this bimodality exists at least out to $z \simeq 1$ (e.g., Bell et al. 2004; Tanaka et al. 2005; Weiner et al. 2005), but with different fractions of galaxies on both sides of the bimodality scale compared to $z = 0$ (Bell et al. 2004; Faber et al. 2005).

An important, and largely open question in galaxy formation regards the origin of this bimodality. In particular, does this bimodality arise early on (the 'nature' scenario), or is it a consequence of various physical processes that operate over a Hubble time (the 'nurture' scenario)? In particular, are there two distinct formation channels, or are galaxies being transformed from one type to the other? In the latter case we need to know where, how and when these transformations occur. Important hints come from the observed correlations between galaxy properties and environment: galaxies in dense environments (i.e., clusters) have predominantly early type morphologies (e.g., Oemler 1974; Dressler 1980; Whitmore, Gilmore & Jones 1993) and low SFRs (e.g., Balogh et al. 1997, 1999; Poggianti et al. 1999). At first sight this seems to suggest that cluster-specific processes, such as galaxy harassment (Moore et al. 1996), ram-pressure stripping (Gunn & Gott 1972) and/or interactions with the cluster potential (Byrd & Valtonen 1990) play a dominant role in transforming galaxy morphologies from late to early types, and in truncating their SFRs. However, starting with the work of Postman & Geller (1984), it has become clear that the environmental dependence of galaxy properties is not restricted to clusters, but smoothly extends to the scale of galaxy groups (see also Zabludoff & Mulchaey 1998; Tran et al. 2001). Consequently, it has been suggested that group-specific processes are of paramount importance for transforming galaxies. In particular, the relatively low velocity dispersion of groups implies that galaxy-galaxy merging, which can transform disk galaxies into ellipticals (e.g., Toomre & Toomre 1972), is effective. In addition, as soon as a galaxy becomes a group member, i.e., becomes a satellite of a bigger system, it is deprived of its reservoir of hot gas. Consequently, it is expected that, after a delay time in which the galaxy consumes (part of) its cold gas, star formation in the galaxy comes to a halt (Larson,

Tinsley & Caldwell 1980; Balogh, Navarro & Morris 2000). This process, often called strangulation, provides a natural explanation for the increasing fraction of red galaxies towards denser environments.

Much of the earlier work on the relation between galaxy properties and environment was based on incomplete samples of clusters and groups. With the advent of large, homogeneous galaxy surveys, it has become possible to investigate this relation in far more detail, and over a much wider range of environments. In particular, using the Las Campanas Redshift Survey (LCRS; Shectman et al. 1996), the Two-Degree Field Galaxy Redshift Survey (2dFGRS; Colless et al. 2001) and the Sloan Digital Sky Survey (SDSS; York et al. 2000; Stoughton et al. 2002) various authors have investigated the relation between environment and morphology (e.g., Hashimoto & Oemler 1999; Goto et al. 2003; Kuehn & Ryden 2005), between environment and star formation rate (e.g., Hashimoto et al. 1998; Lewis et al. 2002; Domínguez et al. 2002; Gómez et al. 2003; Balogh et al. 2004a; Tanaka et al. 2004; Kelm, Focardi & Sorrentino 2005), and between environment and colour (e.g.,Tanaka et al. 2004; Balogh et al. 2004b; Hogg et al. 2004).

One of the numerous results that have emerged from these studies is that galaxy properties only seem to correlate (significantly) with environment above a characteristic surface density, which is roughly consistent with the characteristic density at the perimeter of a cluster or group (Hashimoto & Oemler 1999; Lewis et al. 2002; Gómez et al. 2003; Goto et al. 2003; Tanaka et al. 2004; Balogh et al. 2004a). This has been interpreted as further evidence that group-specific processes play a dominant role in establishing a bimodal distribution of galaxies (e.g., Postman & Geller 1984; Zabludoff & Mulchaey 1998, 2000). However, it is important to understand the physical meaning of the density estimators used. Most studies parameterize 'environment' through the projected number density of galaxies above a given magnitude limit. Typically this number density, indicated by Σ_n, is measured using the projected distance to the nth nearest neighbor, with n typically in the range 5-10 (e.g., Dressler et al. 1980, Lewis et al. 2002; Gómez et al. 2003; Goto et al. 2003; Tanaka et al. 2004; Balogh et al. 2004a,b; Kelm et al. 2005). However, *the physical meaning of Σ_n itself depends on the environment*: in clusters, where the number of galaxies is much larger than n, Σ_n measures a *local* number density, which is a subproperty of the cluster (i.e., Σ_n is strongly correlated with cluster-centric radius). However, in low-density environments, which are populated by haloes which typically contain only one or two galaxies, Σ_n measures a much more global density, covering a scale that is much larger than the halo in which the galaxy resides. This ambiguous, physical meaning of Σ_n severely complicates a proper interpretation of the various correlations between environment and galaxy properties. Note that density estimators that use a fixed metric aperture size, rather than the distance to the nth nearest neighbor, suffer from very similar problems.

Another complication arises from the fact that the bimodality scale, and the fractions of galaxies on either side of it, depend strongly on luminosity and stellar mass (e.g., Kauffmann et al. 2003; Blanton et al. 2003b; Hogg et al. 2004; Baldry et al. 2004; Kelm et al. 2005). This luminosity dependence is also evident from a comparison of the luminosity functions of early and late type galaxies, which shows that late (early) types dominate the faint (bright) end (e.g., Loveday et al. 1992; Marzke & Da Costa 1997; Zucca et al. 1997; Marzke et al. 1998; Blanton et al. 2001; Madgwick et al. 2002). At first sight this seems to suggest that the morphology and SFR of a galaxy is somehow determined by its own (baryonic) mass. On the other hand, this luminosity/stellar mass dependence may also be

a reflection of the correlation between the galaxy luminosity function and environment: as shown by various authors (e.g., Hogg et al. 2003; Blanton et al. 2005b; Mo et al. 2004; Hoyle et al. 2005; Croton et al. 2005), dense environments contain on average brighter galaxies. Therefore, if there is a correlation between galaxy properties and environment, this will introduce a correlation between galaxy properties and luminosity. Of course, the inverse also holds: a physical correlation between galaxy properties and luminosity will introduce an observable correlation between galaxy properties and environment. Clearly, when investigating the physical origin of the bimodality in the distribution of galaxies, it is crucial that one discriminates between environment dependence and luminosity dependence in a proper way (see Girardi et al. 2003 and Blanton et al. 2005b for statistical methods that address this issue).

2.2.1 A physically motivated split of environment

Within our current framework for galaxy formation, in which galaxies are thought to reside in extended dark matter haloes, it is useful to split the 'environment dependence' in three, physically separate, components. Going from small to large scales these are (i) the dependence on halo-centric radius, (ii) the dependence on halo mass, and (iii) the dependence on large-scale environment. In terms of the halo virial radius, $R_{\rm vir}$, these effects measure a dependence on scales $R < R_{\rm vir}$, $R \simeq R_{\rm vir}$, and $R > R_{\rm vir}$. Note that there is a clear, physical motivation for considering the virial radius as an important scale: matter at the virial radius has roughly experienced one dynamical time. In other words, a galaxy inside the virial radius of a given halo can not have been *dynamically* affected (at least not significantly) by any object that is located outside of this virial radius. Thus, if there is any galaxy type dependence on scales $R > R_{\rm vir}$ this must arise from either initial conditions, or from non-gravitational processes such as reionization (e.g., Efstathiou 1992) or preheating (e.g., Mo et al. 2005)[1]. On the other hand, most 'nurture' processes only introduce a (radial) dependence on scales $R < R_{\rm vir}$ Therefore, by investigating 'environment' dependence on scales larger and smaller than the virial radius one may hope to be able to determine which physical processes are most important for setting galaxy properties.

Unfortunately, the presence of a halo mass dependence may complicate the situation. Since the halo mass function is environment dependent, in that overdense regions contain on average more massive haloes than underdense regions (e.g., Lemson & Kauffmann 1999; Mo et al. 2004), a correlation between galaxy properties and halo mass will induce a correlation between galaxy properties and large scale environment. For example, Mo et al. (2004) have shown that the large-scale environment dependence of the galaxy luminosity function of early and late type galaxies, measured on scales of $8h^{-1}$ Mpc by Croton et al. (2005), can be entirely explained as a pure halo mass dependence. In addition, Balogh et al. (2004a), Blanton et al. (2006) and Kauffmann et al. (2004) have shown that various galaxy properties depend on environment, even when the latter is measured over scales of $\sim 5h^{-1}$ Mpc, much larger than the virial radius of the most massive clusters. However, when this large-scale environmental dependence is investigated *at a fixed small-scale environment*, it is no longer present (Blanton et al. 2006; Kauffmann et al. 2004, but see also Balogh et al. 2004a). Finally, Goto et al. (2003) have shown that the mor-

[1] An inferred environmental effect on scales $R \gtrsim R_{\rm vir}$ may also reflect a significant non-sphericity of the dark matter haloes that has not properly been accounted for.

phological fractions are constant at cluster-centric radii that exceed the virial radius. All these results suggest that the environment dependence does not extent beyond the virial radius. This is not only important because it suggests that processes such as reionization and/or preheating have not left a major imprint on galaxy properties, but also because it provides proof for an essential assumption in the halo model (see Cooray & Sheth 2002 and references therein).

A few studies in the past have investigated the correlation between galaxy properties and halo mass using group catalogues. In particular, Martínez et al. (2002) used a group catalogue constructed from the 100K data release of the 2dFGRS by Merchán & Zandivarez (2002) and found that the fraction of early types decreases *continuously* down to the lowest mass haloes probed ($M \sim 3\times10^{12}\,\mathrm{M}_\odot$). This was confirmed by Yang et al. (2005c), who used an independent group catalogue based on the completed 2dFGRS. Tanaka et al. (2004) applied the group-finding algorithm of Huchra & Geller (1982) to the first data release of the SDSS, and examined the median SFR and morphological fraction as function of the group velocity dispersion σ. Splitting the group members into bright and faint galaxies, they find that neither the SFR nor the morphological fraction shows any significant correlation with σ, neither for the bright nor for the faint galaxies. Balogh et al. (2004b) studied the fraction of red galaxies as function of the projected density, Σ_5, and cluster velocity dispersion. While they find a strong dependence on Σ_5, for a fixed luminosity they find no dependence on velocity dispersion over the range $300\,\mathrm{km\,s^{-1}} \lesssim \sigma \lesssim 900\,\mathrm{km\,s^{-1}}$, corresponding to $3\times10^{13}h^{-1}\,\mathrm{M}_\odot \lesssim M \lesssim 10^{15}h^{-1}\,\mathrm{M}_\odot$ (cf., De Propris et al 2004; Goto 2005). Although the comparison is far from straightforward, these findings of Tanaka et al. (2004) and Balogh et al. (2004b) seem difficult to reconcile with those of Martínez et al. (2002)and Yang et al (2005c). A more in-depth investigation, based on a large and well defined sample is required in order to shed some light on these issues, and to examine any possible halo mass dependence in more detail.

2.2.2 The purpose of this work

In this work we investigate the dependence of various galaxy properties, in particular colour, SFR, and concentration, on halo mass and halo-centric radius. To that extent we construct a SDSS group catalogue using the halo-based group finder of Yang et al. (2005a). This group finder has been well tested, and yields high completeness and a low fraction of interlopers. Halo masses are assigned based on the group luminosity, which, as we will show, yields more reliable mass estimates than the conventional velocity dispersion of the group members.

We use the resulting group catalogue to examine the fractions of various galaxy types as function of luminosity, halo mass, and halo-centric radius. Since haloes of different masses host galaxies of different luminosities (e.g., Yang, Mo & van den Bosch 2003; van den Bosch, Yang & Mo 2003), it is important to separate luminosity dependence from halo mass dependence. We address this by studying the halo mass dependence at fixed luminosity and vice versa.

This chapter is organized as follows. In Section 2.3, we describe the data and our classification of galaxy types based on both colour and SFR. In Section 2.4 we present our SDSS group catalogue, which we use in Section 2.5 to investigate the relation between galaxy properties and halo mass. The implications of our findings for the formation and evolution of galaxies is discussed in Section 2.6, while we summarize our results in

Section 2.7. There are two appendices at the end of this thesis which are related to this work: Appendix A gives a detailed description of our group finder and Appendix B presents a number of tests based on mock galaxy redshift surveys to illustrate the robustness of our results.

When required we adopt a standard ΛCDM cosmology with $\Omega_m = 0.3$ and $\Omega_\Lambda = 0.7$. Units that depend on the Hubble constant are expressed in terms of $h \equiv (H_0/100\mathrm{km\,s^{-1}\,Mpc^{-1}})$.

2.3 Classifying Galaxies based on colour and star formation rate

2.3.1 The data

The data used in this work is taken from the Sloan Digital Sky Survey (SDSS; York et al. 2000), a joint, five passband (u, g, r, i, z) imaging and medium-resolution ($R \sim 1800$) spectroscopic survey. In particular, we use the New York University Value-Added Galaxy Catalogue (NYU-VAGC), which is described in Blanton et al. (2005a). The NYU-VAGC is based on the SDSS Data Release 2 (Abazajian et al. 2004), but with an independent set of significantly improved reductions. From this catalogue we select all galaxies in the Main Galaxy Sample, i.e., galaxies with an extinction corrected apparent magnitude brighter than $r = 18$. We prune this sample to those galaxies in the redshift range $0.01 \leq z \leq 0.20$ and with a redshift completeness $c > 0.7$. This leaves a grand total of 184,425 galaxies with a sky coverage of ~ 1950 deg^2.

In addition to these data, we also use estimates of the stellar masses and the star formation rates (SFRs) obtained by Kauffmann et al. (2003) and Brinchmann et al. (2004), respectively. Stellar masses are obtained from the strength of the 4000Å break and the Balmer absorption-line index $\mathrm{H}\delta_A$ as described in Kauffmann et al. (2003), while the SFR is obtained using various emission lines in the SDSS spectra as described in Brinchmann et al. (2004). In this work we mainly use the specific star formation rate (hereafter SSFR), defined as the ratio of the SFR (in $\mathrm{M_\odot\ yr^{-1}}$) to the stellar mass (in $\mathrm{M_\odot}$). The SSFRs used are the average values of the full likelihood distributions obtained by Brinchmann et al. The NYU-VAGC and the stellar mass and SFR catalogues are all publicly available[2]. We have matched these catalogues yielding a (dust-corrected) stellar mass and current SFR (corrected for fiber aperture) for 179,197 of the 184,425 galaxies (~ 97 percent) in our sample.

Note that the fiber aperture corrections are based on the assumption that the SSFR *for given photometric colors* inside the fiber is the same as outside the fiber (see Brinchmann et al. 2004 for details). This, however, is likely to be an oversimplification, as color gradients may also reflect metallicity gradients (see discussion in Wilman et al. 2005). The resulting aperture correction errors will most strongly effect low redshift galaxies, which have a relatively large angular extent. To test the possible impact of inaccurate aperture corrections, we have repeated our full analysis excluding galaxies with $z < 0.05$. Except for a reduction of the dynamic range of luminosities that we can probe, we found virtually no change in the various type fractions analyzed here. This is also consistent with Wilman et al. (2005), who showed that inaccurate aperture corrections leave the

[2]The NYU-VAGC is available at http://wassup.physics.nyu.edu/vagc/#download, while the catalogues with stellar masses and SFRs can be downloaded from http://www.mpa-garching.mpg.de/SDSS/

type fractions largely intact.

Throughout this work we use the Petrosian magnitudes, corrected for Galactic extinction using the dust maps of Schlegel, Finkbeiner & Davis (1998). In order to minimize the errors due to uncertainties in the k-correction we follow Blanton et al. (2005a) and k-correct all magnitudes to a redshift of $z = 0.1$ using the Blanton et al. (2003c) model. We use the notation ${}^{0.1}M_r$ and ${}^{0.1}r$ to indicate the resulting absolute and apparent magnitudes in the r-band, respectively.

The spectroscopic survey of the SDSS suffers from a small incompleteness due to (i) fiber collisions (6 percent), (ii) spectra that did not allow for a useful determination of the redshift (< 1 percent), and (iii) galaxies that were too close to a bright star (Blanton et al. 2006). Of these, the fiber collision incompleteness is the most important one, especially because it creates an incompleteness which is correlated with the local number density of galaxies. Since in this work we are not interested in any absolute number densities, we have not attempted to correct the survey for these fiber collisions. Our main focus is on the *fractions* of various galaxy types *as a function of environment*. Since the galaxies missed because of fiber collisions are a purely random subset of the galaxies in the target field, their absence should have no impact on the type fractions discussed here.

2.3.2 Defining galaxy types

The main purpose of this work is to investigate how galaxy type correlates with halo mass. Roughly, the galaxy population consists of two types: 'early types', which have red colours, low specific star formation rates, and are morphologically reminiscent of ellipticals and S0s, and 'late types', which have blue colours, relatively high specific star formation rates, and are morphologically classified as spiral galaxies.

Unfortunately, whether a galaxy is termed 'early' or 'late' is fairly subjective, and many different approaches have been used in the past, including morphological quantifiers (e.g. Tran et al. 2001; Goto et al. 2003), star formation rate indicators (e.g., Lewis et al. 2002; Martínez et al. 2002; Domínguez et al. 2002; Balogh et al. 2004a; Tanaka et al. 2005) and broad-band colours (Strateva et al. 2001; Baldry et al. 2004; Balogh et al. 2004b; Goto et al. 2004). The 2dFGRS and the SDSS have clearly revealed that the distributions of many of these parameters are (to some extent) bimodal (e.g., Strateva et al. 2001; Madgwick et al. 2002; Blanton et al. 2003b). Although this makes the split more objective, the non-uniqueness of the various type-classifications creates some ambiguity. For example, a genuine, star-forming disk galaxy may appear red due to strong extinction (e.g., when seen edge-on), and thus be termed 'early type' based on its colour, while the SFR and morphology quantifiers would classify it as a 'late-type'.

To partially sidestep these difficulties we classify galaxies using *both* colour and specific star formation rate. The upper left-hand panel of Fig. 2.1 shows the colour-magnitude (CM) relation for a random subsample of 10 percent of all galaxies. The CM relation is clearly bimodal, revealing a narrow red sequence and a much broader blue sequence (see also Blanton et al. 2003b; Baldry et al. 2004; Hogg et al. 2004; Bell et al. 2004). The thick solid line corresponds to

$$ {}^{0.1}(g-r) = 0.7 - 0.032\left({}^{0.1}M_r - 5\log h + 16.5\right) \qquad (2.1) $$

with ${}^{0.1}M_r$ the absolute magnitude in the SDSS r-band, k-corrected to $z = 0.1$. We term galaxies that fall above this line 'red', and galaxies below this line as 'blue'.

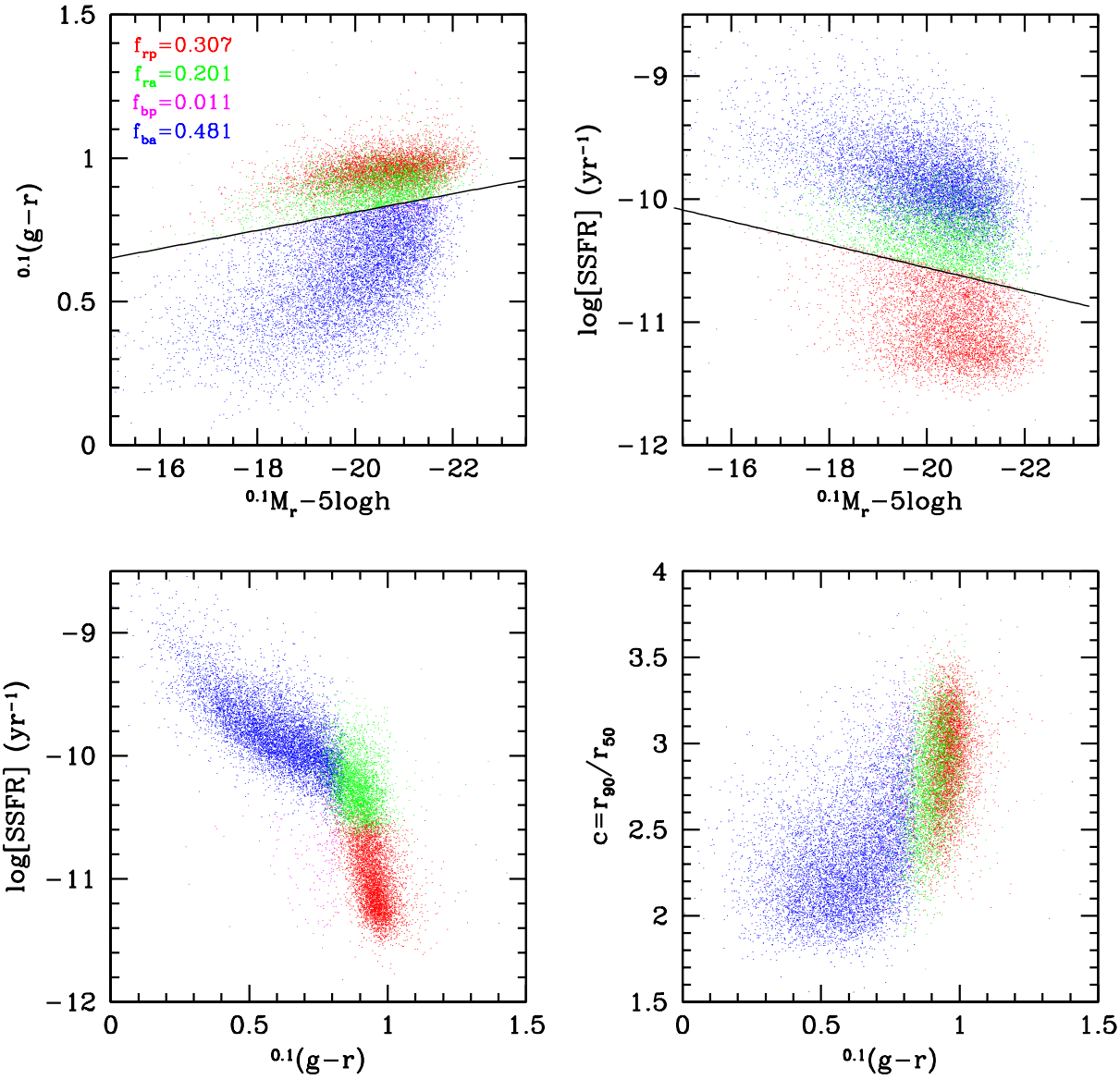

Figure 2.1: *The upper left-hand panel shows the colour-magnitude relation for the galaxies in our sample. The solid line corresponds to equation (2.1) and splits the galaxies into 'red' and 'blue' subsamples. The upper right-hand panel shows the SSFR-magnitude relation for the same galaxies. The solid lines corresponds to equation (2.2) and splits the galaxies into 'active and 'passive' subsamples. Galaxies are colour-coded according to these classifications: red dots (30.7 percent of the population; hereafter 'early'-types) are 'red' and 'passive', blue dots (48.1 percent of the population; hereafter 'late'-types) are 'blue' and 'active', green dots (20.1 percent of the population; hereafter 'intermediate'-types) are 'red' and 'active', and magenta dots are 'blue' and 'passive'. Since the latter only make up for 1.1 percent of all galaxies we do not consider them any further in this work. The lower left-hand panel plots the SSFR as function of colour. Note how the intermediate types are located at the cross-section of the early and late type branches. Finally, the lower right-hand panel plots the concentration of each galaxy, defined as the ratio of r_{90} to r_{50}, as function of colour. For clarity, only a random subsample of 10 percent of all galaxies is shown.*

The upper right-hand panel of Fig. 2.1 plots the SSFR as function of absolute magnitude. Similar to the CM relation, the distribution is clearly bimodal (see also Fig. 2.2). The thick solid line corresponds to

$$\log(\mathrm{SSFR}) = -10.0 + 0.094\left({}^{0.1}M_r - 5\log h + 15.0\right) \tag{2.2}$$

and roughly describes the magnitude dependence of the bimodality scale. Galaxies that fall above this line are termed 'active', and those below it 'passive'.

Galaxies that are 'red' and 'passive' are indicated by red dots in Fig. 2.1 and make up 30.7 percent of the entire population. In what follows we refer to these as early types. Galaxies that are 'blue' and 'active' are represented by blue dots, make up 48.1 percent of the population, and will hereafter be referred to as late-types. A fraction of 20.1 percent of all galaxies are 'red' and 'active'. These are represented by green dots and will hereafter be referred to as intermediate types. The final class of galaxies, those that are both 'blue' and 'passive', only make up 1.1 percent of all galaxies (magenta dots in Fig. 2.1). Thus, although our classification allows for four classes, in practice, 98.9 percent of all galaxies belong to only three of these. This suggests that galaxies occupy only a restricted subspace of the colour-SSFR parameter space. Indeed, as shown in the lower left-hand panel of Fig. 2.1, galaxies follow a roughly one-dimensional distribution in this plane. Most importantly, the different types are clearly separated, with the intermediate types occupying the region in between the early and late types (hence our choice for their nomenclature). The clarity with which the various galaxy types separate out in this colour-SSFR sequence gives a strong, physical motivation for our classification scheme. Note that the intermediate types seem to occupy the region where the late and early type branches overlap. This suggests that they consist of a mix of early and late types, rather than constitute a physically separate class.

Most of the 'blue' and 'passive' galaxies (magenta points) fall off the colour-SSFR sequence: they are clearly not part of the major population of galaxies. Because of this, and since they only make up a negligible fraction of the total population, we no longer consider them in this work.

The lower right-hand panel of Fig. 2.1 plots the concentration parameter $c \equiv r_{90}/r_{50}$ as function of colour. Here r_{90} and r_{50} are the radii that contain 90 and 50 percent of the Petrosian r-band flux, respectively. As expected, early types are, on average, more centrally concentrated than late types. Note also that the intermediate types cover the full range of concentrations expected given their colour. In other words, they are not predominantly low or high concentration systems.

Figure 2.2 shows histograms of the distributions of absolute magnitude, ${}^{0.1}(g-r)$-colour, log(SSFR), and c. The dashed, dotted and dot-dashed curves show the contributions due to late, early, and intermediate types, respectively. Note that no correction has been applied for Malmquist bias (i.e., no $1/V_{\rm max}$ weighting has been applied), so that the distributions shown do not reflect true number density distributions: they merely serve as an illustration. Note how the early and late types are clearly separated in terms of colour and SSFR (by construction), and that the intermediate types have distributions that are truly intermediate to those of the early and late types. The c-distributions of early and late types are clearly skewed towards the opposite extremes, but still show a large range of overlap. Although the intermediate types have a c-distribution that is more reminiscent of that of the early types, they have the same c-distribution as late-type galaxies of the same colour (cf., lower right-hand panel of Fig. 2.1)

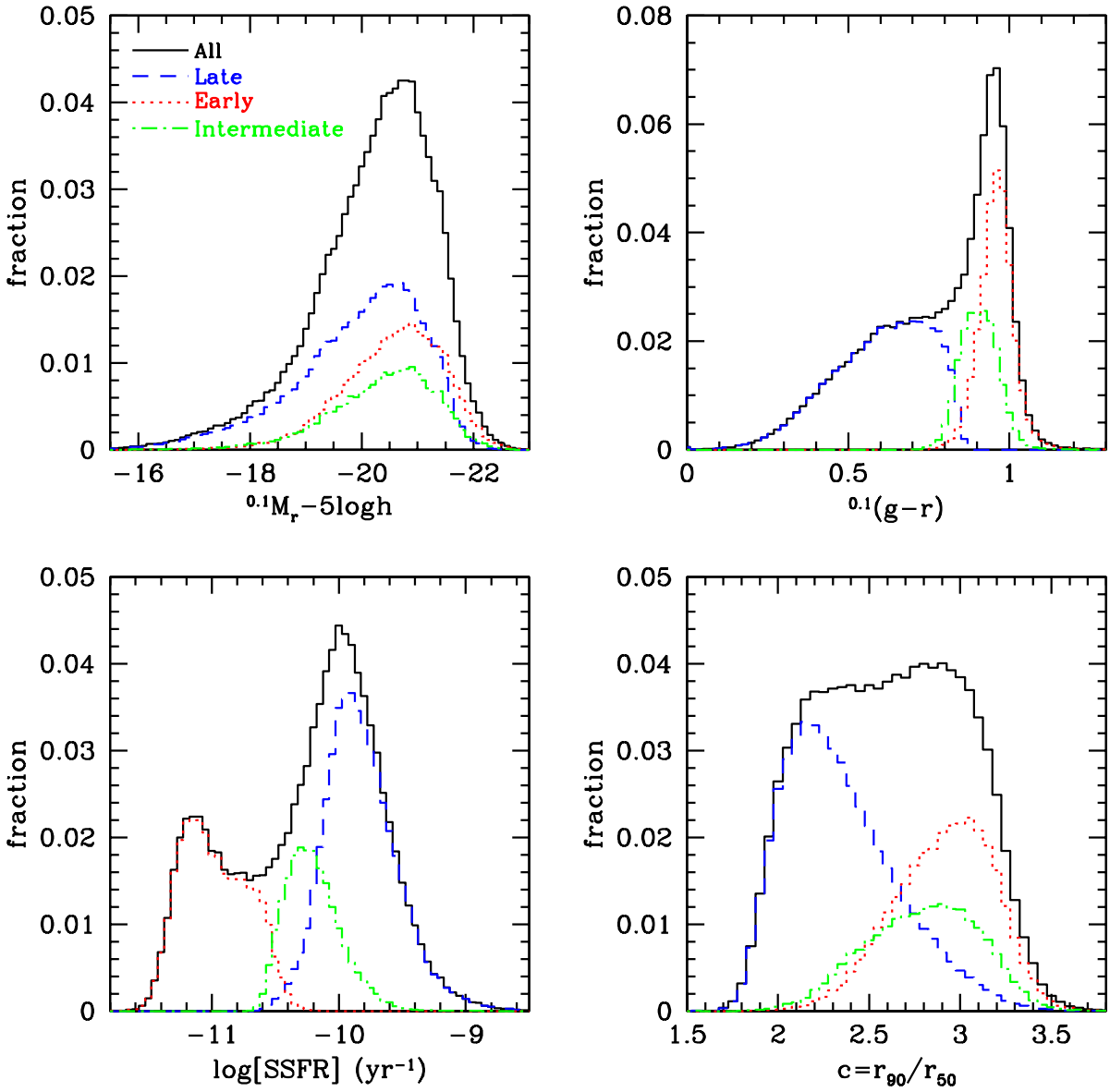

Figure 2.2: *Histograms of the distribution of galaxies as function of absolute r-band magnitude (upper-left panel), $g-r$-colour (upper-right panel), specific star formation rate (lower-left panel), and concentration (lower-right panel). In addition to the distributions for the full sample of galaxies (black, solid lines), we also show the distributions for late types (blue, dashed lines), early types (red, dotted lines), and intermediate types (green, dot-dashed lines). Note that the intermediate types have colours and SSFRs that are intermediate to those of early- and late types, but have luminosities and concentrations that are reminiscent to those of the early types.*

Our class of early types thus consists of red galaxies with a passive SFR and a high concentration, consistent with a typical elliptical. Our class of late types consists of galaxies that are blue, are actively forming stars, and have low concentrations, all consistent with a typical spiral galaxy. The nature of our intermediate types, however, is less clear. They are defined as galaxies that are 'red', yet 'active'. Therefore, it is tempting to interpret them as dusty, star forming galaxies. One possibility is that they are, to a large extent, made up of edge-on disk galaxies where the orientation causes an enhanced extinction. On the other hand, Brinchmann et al. (2004) have stated that due to degeneracies between age, metallicity and dust, the SFR cannot be constrained better than to a factor of 10 at colours redder than ${}^{0.1}(g-r) = 0.7$. Therefore, the intermediate types may also consist of early type galaxies for which the SSFR has been overestimated. Most likely, our class of intermediate types contains examples of both. Indeed, as we will show below, their halo occupation statistics strongly suggest that they consist of a mix of both early and late types.

2.4 The SDSS Group Catalogue

2.4.1 The group finding algorithm

In order to study the relation between galaxy types and halo mass, we construct a group catalogue from the SDSS data described in Section 2.3.1, using all galaxies in our sample, including those for which no stellar mass or SSFR is available.

Our working definition of a galaxy group is the ensemble of galaxies that reside in the same dark matter parent halo; galaxies that reside in subhaloes are considered to be group members that belong to the parent halo in which the subhalo is located. The properties of the halo population in the standard ΛCDM model are well understood, largely due to a combination of N-body simulations and analytical models. Recently, Yang et al. (2005a, hereafter YMBJ) used this knowledge to develop a new group-finding algorithm that is optimized to group galaxies according to their common dark matter halo, and which has been thoroughly tested with mock galaxy redshift surveys. In brief, the method works as follows. First potential group centers are identified using a Friends-Of-Friends (FOF) algorithm or an isolation criterion. Next, the total group luminosity is estimated which is converted into an estimate for the group mass using an assumed mass-to-light ratio. From this mass estimate, the radius and velocity dispersion of the corresponding dark matter halo are estimated using the virial equations, which in turn are used to select group members in redshift space. This method is iterated until group memberships converge. A more detailed description is given in Appendix A. The basic idea behind this group finder is similar to that of the matched filter algorithm developed by Postman et al. (1996) (see also Kepner et al. 1999; White & Kochanek 2002; Kim et al. 2002; Kochanek et al. 2003; van den Bosch et al. 2004, 2005a), although it also makes use of the galaxy kinematics.

In YMBJ the performance of this group finder has been tested in terms of completeness of true members and contamination by interlopers, using detailed mock galaxy redshift surveys. The average completeness of individual groups is ~ 90 percent and with only ~ 20 percent interlopers. Furthermore, the resulting group catalogue is insensitive to the initial assumption regarding the mass-to-light ratios, and the group finder is more successful than the conventional FOF method (e.g., Huchra & Geller 1982; Ramella, Geller & Huchra 1989; Merchán & Zandivarez 2002; Eke et al. 2004a) in associating galaxies according to their

common dark matter haloes.

Thus far this group finder has been applied to the 2dFGRS (Yang et al. 2005a) and used to study the two-point correlation function of groups (Yang et al. 2005b), the galaxy occupation statistics of dark matter haloes (Yang et al. 2005c), the phase-space parameters of brightest halo galaxies (van den Bosch et al. 2005b), and the cross-correlation between galaxies and groups (Yang et al. 2005d). In this work we apply it to the SDSS. The resulting group catalogue is used to investigate the relation between various galaxy properties and halo mass.

2.4.2 Estimating group masses

In order to infer halo occupation statistics from our group samples it is crucial that we can estimate the halo masses associated with our groups. For individual, rich clusters one could in principle estimate halo masses using the kinematics of the member galaxies, gravitational lensing of background sources, or the temperature profile of the X-ray emitting gas. For most groups, however, no X-ray emission has been detected, and no lensing data is available. In addition, the vast majority of the groups in our sample contain only a few members, making a dynamical mass estimate based on its members extremely unreliable (see Appendix B). We thus need to adopt a different approach to estimate halo masses. Following YMBJ we use the group luminosity to assign masses to our groups. The motivation behind this is that one naturally expects the group luminosity to be strongly correlated with halo mass (albeit with a certain amount of scatter). Since the group luminosity is dominated by the brightest members, which are exactly the ones that can be observed in a flux limited survey like the SDSS, the determination of the (total) group luminosity is far more robust than that of the group's velocity dispersion when the number of group members is small.

Clearly, because of the flux limit of the SDSS, two identical groups observed at different redshifts will have a different $L_{\rm group}$, defined as the summed luminosity of all its identified members. To circumvent this bias we first need to bring the group luminosities to a common scale. One possibility is to use the *total* group luminosity, $L_{\rm total}$, which one might define according to

$$L_{\rm total} = L_{\rm group} \frac{\int_0^\infty \Phi(L)\, L\, dL}{\int_{L_{\rm lim}}^\infty \Phi(L)\, L\, dL}\,. \tag{2.3}$$

Here $L_{\rm lim}$ is the minimum luminosity of a galaxy that can be observed at the redshift of the group, and $\Phi(L)$ is the galaxy luminosity function in the $^{0.1}r$-band. Although this approach has been used by many earlier analyzes (e.g., Tucker 2000; Merchán & Zandivarez 2002; Kochanek et al. 2003; Eke et al. 2004b), it is based on the assumption that the galaxy luminosity function in groups is the same as that of field galaxies, independent of the mass of the group. It has been shown, however, that the galaxy luminosity function depends on both halo mass and environment (Yang et al. 2003, 2005c; Mo et al. 2004; Zheng et al. 2005; Croton et al. 2005; Cooray & Milosavljević 2005). Therefore we follow YMBJ and use a more empirical approach. A nearby group selected in an apparent magnitude limited survey should contain all of its members down to a faint luminosity. We can therefore use these nearby groups to determine the relation between the group luminosity obtained using only galaxies above a bright luminosity limit and that obtained using galaxies above a fainter luminosity limit. Assuming that this relation is redshift-independent, one can

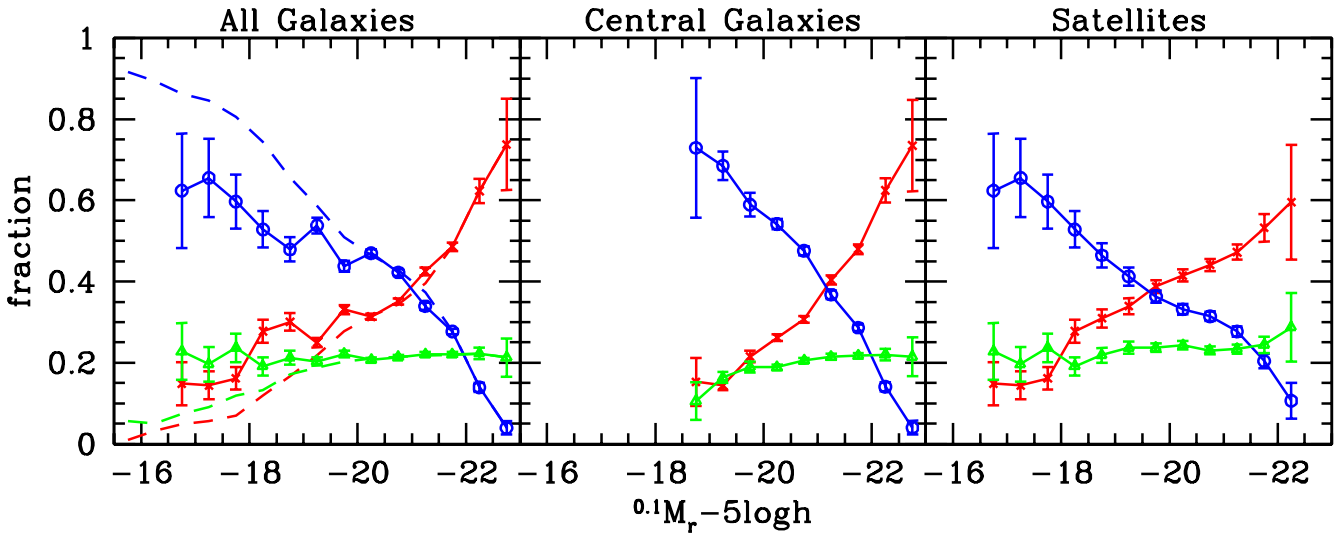

Figure 2.3: *The fraction of late types (open circles with blue lines), early types (crosses with red lines) and intermediate types (open triangles with green lines) as function of absolute magnitude (in r-band, k-corrected to $z = 0.1$). Results are shown for all galaxies in groups (left-hand panel), the central (brightest) group galaxies (middle panel), and satellite galaxies (right-hand panel). In addition, the dashed lines in the left-hand panel show the type fractions for all galaxies, including those not assigned to a group. Errorbars indicate Poisson errors. The fraction of late (early) types decreases (increases) strongly with increasing luminosity. Note that the luminosity dependence is significantly stronger for central galaxies than for satellite galaxies. See text for a detailed discussion.*

correct the luminosity of a high-z group, where only the brightest members are observed, to an empirically normalized luminosity scale.

As common luminosity scale we use $L_{19.5}$, defined as the luminosity of all group members brighter than ${}^{0.1}M_r = -19.5 + 5\log h$. To calibrate the relation between $L_{\rm group}$ and $L_{19.5}$ we first select all groups with $z \leq 0.09$, which corresponds to the redshift for which a galaxy with ${}^{0.1}M_r = -19.5 + 5\log h$ has an apparent magnitude that is equal to the magnitude limit of the survey. For groups with $z > 0.09$ we use this 'local' calibration between $L_{\rm group}$ and $L_{19.5}$ to estimate the latter. $L_{19.5}/L_{\rm group}$ as a function $L_{\rm group}$ for galaxies with $z \leq 0.09$ is shown in Fig. 6.1 in Appendix A. Detailed tests (see YMBJ) have shown that the group luminosities obtained with this method are significantly more reliable than $L_{\rm total}$.

The final step is to obtain an estimate of the group (halo) mass from $L_{19.5}$. This is done using the assumption that there is a one-to-one relation between $L_{19.5}$ and halo mass. For each group we determine the number density of all groups brighter (in terms of $L_{19.5}$) than the group in consideration. Using the halo mass function corresponding to a ΛCDM concordance cosmology with $\Omega_m = 0.3$, $\Omega_\Lambda = 0.7$, $h = H_0/(100\,{\rm km\,s^{-1}\,Mpc^{-1}}) = 0.7$ and $\sigma_8 = 0.9$ we then find the mass for which the more massive haloes have the same number density. Although this has the downside that it depends on cosmology, it is straightforward to convert the masses derived here to any other cosmology. An obvious shortcoming of this method is that the true relation between $L_{19.5}$ and M contains some scatter. This scatter will result in errors in the inferred halo mass. However, as long as the scatter is sufficiently small, which we believe to be the case, given, for example, the small observed scatter in the Tully-Fisher relation, this method of assigning group masses is expected to be significantly more accurate than using the velocity dispersion of group members. In Appendix B we use detailed mock galaxy redshift surveys to demonstrate that this is indeed the case (see also YMBJ and Yang et al. 2005c).

Finally we note that not all groups can have a halo mass assigned to them. First of all, the mass estimator described above does not work for groups in which all members are fainter than ${}^{0.1}M_r = -19.5 + 5\log h$. Secondly, the combination of $L_{19.5}$ and redshift may be such that we know that the halo catalogue is incomplete, which means that there is a significant number of groups at this redshift with the same $L_{19.5}$ but for which the individual galaxies are too faint to be detected (see Fig. 6.2 in Appendix A). Since our mass assignment is based on the assumption of completeness, any group beyond the completeness redshift corresponding to its $L_{19.5}$ is not assigned a halo mass (see Yang et al. 2005a for details).

2.4.3 The SDSS group catalogue

Applying our group finder to the sample of SDSS galaxies described in Section 2.3.1 yields a group catalogue of 53,229 systems with an estimated mass. These groups contain a total of 92,315 galaxies. The majority of the groups (37,216 systems) contain only a single member, while there are 9220 binary systems, 3073 triplet systems, and 3720 systems with four members or more. In what follows we refer to the brightest galaxy in each group as the 'central' galaxy, while all others are termed 'satellites'.

This SDSS group catalogue is publicly available at http://www.astro.umass.edu/~xhyang/Group.html [3]. For each group-member the catalogue contains magnitudes in the five SDSS bands (u,

[3]This website also contains our 2dFGRS group catalogue as well as detailed mock galaxy redshift surveys

g, r, i, z), Petrosian radii, a velocity dispersion, and, for 89,232 galaxies (~ 97 percent of all group members) the stellar mass and present day SFR. In addition to group memberships, the catalogue also contains estimates of the group's characteristic luminosity, $L_{19.5}$, and its mass (derived using the method described above).

2.5 Results

Using the SDSS group catalogue described above, and the definition of galaxy types discussed in Section 2.3.2, we now investigate the ecology of galaxies.

2.5.1 Dependence on Luminosity

We start our investigation by computing how galaxy type depends on luminosity. The left-hand panel of Fig. 2.3 plots the various type fractions as function of the absolute magnitude in the $^{0.1}r$-band. For each luminosity bin, we only consider galaxies with $0.01 \leq z \leq z_{\rm max}$, where $z_{\rm max}$ is the redshift out to which a galaxy at the faint end of the luminosity bin has an apparent magnitude that is equal to the flux limit of the SDSS ($r = 17.77$). In other words, each magnitude bin is a volume limited sample. The points connected by the solid lines indicate the fractions of all galaxies that are member of a group with an assigned mass. Results are only shown for luminosity bins that contain at least 50 galaxies in total and errorbars are calculated using Poisson statistics.

As is well known, the late (early) type fraction decreases (increases) strongly with increasing luminosity (e.g., Baldry et al. 2004; Balogh et al. 2004b; Kelm et al. 2005). The fraction of intermediate type systems, however, is remarkably constant at ~ 20 percent, virtually independent of luminosity.

The dashed lines indicate the type fractions when *all* galaxies are considered, including those that have not been assigned to a group. Note that these fractions differ substantially from those of the group members at the faint end. This is a first indication for a mass dependence of the type fractions; since our group catalogue is incomplete at the low mass end, because its members are too faint for a mass estimate (see Section 2.4.2), the faint galaxies that do make it into the group catalogue are mainly satellite galaxies in more massive haloes. The results shown here suggest that these have a lower late type fraction than galaxies of the same magnitude but which reside in less massive haloes.

The middle and right-hand panels of Fig. 2.3 plot the type fractions for central and satellite galaxies, respectively (again using only galaxies in groups with an assigned halo mass). This shows that the luminosity dependence of the type fractions is stronger for central galaxies than for satellite galaxies. A similar trend was previously noted by Yang et al. (2005c) from an analysis of the 2dFGRS group catalogue. Note that the fraction of intermediate types is, within the errors, equally large among central and satellite galaxies, independent of luminosity.

Although we have stellar masses available, we have chosen to split our sample according to luminosity and not according to stellar mass. The reason is that the former are more accurate than the latter, and that it is straightforward to construct volume limited samples based on luminosities. If one wants to construct volume limited, stellar-mass selected samples, however, one needs to compute the redshift out to which a system of given stellar mass can be detected for the maximum possible stellar mass-to-light ratio (i.e., for a single burst stellar population with an age of ~ 13Gyr). We have performed some tests along

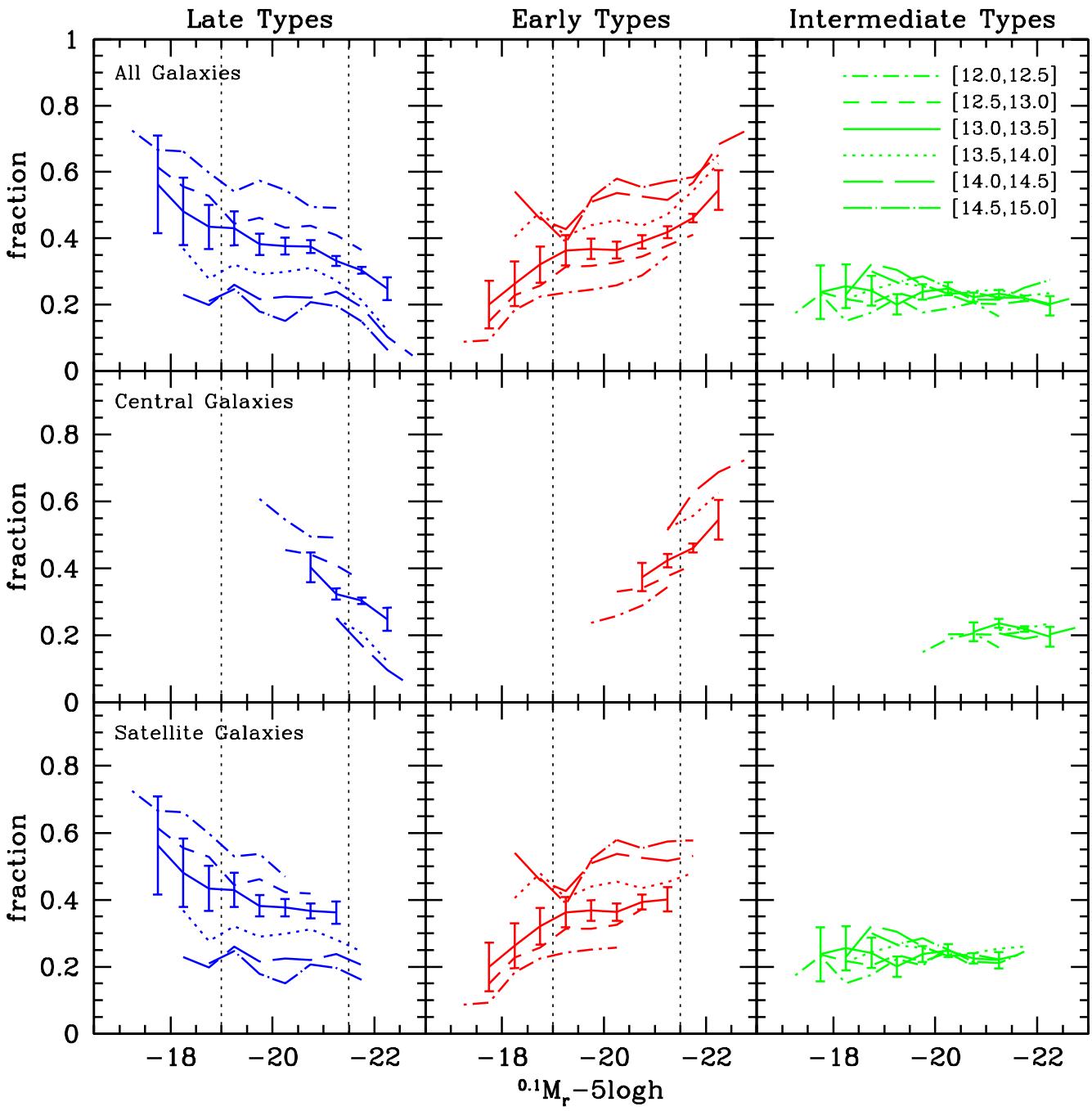

Figure 2.4: *The fractions of late types (left-hand panels), early types (middle panels) and intermediate types (right-hand panels) as function of their absolute magnitude. Results are shown for all galaxies (upper panels), central galaxies (middle row of panels) and satellite galaxies (lower panels), and for 6 different mass bins as indicated (the values in square brackets indicate the range of* $\log(M/h^{-1}\,\mathrm{M}_\odot)$*). Results are only shown for mass-luminosity bins that contain at least 50 galaxies in total, and for clarity (Poissonian) errorbars are only shown for one mass bin. Note that the fraction of early and late types at fixed luminosity is strongly mass-dependent, while luminosity dependence at fixed mass is only evident at the bright and faint ends. In the intermediate range* $-19 \geq^{0.1} M_r - 5\log h \geq -21$ *(indicated by dotted, vertical lines), the luminosity dependence is surprisingly weak, for all halo masses. Note that the fraction of intermediate types is completely independent of both luminosity and halo mass, and does not depend on whether the galaxy is a central galaxy or a satellite.*

this direction, but found that this results in a very significant reduction of the sample size. Since we prefer to have good statistics (which is required when splitting the sample in mass, luminosity, type, and sometimes even radius), we analyze the results as function of luminosity. A similar analysis as function of stellar mass will have to await a larger SDSS sample.

2.5.2 Dependence on Halo Mass

We now investigate how galaxy type depends on halo mass. We start by splitting the group sample in six logarithmic mass bins and determine how their type fractions depend on luminosity. For each bin in mass and luminosity the late type fraction is defined as the total number of late type galaxies in that bin, divided by the total number of galaxies in that bin (i.e., we do not average the late type fraction over individual haloes). The same applies to the early and intermediate types.

The results are shown in the upper panels of Fig. 2.4. In each mass bin the late (early) type fraction decreases (increases) with increasing luminosity, similar as for the entire sample (cf. Fig. 2.3). Note, however, that in the range $-19 \gtrsim {}^{0.1}M_r - 5\log h \gtrsim -21.5$ (indicated by vertical, dotted lines), the luminosity dependence is remarkably weak, for all 6 mass bins. For comparison, an L^* galaxy has ${}^{0.1}M_r - 5\log h = -20.44$ (Blanton et al. 2003a), so that this magnitude range corresponds roughly to $0.25 \lesssim L/L^* \lesssim 2.5$. In Yang et al. (2005c) we found a similar result from an analysis of the early and late type fractions in 2dFGRS groups, despite a different definition of early and late types and the use of luminosities in the b_J-band, rather than the r-band.

At fixed luminosity, the late and early type fractions depend strongly on halo mass: the late type fraction decreases and the early type fraction increases with increasing halo mass. Over the mass range $10^{12}h^{-1}\mathrm{M}_\odot \lesssim M \lesssim 10^{15}h^{-1}\mathrm{M}_\odot$ both fractions change by 30 to 40 percent, at all luminosities. This is a reflection of the well known morphology-density relation (e.g., Dressler 1980; Postman & Geller 1984; Whitmore 1995; Domínguez, Muriel & Lambas 2001; Goto et al. 2003; Tanaka et al. 2004), but now expressed in terms of halo mass rather than galaxy number density.

Panels in the middle and lower row show the same results separately for central and satellite galaxies. As expected, central galaxies mainly occupy the bright end of the distribution. In the, unfortunately small, magnitude range where satellites and central galaxies overlap, there is a weak indication that the early and late type fractions of central galaxies increase and decrease with luminosity, respectively, while those of the satellite galaxies are consistent with no luminosity dependence. However, given the (Poissonian) errors we can not rule out that central and satellite galaxies follow the same trend; a larger data set is required to investigate this in more detail.

The right-hand panels of Fig. 2.4 show that the intermediate type fractions are once again remarkably constant at ~ 20 percent; there is no significant dependence on either luminosity or halo mass, nor does it depend on whether the galaxy is a central galaxy or a satellite galaxy. The implications of this for the nature of intermediate type galaxies are discussed in Section 2.6.3.

Fig. 2.5 shows these results in a complementary way. It shows the type fractions as function of halo mass for five different magnitude bins. For each magnitude bin we only include groups that fall entirely within the volume limit, i.e., for which *all* members have $0.01 \leq z \leq z_{\rm max}$. Whereas the intermediate type fraction, once again, shows no significant

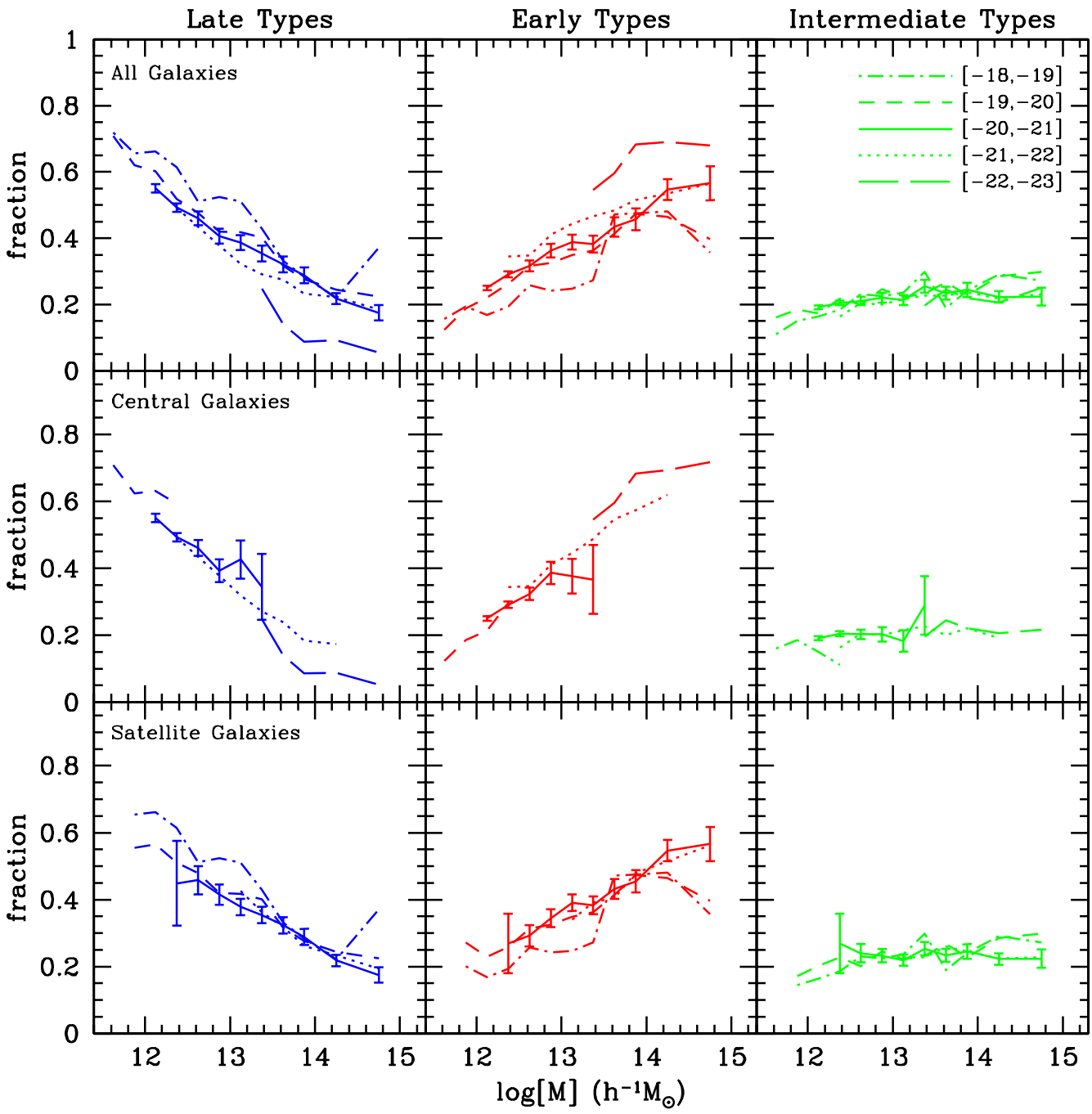

Figure 2.5: *Same as Fig. 2.4, except that this time we plot the type fractions as function of halo mass for five luminosity bins. The values is square brackets in the upper right-hand panel indicate the range of* $^{0.1}M_r - 5\log h$ *used. Note the strong, and smooth halo mass dependence of the early and late type fractions. In particular, there is no indication for any characteristic mass scale. Except for the faintest and brightest luminosity bins, the fractions of early and late type galaxies at fixed halo mass are surprisingly independent of luminosity. Note that there is a weak indication that the mass dependence for central galaxies is stronger than for satellite galaxies. As in Fig. 2.4, the intermediate type fraction is completely independent of luminosity and halo mass, and is the same for central and satellite galaxies. See text for a detailed discussion.*

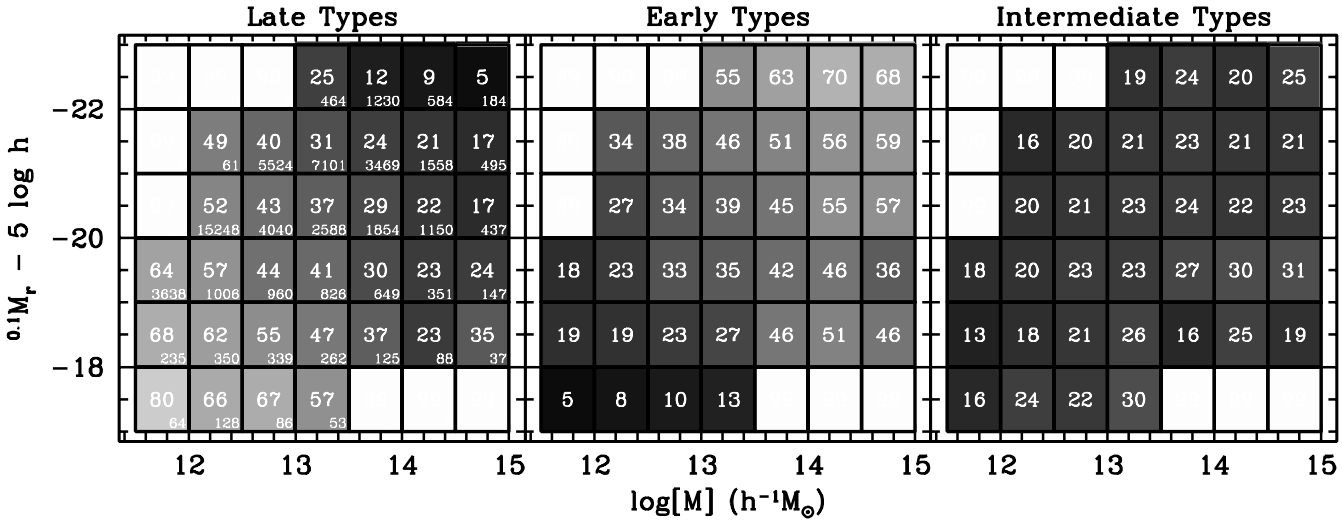

Figure 2.6: *Galaxy type as a function of halo mass and luminosity for the galaxies in our group catalogue. The number in the center of each cell indicates the percentage of late type galaxies (left panel), early type galaxies (middle panel), and intermediate-type galaxies (right panel). Each cell is colour-coded according to this percentage, running from black (0 percent) to white (100 percent). The number in the lower-right corner of each cell in the left-hand panel indicates the total number of galaxies in the corresponding mass-luminosity bin. Only cells with more than 50 galaxies in total are shown.*

mass or luminosity dependence, the early and late type fractions are strongly mass dependent. Most importantly, we find the mass dependence to be remarkably smooth, with no indication at all for any characteristic mass scale.[4]

At fixed halo mass, the luminosity dependence is surprisingly weak, especially over the magnitude range $-19 \gtrsim {}^{0.1}M_r - 5\log h \gtrsim -22$. The early and late type fractions only reveal some luminosity dependence at the very bright and the very faint end of the distribution (cf. Fig. 2.4).

Panels in the middle and lower row of Fig. 2.5 show the various type fractions as function of halo mass for central and satellite galaxies, respectively. There is a weak hint that the mass dependence is stronger for central galaxies (just like their luminosity dependence is stronger, see Fig. 2.3). A confirmation of this trend, however, has to await a larger sample of (SDSS) data.

Note that the functional form of the mass dependence at fixed luminosity is very similar for all magnitude bins considered. Similarly, the functional form of the luminosity dependence at fixed halo mass is very similar for all mass bins. This suggests a simple, separable form for the early and late type fractions as function of luminosity and mass, i.e., $f_{\rm late}(L, M) = g(L)h(M)$, with $g(x)$ and $h(x)$ two (monotonic) functions. Such a separable form was adopted by van den Bosch et al. (2003) and Cooray (2005) in their studies of the conditional luminosity functions of early and late type galaxies in the 2dFGRS. The results presented here provide support for these functional forms, albeit in retrospect.

[4]The only apparent exception occurs for the brightest sample with $-22 \geq {}^{0.1}M_r - 5\log h > -23$, where the late and early type fractions seem to reveal a break at around $10^{14}h^{-1}\,{\rm M}_\odot$. However, an investigation of the Poissonian errorbars (not shown) suggests that this break is not significant.

Finally, for completeness, Fig. 2.6 shows the same results once more, but now in a two-dimensional representation. The grayscale represents the fraction of late, early, and intermediate type galaxies in each mass-luminosity bin. The reader can read off these percentages (big, white number in the center of each cell), as well as the total number of galaxies in each bin (small, white number in lower right corner of each cell).

Our finding that the late type fraction decreases with increasing halo mass is in agreement with previous results from Martínez et al. (2002) and Yang et al. (2005c). On the other hand, Tanaka et al. (2004), de Propris et al. (2004) and Balogh et al. (2004b) find *no* significant dependence of the late or early type fraction on the velocity dispersion of massive groups and clusters. There are two reasons for this apparent discrepancy. First of all, our sample is significantly larger than that of previous studies. This not only results in significantly smaller errorbars, but also allows us to consider a much larger dynamic range in halo masses. Secondly, as we show in Appendix B, using the velocity dispersion as a mass estimator naturally tends to smear out the mass dependence. This is also illustrated in Fig. 2.7, were we plot the early-type fraction of galaxies with $-20 \geq {}^{0.1}M_r - 5\log h > -22$ (using a volume limited sample) as function of the group velocity dispersion. The solid lines use our mass estimator (based on group luminosity), converted to velocity dispersion using equation (A5). Dashed lines use a binning based on the actual velocity dispersion of the member galaxies. Only groups with 6 members or more are included, although the results look similar when using all groups with 3 members or more. Note that over the range $350\,\mathrm{km\,s^{-1}} \lesssim \sigma \lesssim 850\,\mathrm{km\,s^{-1}}$, which is the range used in Balogh et al. (2004a), the early-type fraction is basically flat when using the velocity dispersion of the member galaxies. This explains the discrepancy between the results presented here and those in the previous studies listed above.

Finally, there have been a number of recent studies that used the clustering properties of early and late type galaxies to constrain the type fractions as function of halo mass. Magliocchetti & Porciani (2003), van den Bosch et al. (2003), and Collister & Lahav (2005) all used the two-point correlation functions of early and late type galaxies in the 2dFGRS to infer that the late type fraction has to decrease smoothly with halo mass, in good, qualitative agreement with the results presented here. See also Cooray (2005) for a somewhat different analysis, but with the same result. An exception to this behavior was found by Zehavi et al. (2005), who inferred a late type fraction from the correlation functions extracted from the SDSS DR2 that decreases with halo mass down to a minimum at $10^{13.5}\,\mathrm{M}_\odot$, followed by a subsequent increase. Unfortunately, as demonstrated in van den Bosch et al. (2003), the uncertainties on the type fractions as inferred solely from the clustering data are fairly large, so that we do not consider the results of Zehavi et al. (2005) to be in serious conflict with those presented here.

2.5.3 Dependence on Halo-centric Radius

Thus far we have focussed on the luminosity and mass dependence of galaxy type fractions. Here we address the dependence on halo-centric radius, i.e., we explore the environment dependence on scales $R < R_{\rm vir}$. In order to be able to discriminate type segregation from luminosity segregation we investigate the radial dependence for four magnitude bins. As above, for each magnitude bin we construct a volume limited sample, in which we only include haloes that fall entirely within this volume. For each galaxy we compute the projected distance, R, to the (luminosity weighted) group center, at the (luminosity

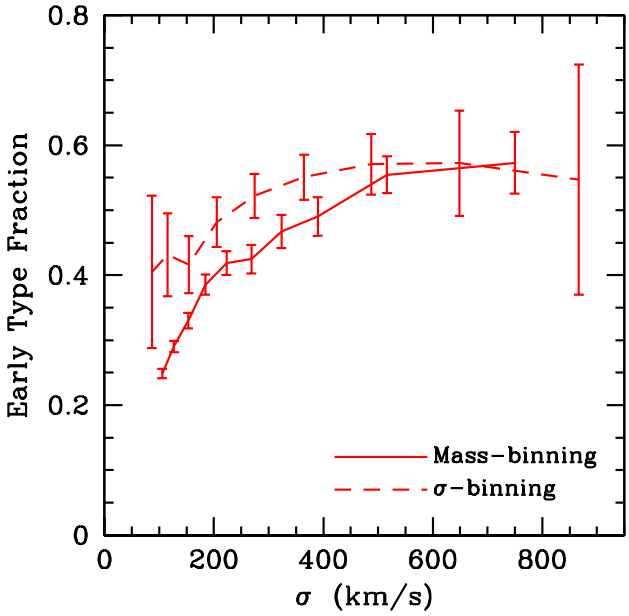

Figure 2.7: *The early-type fraction as function of group velocity dispersion for galaxies with* $-20 \geq {}^{0.1}M_r - 5\log h > -22$. *Solid lines use our mass estimator (based on group luminosity) converted to velocity dispersion using equation (A5). Dashed lines use a binning based on the actual velocity dispersion of the member galaxies. Note that the latter predicts a significantly weaker mass dependence than the former.*

weighted) redshift of the group. In order to allow groups of different masses to be stacked together, we normalize these radii to the group's virial radius $R_{\rm vir}$.[5] Results are shown in Fig. 2.8 for groups in three separate mass ranges. Since central galaxies are special, we have excluded them from our analysis, so that Fig. 2.8 only reflects the type fractions of satellites.

In agreement with previous studies (e.g., Postman & Geller 1984; Biviano et al. 2002; Domínguez et al. 2002; Girardi et al. 2003; Gómez et al. 2003; Goto et al. 2003; Goto et al. 2004) we find that the late type fractions increase towards the outskirts of the groups. Since this trend is virtually identical for all four magnitude bins, it is not a reflection of luminosity segregation (see also Girardi et al. 2003).

Note that at given halo mass and halo-centric radius the type fractions do not depend on luminosity. The only exception is the mass bin $10^{12}h^{-1}\,{\rm M}_\odot < M \leq 10^{13}h^{-1}\,{\rm M}_\odot$, where the faintest galaxies seem to have a slightly larger fraction of late-types than the brighter galaxies at the same halo-centric radius. However, given the Poissonian errors, this difference is only marginally significant. Having established that there is no significant luminosity dependence at fixed halo mass and radius, we now increase the signal to noise by computing the type fractions over the entire magnitude range from $-23 \leq {}^{0.1}M_r - 5\log h \leq -18$ and over the entire redshift range $0.01 \leq z \leq 0.20$. Note that this is not a volume limited sample. However, since we have shown that there is no significant luminosity dependence, Malmquist bias should not affect these results. We have verified that using a

[5]Virial radii are computed from our group masses, which we convert to virial masses using the relation between halo mass and concentration in Bullock et al. (2001).

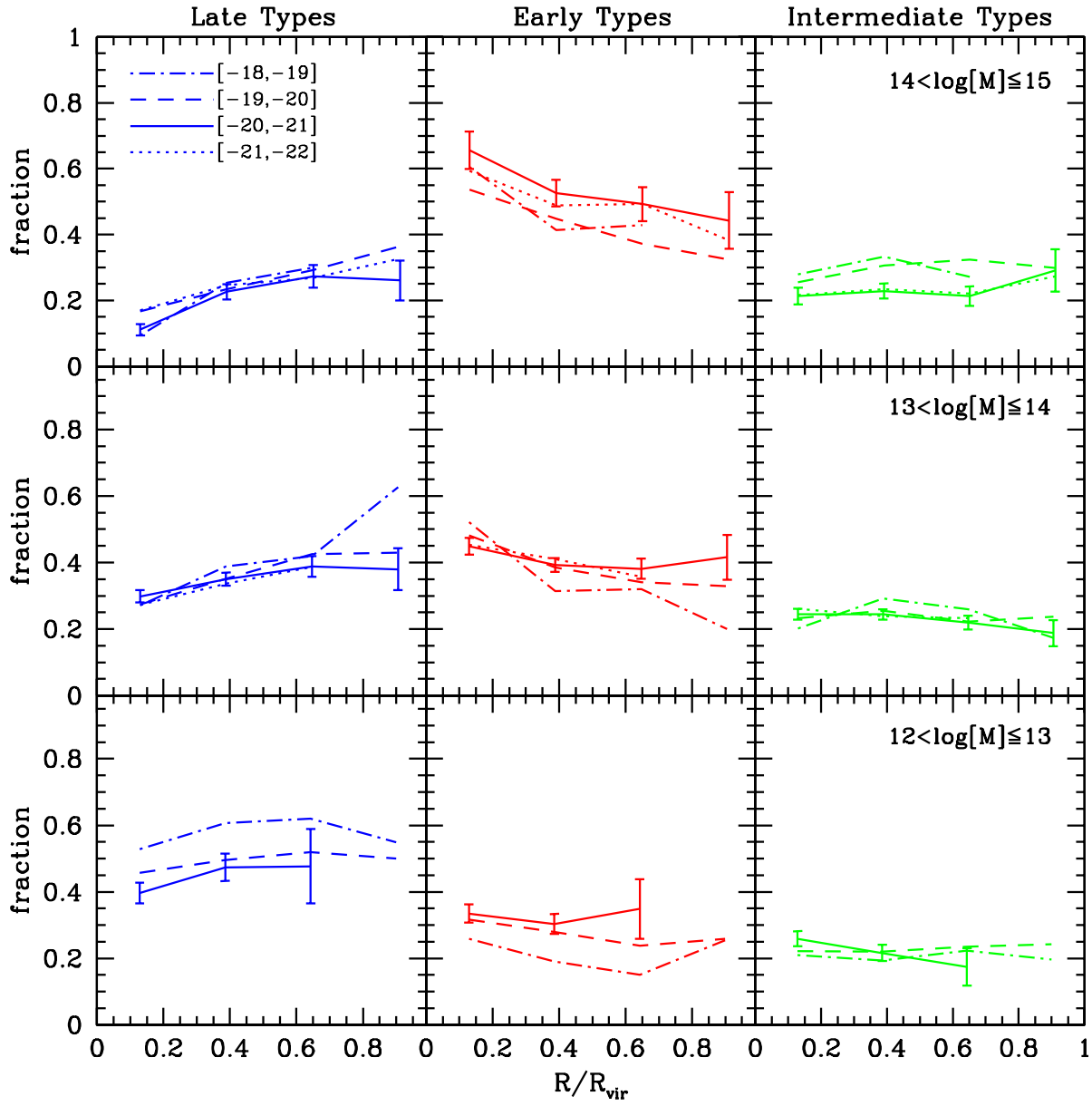

Figure 2.8: *The fractions of satellite galaxies that are late type (left-hand panels), early type (middle panels), and intermediate type (right-hand panels) as function of the projected radius R from the (luminosity-weighted) group center (in units of $R_{\rm vir}$). Results are shown for haloes in three mass ranges (upper, middle and lower panels), and for four bins in absolute magnitude (different line styles, as indicated in the upper left-hand panel). We only show results for bins in radius, magnitude, and mass that contain at least 50 galaxies in total. For clarity, we only show (Poissonian) errorbars for one of the four magnitude bins. Note that the fraction of late (early) type satellite galaxies increases (decreases) significantly with radius, while the fraction of intermediate type satellites does not seem to depend on radius at all. Note also, that at given halo mass and halo-centric radius the type fractions do not depend significantly on luminosity.*

$1/V_{\rm max}$ weighting yields virtually identical results. Results are shown in the upper panels of Fig. 2.9. Except for a normalization offset, which reflects the halo mass dependence of the type fractions, *the radial dependence is the same for all three mass bins*. In all cases, the late type fraction increases by ~ 15 percent going from $R \simeq 0.1R_{\rm vir}$ to $R \simeq 0.9R_{\rm vir}$. Although this may seem a relatively small increase, it is important to realize that we observe the radial dependence in projection. Furthermore, typical orbits in dark matter haloes have fairly large apo- to pericenter ratios of 6 : 1 or larger (e.g., Ghigna et al. 1998; van den Bosch et al. 1999), which together with the projection makes the observed trend appear much weaker than the real trend.

Our result that the radial trend is independent of halo mass is in conflict with Domínguez et al. (2002) who, using the 100K data release of the 2dFGRS, found no significant radial dependence of the late type fraction in haloes with $M \lesssim 10^{13.5}h^{-1}\,{\rm M}_\odot$. There are two reasons for this discrepancy. First of all, our sample is significantly larger, resulting in smaller errorbars. Secondly, as far as we can tell, Domínguez et al. (2002) included the central galaxies in their analysis. If we do the same, we obtain the results shown in the lower panels of Fig. 2.9. Note that the inclusion of central galaxies slightly boosts the late type fraction in the inner most radial bin, especially for low mass haloes. This reduces the overall radial trend, and for the mass bin with $10^{12}h^{-1} < M \leq 10^{13}h^{-1}\,{\rm M}_\odot$ the data is now consistent with no significant radial dependence, in agreement with Domínguez et al. (2002). Since central galaxies are special in many respects, we feel, however, that it is more appropriate to study any radial dependence using satellite galaxies only.

Finally we note that the intermediate type fraction is, in addition to being independent of galaxy luminosity and group mass, also independent of halo-centric radius (in all mass bins, and for all luminosity bins). Thus, a randomly selected galaxy, whether faint or bright, whether in a low mass halo or a cluster, and whether close or far from the group/halo center, has a ~ 20 percent chance of being an intermediate type galaxy (see Section 2.6.3 for discussion).

2.5.4 Dependence on Central Galaxy Type

Next we investigate whether the properties of satellite galaxies correlate with those of their central galaxy. Fig. 2.10 plots the late type fraction as function of halo mass for three different magnitude bins (again computed using volume limited samples). Here we use a different type classification than in the rest of this work. In the upper panels we split galaxies in late and early types only (i.e., no intermediate types are defined here), using the colour cut given by equation (2.1). Galaxies that are bluer than this cut are termed late types. In the lower panels the split in early and late types is based on the SSFR cut of equation (2.2). Galaxies with a SSFR that is higher than this cut are called late types. In each panel in Fig. 2.10 blue, dashed lines indicate the late type fraction of satellites in haloes in which the central galaxy is also a late type. Red, solid lines correspond to haloes with an early type central galaxy. Note that the luminosity of the central galaxy is not restricted to fall within the magnitude bin indicated.

As is evident from Fig. 2.10, haloes with a late type central galaxy have a significantly higher fraction of late type satellites than haloes of the same mass but with an early type central galaxy. This difference is evident over the entire ranges of masses and luminosities explored. Apparently, satellite galaxies 'know' about the properties of their central galaxy. We have verified that this effect also exists with respect to the second-, third- and fourth

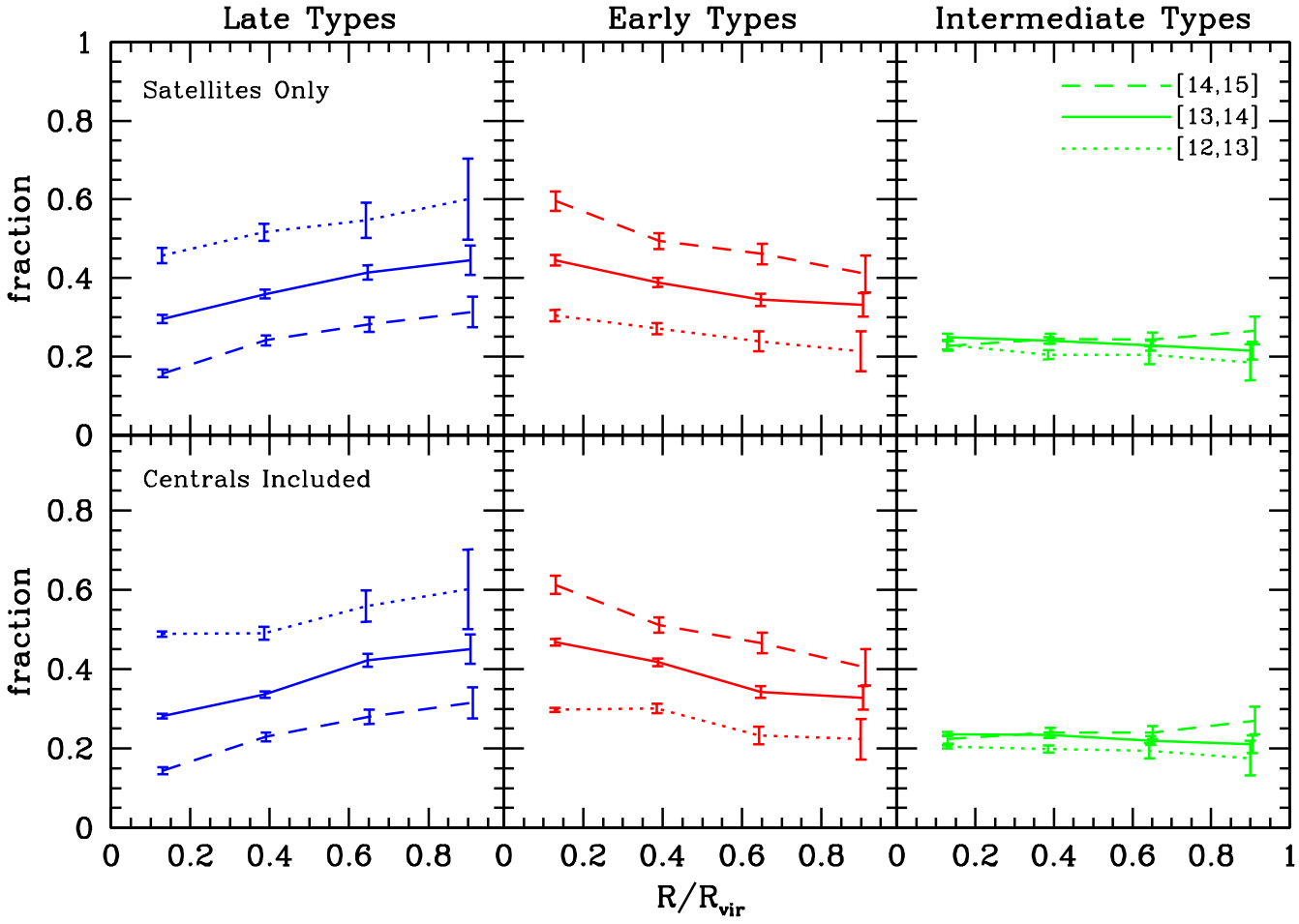

Figure 2.9: *he upper panels are the same as Fig. 2.8 except that this time we consider all galaxies in the magnitude interval* $-23 \leq^{0.1} M_r - 5\log h \leq -18$ *and in the redshift range* $0.01 \leq z \leq 0.2$. *Results are shown for three mass bins. The values in square brackets in the upper right-hand panel indicate the values of* $\log(M)$ *(in* $h^{-1}\,\mathrm{M}_\odot$*) used. Except for an offset, which reflects the halo mass scaling shown in Fig. 2.5, the radial dependence is independent of halo mass. For comparison, the lower panels reveal the same type fractions, but this time central galaxies are included. This introduces a weak mass dependence, in that lower mass haloes seem to reveal a weaker dependence on radius. See text for a detailed discussion.*

brightest galaxy. Haloes whith a late type second ranked galaxy have an enhanced overall late type fraction in comparison to haloes of the same mass but with an early type second ranked galaxy. The same also holds for the third and fourth ranked galaxy. This shows that the effect described above is real and cannot be solely a result of an underestimate of the masses of haloes with an early type central galaxy, although this could lead to a slight artificial strengthening of the effect.

The phenomenon described above, which we term 'galactic conformity', is a new result that has not been noticed before. Some studies, however, have found correlations that point in the same direction. Wirth (1983), studying the galaxy content of groups and clusters using photographic plates, noted that the direct environment of elliptical galaxies contain a higher fractions of early types than the average of the field. Hickson et al. (1984), studying compact groups, noticed that if the brightest galaxy is a spiral the fainter group members also tend to be spirals. Ramella et al. (1987), analyzing the morphological content of loose groups in the catalogue of Geller & Huchra (1983), noticed that the fraction of elliptical galaxies is significantly higher if the first-ranked group member is also an elliptical. None of these studies, though, performed the analysis as a function of group mass. Since the early type fraction increases with halo mass for both central and satellite galaxies (see Section 2.5.2), a type-correlation between the central galaxy and its satellites arises naturally when using a sample of groups that span a range in masses. Indeed, Osmond & Ponmon (2004), studying a sample of 60 galaxy groups with existing X-ray data, also noticed that the spiral fraction was significantly higher if the brightest group galaxy also was a late type. The corresponding groups, however, where found to have a lower velocity dispersion and no detected X-ray emission, suggesting that they had a lower mass on average. What is special about the 'galactic conformity' presented here, is that such a correlation exists *at a fixed halo mass*, and for satellites of a fixed range in magnitudes. This finding puts intriguing new constraints on galaxy formation models, which we briefly address in Section 2.6.2.

2.5.5 The Correlation between Galaxy Properties and Halo Mass

Thus far we have only focussed on the *fractions* of early, late and intermediate type galaxies. We now examine how the *median* colour, SSFR, and concentration of galaxies scale with halo mass. As before, we discriminate between luminosity dependence and halo mass dependence by splitting the galaxy population in a number of magnitude bins. For each bin we construct a volume limited sample, and only consider groups that fall entirely within this volume. Results are shown in Fig. 2.11, which plots the median colour (upper panels), SSFR (panels in middle row), and concentration (lower panels) as function of halo mass[6]. Results are shown for five magnitude bins and separately for all galaxies, late type galaxies, early type galaxies and intermediate type galaxies.

If we first focus on the relations for all galaxies (panels in left column), one notices that the correlations of all three galaxy properties with halo mass are fairly weak *at fixed luminosity*. To make this a bit more quantitative, we estimate the gradients of the median properties as function of mass at fixed luminosity, and as function of luminosity at fixed

[6]We have also examined the *average* properties (not shown), and found the relations to be extremely similar.

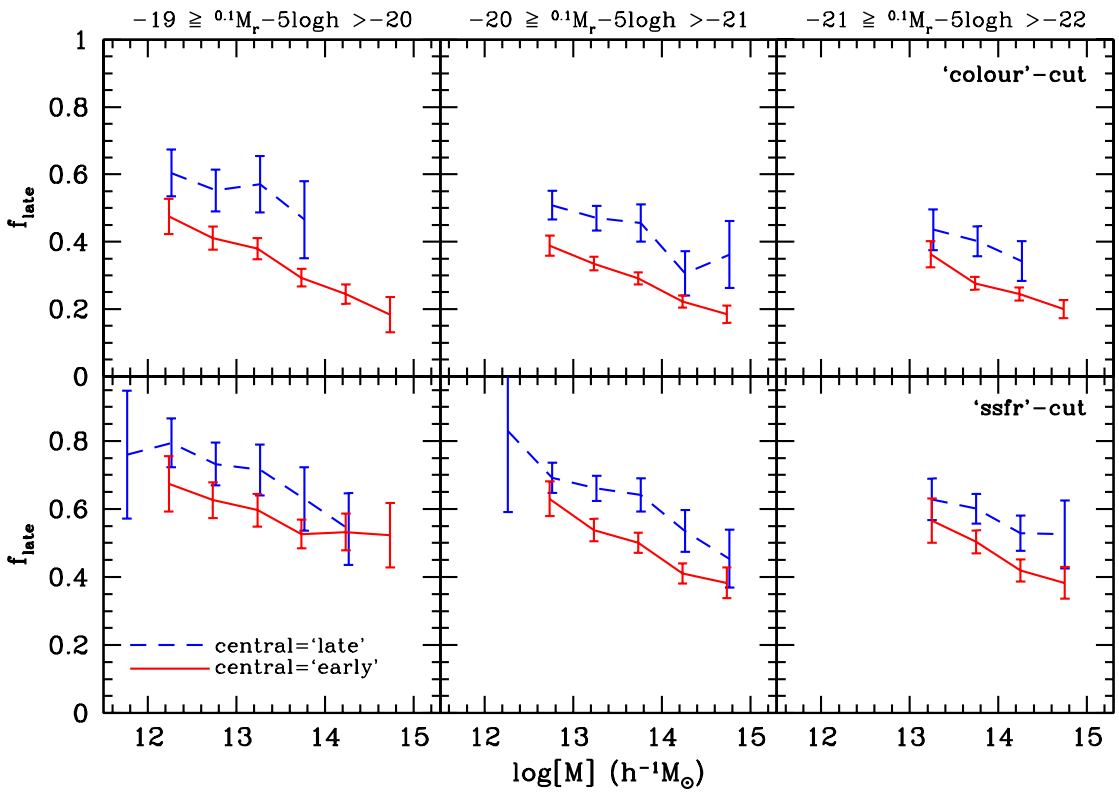

Figure 2.10: *The late type fraction of satellites galaxies as function of halo mass for haloes with a central early type galaxy (red, solid curves) and a central late type galaxy (blue, dashed curves). Results are shown for three different volume limited samples, as indicated. In the upper panels, galaxy type is determined using a colour cut (equation [2.1]), while in the lower panels a cut based on the SSFR (equation [2.2]) has been used. Results are only shown for mass-luminosity bins with at least 50 galaxies in total, and errorbars denote Poissonian errors. Note that haloes with a late type central galaxy have a significantly higher fraction of late type satellites than haloes with an early type central galaxy, a phenomenon we term 'galactic conformity'.*

mass. For the luminosity and mass dependence of the median colour we find

$$\left.\frac{\mathrm{d}^{0.1}(g-r)}{\mathrm{d}\log M}\right|_L \approx +0.06 \qquad \left.\frac{\mathrm{d}^{0.1}(g-r)}{\mathrm{d}\log L}\right|_M \approx +0.09 \tag{2.4}$$

For the SSFR these gradients are

$$\left.\frac{\mathrm{d}\log \mathrm{SSFR}}{\mathrm{d}\log M}\right|_L \approx -0.20 \qquad \left.\frac{\mathrm{d}\log \mathrm{SSFR}}{\mathrm{d}\log L}\right|_M \approx -0.35 \tag{2.5}$$

and for the concentration we find

$$\left.\frac{\mathrm{d}c}{\mathrm{d}\log M}\right|_L \approx +0.07 \qquad \left.\frac{\mathrm{d}c}{\mathrm{d}\log L}\right|_M \approx +0.25 \tag{2.6}$$

Although these numbers are fairly rough estimates, it is clear that in all three cases the luminosity dependence is stronger than the halo mass dependence (when both luminosity and mass are expressed in solar units).

Note that this contrasts strongly with the type fractions, which depend more strongly on halo mass than on luminosity (see Section 2.5.2). We can reconcile this with the strong luminosity dependence of the median colour and SSFR by realizing that the cuts in colour and SSFR used to define the galaxy types scale with luminosity according to

$$\frac{\mathrm{d}^{0.1}(g-r)}{\mathrm{d}\log L} = +0.08 \qquad \frac{\mathrm{d}\log \mathrm{SSFR}}{\mathrm{d}\log L} = -0.24 \tag{2.7}$$

(cf. equations [2.1] and [2.2]). Note that these gradients are comparable to those of the median properties at fixed mass. This shows that at fixed halo mass, the median colour and SSFR scale roughly with luminosity in the same way as the corresponding bimodality scales. The fractions of galaxies on either site of this bimodality scale, however, only depend weakly on luminosity at fixed halo mass.

As is evident from the three right-hand columns of Fig. 2.11 the median properties of a galaxy of given luminosity *and type* are virtually independent of halo mass. The mass dependence of the median properties of *all* galaxies, therefore, owes entirely to the mass dependence of the type fractions. In as far as halo mass is a reliable proxy for the local surface density of galaxies, this is in agreement with Balogh et al. (2004a) and Tanaka et al. (2004) who found that although the *fraction* of star forming galaxies (defined according to the equivalent width of the Hα line) depends strongly on Σ_5, the median equivalent width of star forming galaxies (those with EW(Hα) > 4Å) does not show any Σ_5-dependence. Our results also agree with those of Kauffmann et al. (2004), who found that the concentration parameter of galaxies is independent of galaxy number density at fixed stellar mass.

2.5.6 Conditional Probability Distributions

The type fractions and medians discussed thus far are simple scalars expressing some properties of the underlying probability distributions. For completeness, we now present, for some illustrative cases, these full distributions. First we split our sample of galaxies (those that have been assigned to groups) according to type and luminosity (using five volume limited magnitude bins). For each galaxy in each luminosity-type bin we look up

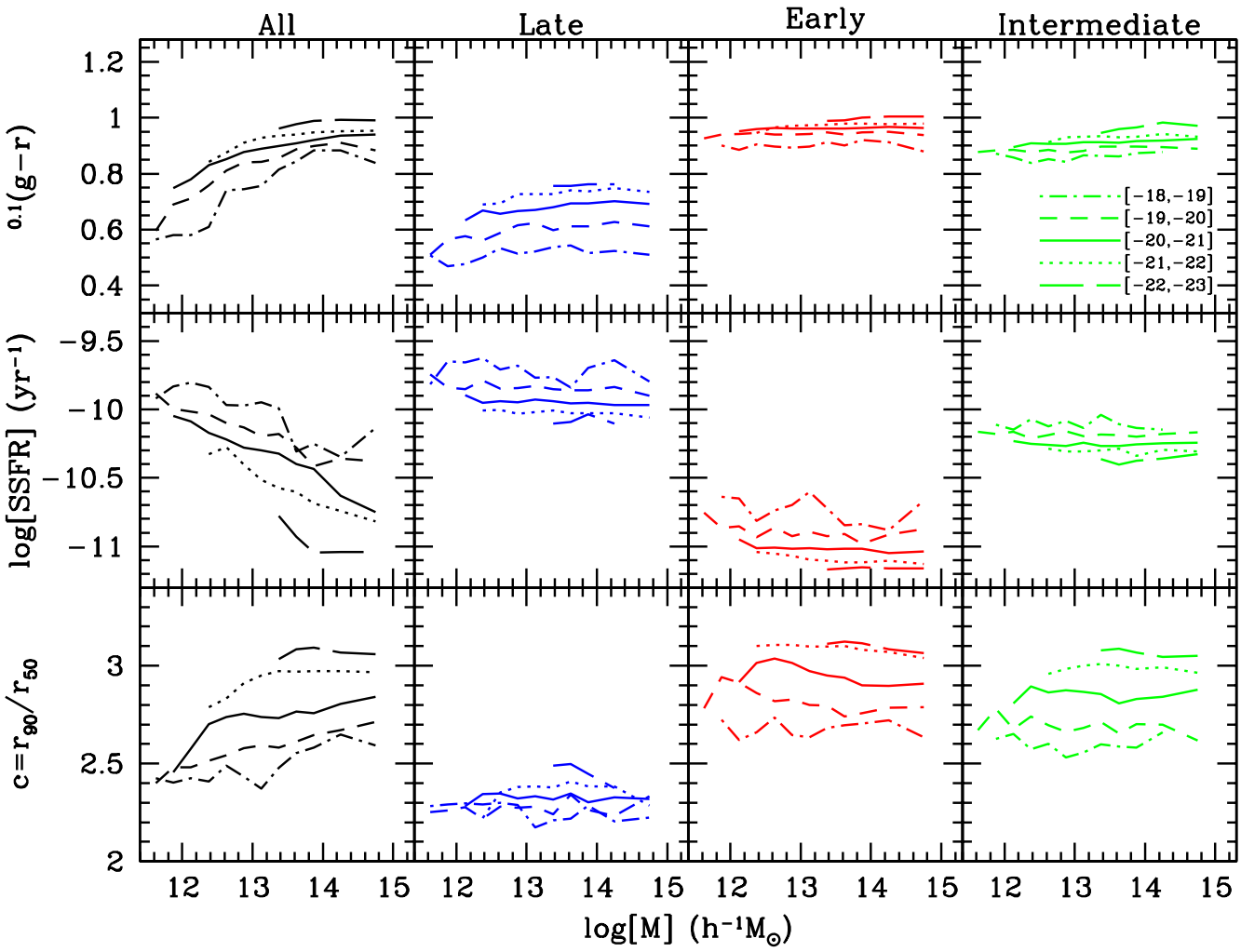

Figure 2.11: *The* median *colour, SSFR, and concentration of galaxies as function of halo mass. Results are shown for five magnitude bins (as indicated), and separately for all galaxies, late type galaxies, early type galaxies and intermediate type galaxies. Results are only shown for mass-luminosity bins that contain at least 20 galaxies in total.*

the mass of the group of which it is a member. Fig. 2.12 plots the resulting conditional mass functions $P(M|L, \mathrm{type})$, with L the luminosity in the ${}^{0.1}r$-band. The histograms in the upper panels show $P(M|L)$. As expected, bright galaxies always reside in massive haloes. The conditional mass function for faint galaxies, however, reveals a bimodal distribution: a narrow peak at low halo masses, corresponding to central galaxies, and a very broad wing to high halo masses, corresponding to satellite galaxies. Note that the functional form of $P(M|L)$ derived here is in good agreement with predictions based on the conditional luminosity function presented in Yang et al. (2003) and Cooray (2005). The blue, red and green histograms in the upper panels indicate the contributions to $P(M|L)$ due to late, early and intermediate type galaxies, respectively. In agreement with the results shown above, bright galaxies in massive haloes are predominantly early types, while faint galaxies in low mass haloes are dominated by late types. However, one can also see that those faint galaxies that reside in the most massive haloes are more likely to be an early type.

The latter is more evident when one compares the conditional mass functions of early and late type galaxies, shown in the panels in the middle two rows. For faint galaxies, $P(M|L, \mathrm{late})$ and $P(M|L, \mathrm{early})$ are clearly different, in that the former is clearly more skewed towards low M. This implies that a faint, early type galaxy lives in a halo that, on average, is more massive than a halo hosting a late type galaxy of the same luminosity. This is in good agreement with other studies. In particular, Blanton et al. (2005b) studied the relationship between environment and various properties of galaxies in the SDSS. They computed the *mean* local overdensity as function of both luminosity and several other parameters, including colour and Sersic index. Although their overdensities are measured using a fixed metric scale of $1h^{-1}\,\mathrm{Mpc}$, which, as we have argued in Section 2.2, is difficult to interpret in terms of halo masses, their results paint a very similar picture: blue faint galaxies live in low density regions (i.e., are central galaxies in their own, low mass haloes), while red faint galaxies reside in regions with a similar overdensity as that of red bright galaxies (i.e., they are satellite galaxies in clusters). This is also consistent with clustering data. In particular, Norberg et al. (2002) have shown that the correlation length of faint early types is much higher than that of late type galaxies of the same luminosity, indicating that they live in more massive haloes.

Fig. 2.13 plots the conditional colour distributions $P({}^{0.1}(g-r)|L, M)$ for three bins in halo mass and five (volume limited) bins in absolute magnitude. There is a clear trend that the fraction of red galaxies increases with both luminosity and with halo mass, in agreement with the results presented above. Note also that, at fixed halo mass, the colour distributions for $-19 \geq^{0.1} M_r - 5\log h > -20$ and for $-20 \geq^{0.1} M_r - 5\log h > -21$ are remarkably similar, consistent with the fact that the galaxy type fractions are independent of luminosity over this magnitude range (cf. Fig. 2.4). Finally, Fig. 2.14 plots the distributions of galaxy concentration conditional on luminosity and halo mass. These nicely illustrate how the average concentration increases with both halo mass and luminosity, as already shown in Fig. 2.11. Although all main trends visible in Figs. 2.12 – 2.14 are already evident from the previous discussion based on type fractions and median properties, the full distributions shown here contain useful, additional information not evident from the fractions or the means.

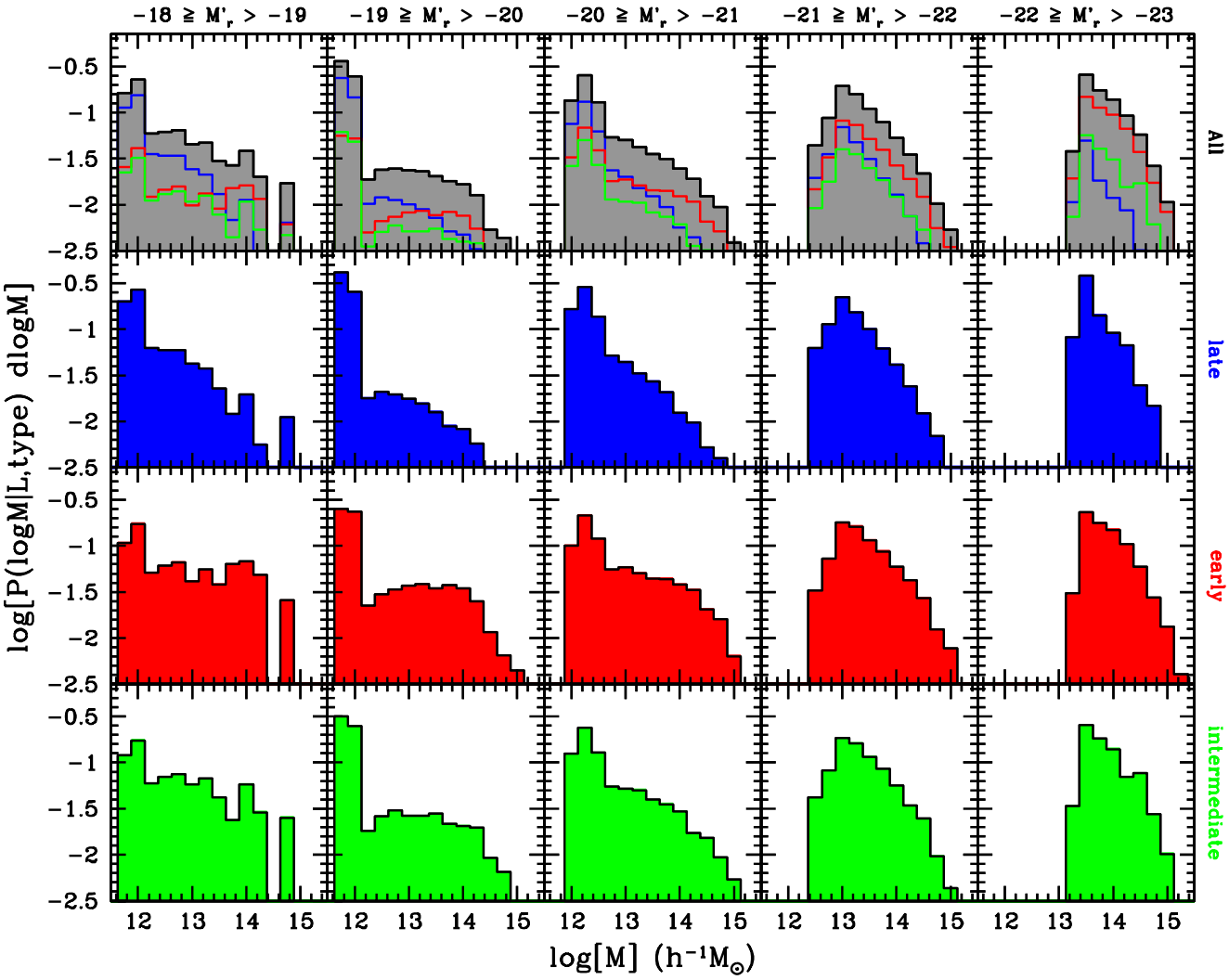

Figure 2.12: *The logarithm of the conditional probability distribution* $P(\log[\mathrm{M}]|\mathrm{L},\mathrm{type})$ *that a galaxy of given luminosity* L *(in the* $^{0.1}r$*-band) and given type resides in a halo of mass* M*. Results are shown for five magnitude bins (indicated at top of each column, with* $M'_r = ^{0.1} M_r - 5\log h$*) and for late types (panels in second row), early types (panels in third row) and intermediate types (panels in bottom row). The upper row of panels plots the conditional probability distribution* $P(M|L)$ *(gray scale). The blue, red and green histograms in these panels indicate the contributions to* $P(M|L)$ *due to late, early and intermediate types, respectively.*

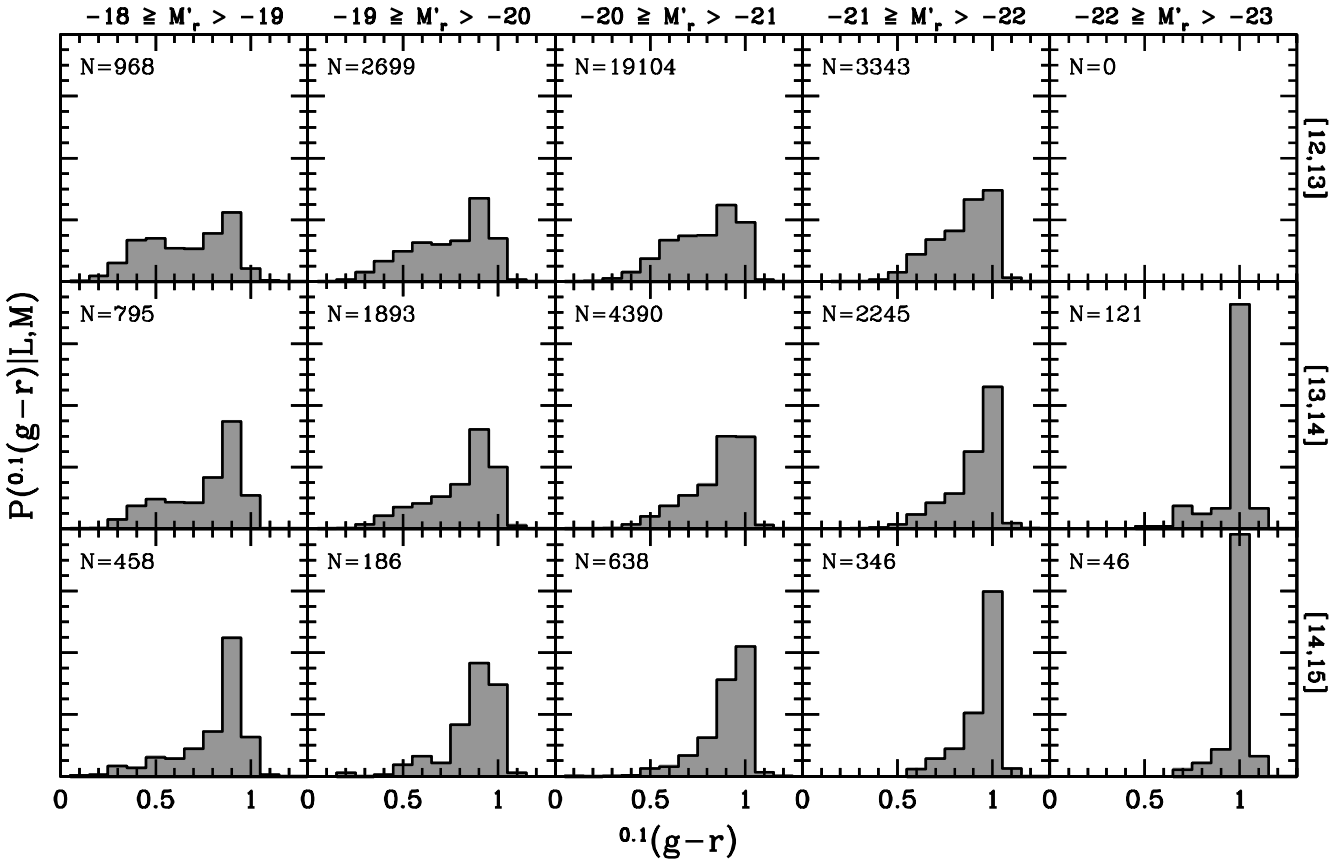

Figure 2.13: *The conditional probability distribution* $P(^{0.1}(g-r)|L,M)$ *for three different bins in halo mass (values in square brackets on the right site of each row indicate the range of* $\log[M]$ *used) and five different bins in luminosity (indicated at top of each column, with* $M'_r = ^{0.1} M_r - 5\log h$*). The total number of galaxies in each distribution,* N*, is indicated in the upper left corner of each panel.*

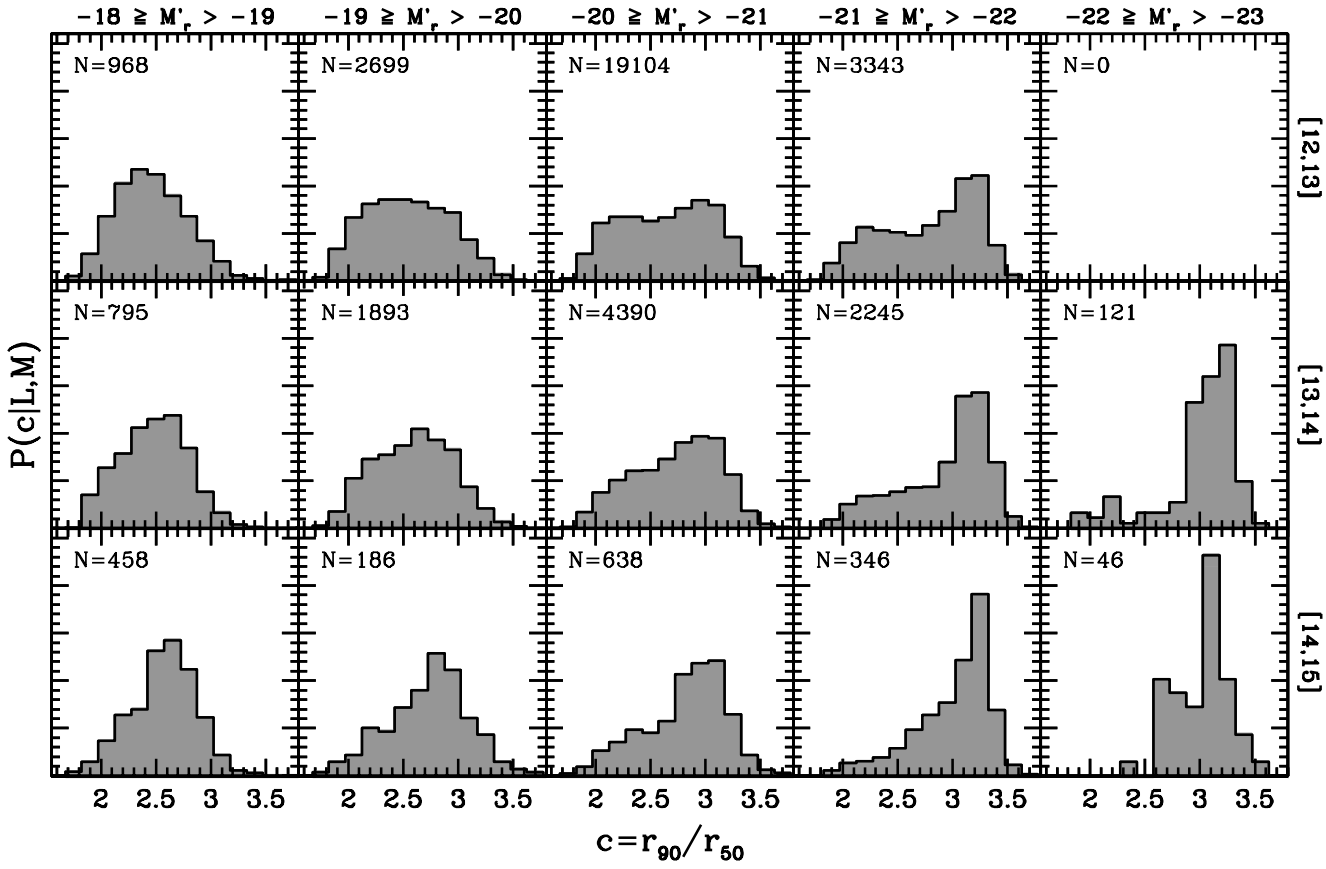

Figure 2.14: *Same as Fig. 2.13 except that this time we plot the conditional probability distribution $P(c|L, M)$, with $c = r_{90}/r_{50}$ the galaxy concentration.*

2.6 Discussion

2.6.1 Implications for Galaxy Formation & Evolution

In the current paradigm of galaxy formation, galaxies form in extended dark matter haloes. In the pure 'nature' scenario, the properties of a galaxy depend only on the mass and formation history of the dark matter halo in which it resides. However, a galaxy also experiences interactions of various kinds with its environment. Examples of these are ram-pressure stripping, strangulation, and galaxy harassment. These, and other, 'nurture' processes may also play an important role in setting the final properties of a galaxy.

Ever since the discovery that galaxy properties correlate with their environment, their has been an ongoing debate as to the relative importance of nature versus nurture processes in regulating galaxy properties. In this work we have analyzed how a variety of galaxy properties depend on halo mass, using a sample of $\sim 90,000$ galaxies distributed over $\sim 53,000$ haloes (galaxy groups). These results provide a testbed for comparison with galaxy formation models, and may provide important insights regarding the nature-versus-nurture debate.

Unfortunately, many poorly understood, intertwined processes play a role in galaxy formation, so that an interpretation of our results is far from straightforward. For example, although the mere presence of a correlation between galaxy properties and environment is often taken as evidence for a dominant role of 'nurture' processes, it is important to realize that many, if not all, of these correlations can equally well be explained within a pure 'nature' scenario (see below). This makes it extremely difficult to discriminate between the various physical processes. Below we briefly discuss some of these processes, and emphasize how their (often crude and speculative) predictions compare to the results presented above.

2.6.1.1 The nature scenario

In the 'nature' scenario, the global properties of the galaxy population owe mainly to the formation history of their dark matter haloes. During quiescent growth phases gas can cool and form a centrifugally supported disk. Star formation slowly and continuously converts the gas into stars, resulting in a typical late-type galaxy with blue colors and an ongoing SFR. During a major merger of two dark matter haloes, the (central) galaxies are likely to merge as well due to dynamical friction. If their mass ratio is sufficiently small, the outcome of this merger event will most likely resemble a spheroid (e.g., Toomre & Toomre 1972), while most gas is likely to be consumed in a starburst (e.g., Mihos & Hernquist 1996). If new accretion of gas can somehow be prevented, for example by invoking AGN feedback (Croton et al. 2005), the resulting galaxy will quickly become 'red and dead', characteristic of a genuine early-type. If, however, the accretion of new gas can not be prevented, a new disk may start to grow around the spheroid, slowly transforming the early type into a late type.

This is the standard picture adopted in virtually all semi-analytical models for galaxy formation. When assigning galaxy types according to their bulge-to-disk ratio, these models yield an increasing fraction of early types with increasing halo mass and with decreasing halo-centric radius (Diaferio et al. 2001; Okamoto & Nagashima 2001; Springel et al. 2001; Berlind et al. 2003), all in qualitative agreement with observations. This suggests that the global morphology-density relation is built in at a very fundamental level

in hierarchical formation theories and can be explained within the 'nature' scenario (see also Evrard, Silk & Szalay 1990). However, all models have problems in trying to match the radial dependence of S0s, which seems to require additional ('nurture') processes.

In addition, a more detailed comparison between the model predictions and the results presented here indicates another potential problem. Since galaxy-galaxy merging is inefficient in massive haloes, all semi-analytical models predict a 'saturation' of the early type fraction in haloes above a certain mass. For example, the models of Diaferio et al. (2001) predict that the fraction of early types (defined according to bulge-to-disk ratio) increases with halo mass up to $\sim 10^{13.5}h^{-1}\,\mathrm{M}_\odot$, after which the early type fraction reveals a modest decline. This is inconsistent with our results, which show that the early type fraction continues to decrease up to the most massive haloes analyzed ($M \simeq 10^{15}h^{-1}\,\mathrm{M}_\odot$). Berlind et al. (2003) and Zheng et al. (2005) have shown that the semi-analytical models of Cole et al. (2000) predict that the fraction of 'young' galaxies decreases with increasing halo mass up to $\sim 10^{13}h^{-1}\,\mathrm{M}_\odot$, after which the fraction remains constant. Although 'young' galaxies are not necessarily the same as our late types, this again seems inconsistent with the findings reported here. It remains to be seen whether this inconsistency disappears when for example AGN feedback is taken into account, or whether it signals the need for additional processes to describe type transformations.

2.6.1.2 Ram pressure stripping

Whenever a galaxy orbits a hot, gaseous halo it may experience ram-pressure stripping (Gunn & Gott 1972). This causes a rapid removal of gas, shutting off star formation, and transforming a late type into an early type. Note, however, that the morphology of the galaxy is not modified: a disk will remain a disk. Ram pressure stripping is therefore mainly invoked as a mechanism to transform spirals into S0s. Since the latter are typically red and passive, they are part of the early types in our classification scheme.

In order to estimate how the effectiveness of ram pressure stripping depends on the masses of the host halo and the galaxy, consider a halo of mass M and circular velocity V. In addition, we assume that the galaxy is embedded in a subhalo of mass m and circular velocity v. We assume that both M and m obey the virial relations so that $M \propto V^3$ and $m \propto v^3$. Now consider a disk with surface density $\Sigma_{\rm disk}$, consisting of both stars and gas, embedded within m. The pressure exerted on the gas in this disk due to the hot gas associated with M is $P \propto \rho_{\rm hot}V^2 \propto f_{\rm hot}V^2$, where $f_{\rm hot}$ is the baryonic mass fraction of M that is in a hot component (note that all virialized haloes have the same average density, independent of halo mass). The restoring force per unit area on the gas disk due to the self-gravity of the disk is $F_{\rm res}/A = 2\pi G\Sigma_{\rm gas}\Sigma_{\rm star} = 2\pi G(1-f_*)f_*\Sigma^2_{\rm disk}$, with f_* the disk mass fraction in stars. To relate $\Sigma_{\rm disk}$ to the subhalo mass m we use the disk formation models of Mo, Mao & White (1998), according to which $\Sigma_{\rm disk} \propto v \propto m^{1/3}$.

Ram pressure stripping occurs when $P > F_{\rm res}/A$, which is the case whenever

$$\frac{f_{\rm hot}}{f_*(1-f_*)}\left(\frac{m}{M}\right)^{-2/3} > c \tag{2.8}$$

with c some constant. In a galaxy that obeys this criterion, the force per unit mass on the gas disk is proportional to $[P - F_{\rm res}/A]\Sigma^{-1}_{\rm disk} \propto [aM^{2/3} - bm^{2/3}]m^{-1/3}$, with a and b some constants that depend, among others, on $f_{\rm hot}$ and f_*, respectively. Per crossing time, which is independent of M, the distance travelled by m is proportional to $M^{1/3}$, so

that the work done on the gas per unit mass per unit time is

$$\frac{\mathrm{d}W}{\mathrm{d}m\,\mathrm{d}t} \propto \left[aM^{2/3} - bm^{2/3}\right] \left(\frac{m}{M}\right)^{-1/3} \tag{2.9}$$

From equations (2.8) and (2.9) is thus is evident that, at fixed m, ram pressure stripping is more likely to occur, and with a higher efficiency, in more massive haloes. If we (naively) assume that satellite luminosity is a reasonable proxy for m, and that ram pressure stripping transforms a late type system into an early type system, this predicts that the late type fraction of galaxies of fixed luminosity decreases with increasing halo mass, as observed. Note that this effect will only be stronger if $f_{\rm hot}$ increases with M as suggested by X-ray measurements.

At fixed halo mass M, however, equations (2.8) and (2.9) predict that a satellite is more likely to experience ram pressure stripping, and with a larger efficiency, if m is lower. This therefore predicts that the late type fraction should increase with luminosity at fixed M, in clear conflict with the data. Furthermore, if ram pressure stripping is the main process responsible for the radial type dependence, one predicts the effect to be more pronounced in more massive haloes, and in haloes of fixed mass to be less pronounced for more luminous satellites. Both of these predictions are inconsistent with the data, which shows no luminosity dependence at fixed halo mass, and an equally strong radial trend for all halo masses. We therefore conclude that ram pressure stripping can not be the dominant effect that causes type transformations. A similar conclusion was recently obtained by Goto (2005) based on a detailed study of the velocity distribution of galaxies within clusters.

2.6.1.3 Strangulation

As long as a (central) galaxy continues to accrete new gas, it can continue to form stars. As soon as it enters a larger system, and becomes a satellite galaxy, it is deprived of its hot gas reservoir. This shuts off the accretion of new gas, so that the star formation rate will come to a halt after the galaxy has consumed (part of) its cold gas. This supply-driven decline in star formation rates of satellite galaxies was first suggested by Larson, Tinsley & Caldwell (1980), and is often called 'strangulation' (Balogh, Navarro & Morris 2000).

The main difference between strangulation and ram pressure stripping is that the time scale for strangulation is much longer than for stripping. It has been argued that such long quenching time scales are inconsistent with the observation that the distribution of Hα equivalent widths of starforming galaxies is independent of environment (Balogh et al. 2004a). However, using the relations between three different SFR indicators, Kauffmann et al. (2004) have actually argued in favor of a long time scale (> 1 Gyr) for star formation suppression. More detailed modeling is required to investigate these issues in more detail. Important constraints may also come from the pronounced bimodality in the colour magnitude relation (e.g., Balogh et al. 2004b; Bell et al. 2004).

Unlike ram pressure stripping and harassment, strangulation is a standard ingredient in most semi-analytical models for galaxy formation (Kauffmann, White & Guiderdoni 1993; Diaferio et al. 2001), where it helps to explain the enhanced early type fraction in more massive haloes, simply because they contain more satellite galaxies. As with ram pressure stripping, however, strangulation will only modify the colours and SFRs, but will not transform a disk into a spheroidal. Thus, while it may be an important process to

explain the enhanced fraction of S0 galaxies in dense environments, it can not explain the enhancement of spheroidals.

2.6.1.4 Harassment

Dark matter haloes are populated with numerous subhaloes of a wide range of masses (e.g., Gao et al. 2004; van den Bosch, Tormen & Giocoli 2005c). A satellite galaxy embedded in one of these subhaloes, is subject to frequent high speed encounters with other subhaloes (some of which may not host a luminous satellite galaxy). The impulsive heating due to these numerous encounters is termed galaxy harassment (Moore et al. 1996), and may cause morphological transformations. In the tidal approximation (Spitzer 1958), the amount of heating per encounter scales as $\Delta E \propto b^{-4}$, with b the impact parameter. To get an estimate of the total heating due to impulsive encounters, it is therefore important to accurately account for the encounters with small impact parameters. Unfortunately, the tidal approximation is only valid for relatively large impact parameters (Aguilar & White 1985). This makes it extremely difficult to make accurate predictions regarding the scaling of the harassment efficiency with halo mass.

Nevertheless, one point is worth making. Galaxy harassment is often considered a mechanism that only operates in clusters of galaxies. This seems to be motivated by the fact that clusters contain hundreds to thousands of galaxies, very different from groups and galaxy sized haloes. However, in terms of dark matter subhaloes, the CDM paradigm predicts that lower mass haloes are simply scaled-down versions of cluster-sized haloes, albeit with a relatively small, mass dependent normalization (e.g., van den Bosch et al. 2005c). Since dark matter subhaloes without a luminous satellite galaxy can also cause impulsive heating, galaxy harassment is expected to occur in haloes of all masses.

Although we cannot make a robust prediction for how the harassment efficiency scales with halo mass, we may use the tidal approximation to estimate how it scales with the mass of the perturbed system. Consider a system s, with mass m_s, that experiences an impulsive encounter with a perturbed p of mass m_p. The energy increase of s is given by

$$\Delta E = \frac{4}{3} G^2 m_s \frac{m_p^2}{V^2} \frac{\langle r_s^2 \rangle}{b^4} \tag{2.10}$$

(Spitzer 1958), with b the impact parameter, V the encounter velocity, and $\langle r_s^2 \rangle$ the mean square radius of s. We can express the harassment efficiency as the ratio of this energy change to the gravitational binding energy of s, $W \propto G m_s^2 / r_s$. If we use that $\langle r_s^2 \rangle \propto r_s^2$, which holds as long as all systems have a similar density distribution, and we assume that the virial relation $m_s \propto r_s^3$ holds, we obtain that

$$\epsilon_{\rm haras} \equiv \frac{\Delta E}{W} \propto \left(\frac{m_p}{V}\right)^2 \frac{1}{b^4} \tag{2.11}$$

Note that this is independent of m_s. If harassment is the main cause of type transformations, and m_s is a reasonable proxy for satellite luminosity, this scaling relation predicts that the type fraction should be independent of luminosity at fixed halo mass. As we have shown in Section 2.5.2 this is in reasonable agreement with the data, but only over the luminosity range $0.25 \lesssim L/L^* \lesssim 2.5$. However, this argument is based on the assumption of self-similarity. Although this is a reasonable assumption for dark matter subhaloes, it does not apply for the satellite galaxies that reside in these subhaloes. As shown by

Moore et al. (1999), low surface brightness (LSB) galaxies are much more vulnerable to harassment than high surface brightness (HSB) galaxies in a halo of the same mass. Since LSB galaxies have typically lower luminosities than HSB systems, they are expected to reside in lower mass subhaloes, on average. In this case, harassment will tend to have a bigger impact on lower mass systems. If harassment transforms late type galaxies into early type galaxies, this will result in a late-type fraction that increases with increasing luminosity (in a halo of fixed mass), in disagreement with the data. Although clearly more detailed studies of the impact of galactic harassment are needed, these simple arguments seem to disfavor harassment as a dominant physical process.

2.6.2 Galactic Conformity

In the standard 'nature' picture, adopted in all semi-analytical models of galaxy formation, the morphology of a central galaxy is related to the epoch of the last major merger, and thus to the assembly history of its dark matter halo: haloes that experienced a recent major merger, and thus assembled recently, are more likely to host a central early type. Interestingly, using a large numerical simulation, Gao, Springel & White (2005) have recently shown that haloes *of given mass* that assemble later are less strongly biased (i.e., are less strongly clustered). If, for some reason, a less strongly biased region produces a larger fraction of early types, this correlation between assembly redshift and halo bias might provide an explanation for galactic conformity. However, this picture has two important shortcomings. First of all, it is well known that less massive haloes are less strongly biased (e.g., Mo & White 1996). If a higher bias indeed results in a smaller early type fraction, one would therefore expect an early type fraction that decreases with increasing halo mass, opposite to what is observed. Secondly, Gao et al. (2005) have shown that the bias only depends on halo assembly time for haloes less massive than $\sim 10^{13}h^{-1}\,\mathrm{M}_{\odot}$. Our results, however, indicate that galactic conformity is present in haloes both more massive and less massive than this.

Alternatively, galactic conformity might owe to 'nurture' processes. For example, X-ray observations show that haloes with pronounced X-ray emission contain virtually always an early type central galaxy (e.g., Ebeling, Voges & Böhringer 1994; Osmond & Ponmon 2004). Since the presence of X-ray emission indicates a relatively dense, hot gas halo, conformity might simply reflect an enhanced early type fraction of satellites due to ram pressure stripping. However, as we have argued above, if ram pressure stripping is the dominant process responsible for type transformations, one would expect that, at given halo mass, the early type fraction decreases with increasing satellite luminosity, opposite to what is observed. Alternatively, conformity might be related to strangulation, in which case satellites in haloes with a late type central galaxy need to have been accreted more recently (so that their SFRs are not yet completely quenched). It is unclear, however, why this would be the case. The final nurture process that we have discussed in this work, harassment, does not seem to provide a natural explanation for conformity either: there is no obvious reason why haloes with an early type central should have an enhanced harassment rate compared to haloes of the same mass, but with a late type central.

Clearly, galactic conformity poses an intriguing, new challenge for galaxy formation models. It remains to be seen whether the latest semi-analytical models that include AGN feedback (Croton et al. 2005) can explain conformity, or whether additional, new model ingredients are required.

2.6.3 The Physical Nature of Intermediate Type Galaxies

We have shown that the fraction of intermediate type galaxies is ~ 0.2, independent of luminosity, independent of halo mass, independent of halo-centric radius, and independent of whether the galaxy is a central galaxy or a satellite. Intermediate type galaxies are defined as galaxies that are 'active', yet 'red' (both with respect to the magnitude-dependent bimodality scales). They occupy the region in the colour-SSFR plane where the early and late type branches overlap. Therefore, it seems natural to assume that they consist of a mix of dusty late types (probably due to an edge-on appearance, which enhances the amount of extinction) and early types with a SSFR that is overestimated. As discussed in Brinchmann et al. (2004), the star formation rate of galaxies with colours redder than ${}^{0.1}(g-r) \simeq 0.7$ are uncertain by an order of magnitude, due to degeneracies between age, metallicity and dust.

One might worry that the intermediates are mainly a class of galaxies for which the colour and/or SSFR has not been well determined. In particular, Brinchmann et al. (2004) identified two 'classes' of galaxies for which the determination of the SSFR is likely to be less certain. These are the AGN, identified as such in the BPT diagram (Baldwin, Phillips & Terlevich 1981), and the galaxies which Brinchmann et al. termed 'unclassifiable' and which have no or very weak emission lines. For both of these classes the SSFR has been determined using the measured D4000 value, rather than the emission lines. We find that ~ 25 percent of all AGN and ~ 25 percent of all 'unclassifiable' galaxies end up as 'intermediates' with our classification. Note that this is very close to the overall fraction of intermediates (20.1 percent), indicating that neither the AGN nor the unclassifiable galaxies end up predominantly as intermediates. This is further strengthened by the following statistics: of the late types 7% are AGN and 3.8% are 'unclassifiable'; of the early types 18.8% are AGN and 61.8% are 'unclassifiable'; of the intermediate types 22% are AGN and 38.6% are 'unclassifiable'. Clearly, the intermediates are not overrepresented by either AGN or galaxies that are 'unclassifiable'.

If the intermediate types are predominantly early (late) types, their halo occupation statistics should reflect those of the early (late) types, which they clearly do not. Therefore, if indeed the intermediate types consist of early and late types, their fractional contribution must be close to 50 percent at all luminosities, in haloes of all masses, and at all halo-centric radii. This seems extremely contrived. However, alternative explanations seem even more implausible. For example, if the intermediate types are a class of galaxies that are truly distinct from early and/or late types, it is at least as puzzling why they account for 20 percent of all galaxies independent of luminosity, mass, or radius. Clearly, a more in-depth investigation regarding the nature of this class of galaxies is required to provide more insight into their nature.

2.7 Summary

Using the halo-based group finder of Yang et al. (2005a), we have constructed a large galaxy group catalogue from the SDSS NYU-VAGC of Blanton et al. (2005a). Group (halo) masses are determined from the group luminosity, which, as we have demonstrated, yields more reliable halo masses than using the velocity dispersion of the group members. Our catalogue also contains 'groups' (haloes) with only a single member. This allows us to consider a significantly larger dynamic range of halo masses. The final catalogue consists of

$\sim 92,000$ galaxies in $\sim 53,000$ groups with masses $M \gtrsim 3 \times 10^{11} h^{-1}\,\mathrm{M}_\odot$. For 97 percent of these galaxies we have obtained the stellar masses and SFRs from the catalogues of Kauffmann et al. (2003) and Brinchmann et al. (2004), respectively.

In this first work in a series, we have investigated the correlation between various galaxy properties and halo mass. Using the magnitude dependent bimodality scale in the colour-magnitude relation we have split the population of galaxies into 'red' and 'blue' subsamples. In addition, we have used the relation between magnitude and SSFR to split the galaxies into 'active' and 'passive'. The majority of galaxies are either 'red' and 'passive' (we call these early types) or 'blue' and 'active' (which we call late types). About 20 percent of all galaxies, however, are 'red' and 'active', while only one percent are 'blue' and 'passive'. Except for this latter minority class, galaxies follow a tight correlation between colour and SSFR, with two distinct branches: one populated by early types, the other by late types. These two branches overlap at ${}^{0.1}(g-r) \sim 0.9$ and $\log(\mathrm{SSFR}/\mathrm{yr}^{-1}) \sim -10.2$, where the 'red' and 'active' galaxies are located. Without further information it is unclear whether these are a physically distinct class of galaxies, or whether they are mainly early types (probably with an overestimated SSFR) or mainly late types (probably edge-on disks). Therefore, we have provisionally called them intermediate types.

Using our group catalogue, we have investigated the various type fractions as function of halo mass, halo-centric radius, and central galaxy type. The main results are:

- The early (late) type fraction increases (decreases) strongly with increasing luminosity. This luminosity dependence is stronger for central galaxies than for satellite galaxies (Section 2.5.1).

- At fixed halo mass, the early type fraction increases only weakly with increasing luminosity. Most of the luminosity dependence is only evident at the bright and faint end. In the regime $0.25 \lesssim L/L^* \lesssim 2.5$ the luminosity dependence is insignificant. This holds over the entire mass range probed ($10^{12} h^{-1}\mathrm{M}_\odot \leq M \leq 10^{15} h^{-1}\mathrm{M}_\odot$), and implies that halo mass is more important for determining the properties of a galaxy than is galaxy luminosity. A significant part of the strong luminosity dependence is simply a reflection of the fact that more luminous galaxies reside in more massive haloes (Section 2.5.2).

- At fixed luminosity, the early (late) type fraction increases (decreases) with increasing halo mass. Most importantly, we find that this mass dependence is smooth and that it persists over the entire mass range probed: *there is no break or feature at any mass scale*. This differs from previous work. In particular, various studies have found that the environment dependence becomes weaker, or completely vanishes, below a characteristic density scale. This has been interpreted as indicating that group-specific processes are the dominant cause of type transformations. We have argued, however, that this characteristic scale merely reflects the scale at which the physical meaning of the density estimator transits from a local density ($R < R_{\mathrm{vir}}$) estimator to a global, large scale density ($R > R_{\mathrm{vir}}$) estimator. Our results, based on halo masses, find no indication whatsoever that group- and/or cluster-specific processes play a dominant role in type transitions (Section 2.5.2).

- The early (late) type fraction decreases (increases) with increasing halo-centric radius. Contrary to previous studies, who found no radius dependency in haloes with

$M \lesssim 10^{13.5} h^{-1}\,\mathrm{M}_\odot$, we find a self-similar dependence in haloes of all masses probed ($10^{12} h^{-1}\,\mathrm{M}_\odot \leq M \leq 10^{15} h^{-1}\,\mathrm{M}_\odot$). This discrepancy is most likely due to the fact that previous studies included the central galaxies and were based on significantly smaller samples (Section 2.5.3).

- The intermediate type fraction is ~ 20 percent, independent of luminosity, independent of halo mass, independent of halo-centric radius, and independent of whether the galaxy is a central galaxy or a satellite galaxy. Probably the easiest explanation is that intermediates consist of an equal mix of early and late types. Although consistent with the fact that intermediate types lie in the region in the colour-SSFR plane where the early and late type branches overlap, it is extremely puzzling that the fractional mix does not scale with luminosity, halo mass, or halo-centric radius. A more in-depth study is required to investigate the nature of this class of galaxies in more detail (Sections 2.5.2 and 2.5.3).

- The properties of a satellite galaxy are strongly correlated with those of its central galaxy. In particular, we have shown that the early type fraction of satellites is significantly higher for a halo with an early type central galaxy than for a halo *of the same mass* but with a late type central galaxy. This phenomenon, which we call 'galactic conformity', is present in haloes of all masses and for satellites of all luminosities (Section 2.5.4).

- The median physical properties of late, early, and intermediate type galaxies of a given luminosity do not depend on halo mass. The relative fractions of these types, however, do. Since different galaxy types have different median properties, this halo mass dependence of the type fractions causes a halo mass dependence of the median properties of the full galaxy population (Section 2.5.5).

We have discussed the possible implication of these findings for our understanding of galaxy formation and evolution. Using simple scaling arguments, we have argued that both ram pressure stripping and galaxy harassment are not the major processes responsible for galaxy transformations, as they predict an increasing late type fraction with increasing luminosity in haloes of fixed mass, opposite to what is observed. We therefore suggest that merger history and strangulation (i.e., the quenching of star formation as soon as a galaxy becomes a satellite galaxy) are the main ingredients required to predict whether a galaxy ends up as an early or a late type galaxy.

This conclusion, however, is still extremely speculative. For example, it still needs to be seen, whether the semi-analytical models that use strangulation and the merger history to predict galaxy types, are indeed consistent with the various observational trends presented here. In particular, we have argued that galactic conformity poses an intriguing new challenge for galaxy formation models. Although the correlations between galaxy properties and halo mass presented here provide an interesting testbed for galaxy formation models, a definite explanation for the origin of the bimodality of galaxy properties will most likely have to await a similar analysis as performed here, but at different epochs (i.e., different redshifts). It is reassuring that promising work in this direction is already under way (e.g., Gerke et al. 2005; Cooper et al. 2005).

2.8 Acknowledgements

We are extremely grateful to Michael Blanton, Guinevere Kauffmann, Jarle Brinchmann and all other people within the SDSS collaboration for producing a wonderful data set and for making their various catalogues publicly available. Michael Blanton is also acknowledged for his help with the NYU-VAGC, and the anonymous referee and David Wilman for their helpful comments that greatly helped to improve the presentation. Frank van den Bosch acknowledges useful discussions with Eric Bell, Aaron Dutton, and Anna Pasquali.

Chapter 3

Galaxy Groups in the SDSS: The Dependence of Galaxy Type on AGN Feedback and Star Formation Truncation[1]

In answer to the question of why it happened, I offer the modest proposal that our Universe is simply one of those things which happen from time to time.

Edward P. Tryon

3.1 Abstract

Successfully reproducing the galaxy luminosity function and the bimodality in the galaxy distribution requires a mechanism that can truncate star formation in massive haloes. Current models of galaxy formation consider two such truncation mechanisms: strangulation, which acts on satellite galaxies, and AGN feedback, which predominantly affects central galaxies. The efficiencies of these processes set the blue fraction of galaxies, $f_{\rm blue}(L, M)$, as function of galaxy luminosity, L, and halo mass, M. In this paper we use a galaxy group catalogue extracted from the Sloan Digital Sky Survey (SDSS) to determine $f_{\rm blue}(L, M)$. To demonstrate the potential power of these data as a benchmark for galaxy formation models, we compare the results to the semi-analytical model for galaxy formation of Croton et al. (2006). Although this model accurately fits the *global* statistics of the galaxy population, as well as the shape of the conditional luminosity function, there are significant discrepancies when the blue fraction of galaxies as a function of mass and luminosity is compared between the observations and the model. In particular, the model predicts (i) too many faint satellite galaxies in massive haloes, (ii) a blue fraction of satellites that is much too low, and (iii) a blue fraction of centrals that is too high and with an inverted luminosity dependence. In the same order, we argue that these discrepancies owe to (i)

[1]This chapter has been published in MNRAS (Weinmann et al., 2006b)

the neglect of tidal stripping in the semi-analytical model, (ii) the oversimplified treatment of strangulation, and (iii) improper modeling of dust extinction and/or AGN feedback. The data presented here will prove useful to test and calibrate future models of galaxy formation and in particular to discriminate between various models for AGN feedback and other star formation truncation mechanisms.

3.2 Introduction

One of the most challenging outstanding problems in galaxy formation is to explain the detailed shape of the galaxy luminosity function (hereafter LF). In particular, the relatively shallow faint-end slope and the exponential cut-off at the bright end of the LF have proven difficult to explain (e.g., White & Frenk 1991; Benson et al. 2003). In the traditional scenario for galaxy formation, it is envisioned that lower cooling efficiencies in massive galaxies would explain the exponential tail of the LF (Rees & Ostriker 1977; Silk 1977; White & Rees 1978), while supernova feedback is typically invoked to reduce the star formation efficiency in low mass haloes (Larson 1974; White & Rees 1978; Dekel & Silk 1986). Although the latter can indeed be tuned to reproduce the faint-end slope of the galaxy LF, it worsens the problems at the bright end. As nicely demonstrated by Benson et al. (2003), supernova feedback causes a drastic increase of the amount of diffuse hot gas that remains in larger halos. This gas is able to cool onto the central galaxies in these haloes, producing too many bright galaxies. In addition, this causes the bright model galaxies to have relatively young stellar populations, in disagreement with observations (e.g., Kauffmann & Charlot 1998; Heavens et al. 2004; Thomas et al. 2005). What is needed is a mechanism that can truncate the star formation in these massive, central galaxies at relatively late times.

Star formation truncation is also the main mechanism that is thought to underlie the bimodality of galaxy properties. The local population of galaxies consists roughly of two types: red galaxies, which reveal an early type morphology and which have very little or no ongoing star formation, and blue galaxies with active star formation and a late-type morphology (e.g., Strateva et al. 2001; Blanton et al. 2003a; Kauffmann et al. 2003, 2004; Baldry et al. 2004; Brinchmann et al. 2004; Balogh et al. 2004a,b). Although a non-negligible fraction of red galaxies are clearly edge-on disk galaxies that owe their red colour to an enhanced extinction, the most pronounced distinction between 'red sequence' and 'blue sequence' galaxies is their current star formation rate. Since only relatively small amounts of ongoing star formation tend to make a galaxy appear 'blue', the colour bimodality basically reflects star formation truncation: red sequence galaxies have their star formation truncated, while blue sequence galaxies are still forming stars today.

Semi-analytical models for galaxy formation consider a number of mechanisms that can prevent, delay or truncate star formation. In low mass haloes one typically invokes reionization and supernova feedback in order to suppress or truncate star formation. In haloes with $M \gtrsim 10^{12} h^{-1}\,\mathrm{M}_{\odot}$, on which we will focus in this work, two additional truncation effects are considered. The first one, called strangulation, only affects satellite galaxies. As soon as a dark matter halo is accreted by a larger halo, its central galaxy becomes a satellite galaxy. It is often assumed that this accretion process causes the satellite galaxy to be stripped of its hot gas reservoir. Consequently, after a delay time in which the galaxy consumes (part of) its cold gas, star formation is truncated, and the

satellite galaxy becomes red (Larson, Tinsley & Caldwell 1980; Balogh, Navarro & Morris 2000). Ram-pressure stripping (Gunn & Gott 1972) may shorten the time-delay, by also stripping the satellite of its cold gas reservoir, but since the time scale for strangulation is already relatively short, the addition of ram-pressure stripping does not have a large impact. Virtually all semi-analytical models of galaxy formation, starting with Kauffmann, White & Guiderdoni (1993), have taken this strangulation mechanism into account. In fact, it is the main mechanism that causes red-sequence model galaxies to preferentially reside in overdense regions such as groups and clusters of galaxies, in good agreement with observations (e.g. Oemler 1974; Dressler 1980; Hogg et al. 2004; Balogh et al. 2004b; Weinmann et al. 2006).

The second star formation truncation mechanism that operates in massive haloes is feedback from active galactic nuclei (AGN), which predominantly affects central galaxies. Although the potential importance of AGN feedback has long been recognized (e.g., Tabor & Binney 1993; Ciotti & Ostriker 1997), it only recently has been given serious consideration in galaxy formation models. This has largely been motivated by X-ray observations which reveal that AGN can indeed impact the hot IGM of galaxy clusters (e.g., Fabian et al. 2003; McNamara et al. 2005). Numerous recent studies have demonstrated that the inclusion of AGN feedback in galaxy formation models can help to explain the bright end exponential cut-off of the galaxy luminosity function (e.g. Granato et al. 2004; Croton et al. 2006; Cattaneo et al. 2006; Sijacki & Springel 2005; Bower et al. 2006) and the fact that the most massive galaxies contain the oldest stars (Croton et al. 2006; Scannapieco, Silk & Bouwens 2005; Bower et al. 2006).

Despite these successes, we are still far from a proper understanding of how AGN feedback may establish an equilibrium state where it can efficiently suppress star formation in the centers of massive haloes. In the studies mentioned above, AGN feedback is typically modeled using oversimplified, heuristic scaling relations, often based on very different views of how AGN feedback might operate. In particular, it is still unclear which mode of AGN activity is most important for the star formation truncation discussed above; the merger induced 'quasar mode' which leads to an initial starburst followed by a quenching of star formation, or the 'radio mode', which is caused by continual and quiescent accretion of hot gas onto the central supermassive black hole. Hopkins et al. (2006) have suggested that merger-induced AGN activity (the 'quasar mode') is responsible for the transition from blue, star forming to red, passive galaxies. Springel, Di Matteo & Hernquist (2005a), Menci et al. (2005) and Kang, Jing & Silk (2005) have shown that this 'quasar mode' feedback can indeed terminate star formation and expel the gas from the center of the galaxy, once the supermassive black holes become sufficiently massive. On the other hand, Croton et al. (2006), Bower et al. (2006), Cattaneo et al. (2006), Nusser et al. (2006) and Sijacki & Springel (2006) have argued that the 'radio mode' of AGN activity (or AGN feedback operating in quasi-hydrostatically cooling haloes) is the main mechanism to truncate star formation in massive galaxies. How exactly this radio mode feedback operates, however, is still unclear, as is evident from the fact that the aforementioned studies all use very different formulations.

All these different AGN feedback models mainly differ in the way in which the feedback efficiency scales with halo mass and with galaxy properties such as black hole mass and gas mass fraction. Since AGN feedback causes star formation truncation, one way to discriminate between these various models is therefore to investigate the relative fractions of blue and red galaxies as function of halo mass and galaxy properties. Such a study will

also help to improve our understanding of strangulation, the star formation truncation mechanism for satellites. Although strangulation is typically modeled as being independent of halo mass, one might argue that the ability of a host halo to strip a subhalo of its hot gas reservoir depends on the presence and density of the hot corona of the host halo, which in turn may well be mass dependent. Again, knowledge of the fractions of blue and red (satellite) galaxies as function of halo mass should allow us to discriminate between these different possibilities.

Nowadays, with large galaxy surveys, such as the Two Degree Field Galaxy Redshift Survey (Colless et al. 2001) and the Sloan Digital Sky Survey (York et al. 2000), the number of galaxies is sufficiently large that, in principle, one could accurately measure the red and blue fractions as a function of various variables. In this work, we use our SDSS group catalogue, presented in Weinmann et al. (2006, hereafter paper I), to compute the fractions of blue and red galaxies as function of both halo mass and galaxy luminosity. To emphasize the potential constraining power of these data we compare our results to the semi-analytical galaxy formation model of Croton et al. (2006), which includes both strangulation and 'radio-mode' AGN feedback. We show that although this model accurately fits the galaxy luminosity function, the color-bimodality, and many other *global* statistics of the galaxy population, it fails dramatically when it comes down to the blue fraction of galaxies as a function of halo mass and luminosity. We argue that this has its origin in the way that strangulation and AGN feedback have been incorporated and we briefly discuss possible modifications. The aim of this work, however, is not to present a new, improved model for star formation truncation, but merely to present observational constraints that will hopefully prove useful in discriminating between the various models.

This chapter is organized as follows. Section 3.3 describes our SDSS group catalogue, which we compare to a similar group catalogue extracted from the semi-analytical model of Croton et al. (2006) described in Section 3.4. The actual comparison is presented in Section 3.5, while Section 3.6 discusses the possible implications for galaxy formation models. We summarize our results in Section 3.7.

3.3 The SDSS Group Catalogue

3.3.1 Data

The Sloan Digital Sky Survey (SDSS; York et al. 2000) is a joint, five passband (u, g, r, i and z) imaging and medium-resolution ($R \sim 1800$) spectroscopic survey. In this work, we focus on the subset of galaxies that are in the New York University Value-Added Galaxy Catalogue (NYU-VAGC) based on the SDSS Data Release 2 (Blanton et al. 2005). This NYU-VAGC is based on an independent, significantly improved data reduction. From this catalogue we select all galaxies with an extinction corrected apparent magnitude brighter than $r = 17.77$, with redshifts in the range $0.01 \leq z \leq 0.20$, and with a redshift completeness $\mathcal{C} > 0.7$. This leaves a grand total of $184,425$ galaxies. In what follows, we use M_r and ${}^{0.1}M_r$ to indicate the absolute magnitude in the r-band, k-corrected to $z = 0$ and $z = 0.1$, respectively. All k-corrections are based on the model described in Blanton et al. (2003b).

We split the galaxies into 'red' and 'blue' subsamples using a magnitude dependent cut, which roughly follows the observed bimodality scale in the colour-magnitude relation:

$$ {}^{0.1}(g-r)_{\rm cut} = 0.7 - 0.032 \left[{}^{0.1}M_r + 16.5 \right] \tag{3.1} $$

(cf. paper I). In what follows, we refer to galaxies that are redder and bluer than $^{0.1}(g-r)_{\rm cut}$ as 'red' and 'blue' galaxies, respectively.

3.3.2 The group-finding algorithm

Our working definition of a galaxy group is the ensemble of galaxies that reside in the same dark matter parent halo; galaxies that reside in subhaloes are considered to be group members that belong to the parent halo in which the subhalo is located. We have used the halo-based group finder developed by Yang et al. (2005a, hereafter YMBJ) in order to group the galaxies in the above mentioned galaxy catalogue. This particular group finder has been optimized to group galaxies according to their common dark matter halo, and has been thoroughly tested with mock galaxy redshift surveys. In brief, the method works as follows. First, potential group centers are identified using a Friends-Of-Friends (FOF) algorithm or an isolation criterion. Next, the total group luminosity is estimated which is converted into an estimate for the group mass using an assumed mass-to-light ratio. From this mass estimate, the radius and velocity dispersion of the corresponding dark matter halo are estimated using the virial equations, which in turn are used to select group members in redshift space. This method is iterated until group memberships converge. A more detailed description is given in Appendix A.

In YMBJ the performance of this group finder has been tested in terms of completeness of true members and contamination by interlopers, using detailed mock galaxy redshift surveys. The average completeness of individual groups was found to be ~ 90 percent, with only ~ 20 percent interlopers. Furthermore, the resulting group catalogue is insensitive to the initial assumption regarding the mass-to-light ratios, and the group finder is more successful than the conventional FOF method (e.g., Huchra & Geller 1982; Ramella, Geller & Huchra 1989; Merchán & Zandivarez 2002; Eke et al. 2004; Berlind et al. 2006) in associating galaxies according to their common dark matter haloes.

3.3.3 Estimating group masses

Following YMBJ we use the group luminosity to assign masses to our groups. The motivation behind this is that one naturally expects the group luminosity to be strongly correlated with halo mass (albeit with a certain amount of scatter). Since the group luminosity is dominated by the brightest members, which are exactly the ones that can be observed in a flux limited survey like the SDSS, the determination of the (total) group luminosity is more robust than that of the group's velocity dispersion, especially when the number of group members is small (see Appendix B in paper I).

Clearly, because of the flux limit of the SDSS, two identical groups observed at different redshifts will have a different $L_{\rm group}$, defined as the summed luminosity of all its identified members. To circumvent this bias we first need to bring the group luminosities to a common scale. A nearby group selected in an apparent magnitude limited survey should contain all of its members down to a faint luminosity. We can therefore use these nearby groups to determine the relation between the group luminosity obtained using only galaxies above a bright luminosity limit and that obtained using galaxies above a fainter luminosity limit. Assuming that this relation is redshift-independent, one can correct the luminosity of a high-z group, where only the brightest members are observed, to an empirically normalized luminosity scale.

As common luminosity scale we use $L_{19.5}$, defined as the luminosity of all group members brighter than ${}^{0.1}M_r = -19.5 + 5\log h$. To calibrate the relation between $L_{\rm group}$ and $L_{19.5}$ we first select all groups with $z \leq 0.09$, which corresponds to the redshift for which a galaxy with ${}^{0.1}M_r = -19.5 + 5\log h$ has an apparent magnitude that is equal to the magnitude limit of the survey. For groups with $z > 0.09$ we use this 'local' calibration between $L_{\rm group}$ and $L_{19.5}$ to estimate the latter. Detailed tests have shown that the resulting group luminosities are significantly more reliable than those in which the correction for missing members is based on the assumption of a universal luminosity function (see YMBJ for details).

The final step is to obtain an estimate of the group (halo) mass from $L_{19.5}$. This is done using the assumption that there is a one-to-one relation between $L_{19.5}$ and halo mass. For each group we determine the number density of all groups brighter (in terms of $L_{19.5}$) than the group in consideration. Using the halo mass function corresponding to a ΛCDM concordance cosmology with $\Omega_m = 0.3$, $\Omega_\Lambda = 0.7$, $h = H_0/(100\,{\rm km\,s^{-1}\,Mpc^{-1}}) = 0.7$ and $\sigma_8 = 0.9$ we then find the mass for which the more massive haloes have the same number density. Although the masses thus derived depend on cosmology, it is straightforward to convert the masses derived here to any other cosmology.

Finally we note that not all groups can have a halo mass assigned to them. First of all, the mass estimator described above does not work for groups in which all members are fainter than ${}^{0.1}M_r = -19.5 + 5\log h$. Secondly, the combination of $L_{19.5}$ and redshift may be such that we know that the halo catalogue is incomplete, which means that there is a significant number of groups at this redshift with the same $L_{19.5}$ but for which the individual galaxies are too faint to be detected. Since our mass assignment is based on the assumption of completeness, any group beyond the completeness redshift corresponding to its $L_{19.5}$ is not assigned a halo mass (see Yang et al. 2005b for details).

3.3.4 The SDSS group catalogue

Applying our group finder to the sample of SDSS galaxies described in Section 3.3.1 yields a group catalogue of 53,229 systems with an estimated mass. These groups contain a total of 92,315 galaxies. The majority of the groups (37,216 systems) contain only a single member, while there are 9220 binary systems, 3073 triplet systems, and 3720 systems with four members or more (see paper I for details)[1]. In what follows we refer to the brightest galaxy in each group as the 'central' galaxy, while all others are termed 'satellites'.

3.4 The Semi-Analytic Model

The semi-analytic model (hereafter SAM) to which we compare the SDSS group catalogue discussed above is based on an output of the Millennium Run N-body simulation (Springel et al. 2005b) and is described in detail in Croton et al. (2006; hereafter C06). The simulation is based on the cosmological parameters $\Omega_m = 0.25$, $\Omega_\Lambda = 0.75$, $\Omega_b = 0.045$, $h = 0.73$ and $\sigma_8 = 0.9$ and has a volume of $0.125h^{-3}{\rm Gpc}^3$. Dark matter haloes are identified with a FOF group finder, and subsequently populated with galaxies following the semi-analytical model described in C06.

[1]This SDSS group catalogue is publicly available at http://www.astro.umass.edu/~xhyang/Group.html

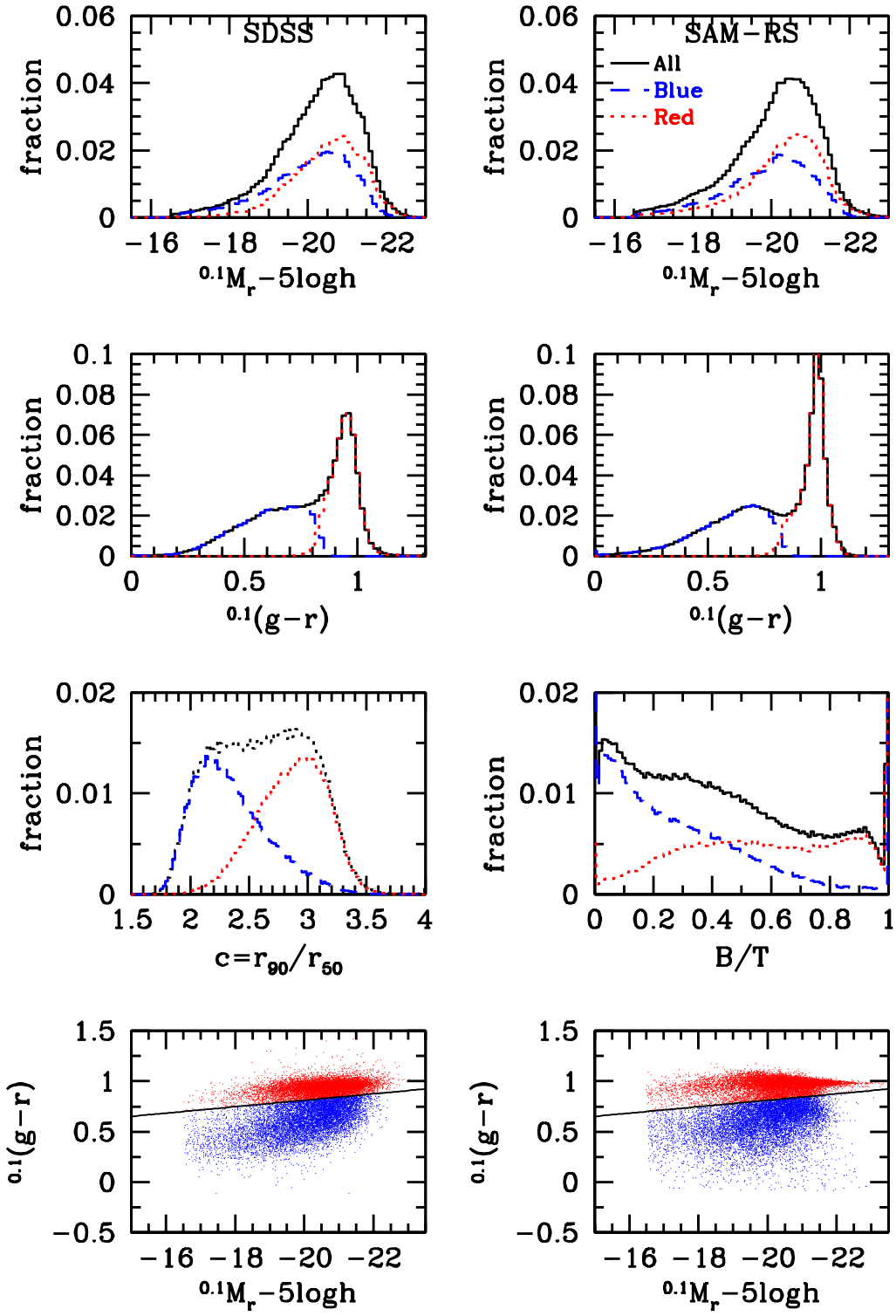

Figure 3.1: *A comparison of global statistics of the SAM-RS (right-hand panels) with the SDSS (left-hand panels). Panels in the first and second row show histograms of absolute* $^{0.1}r$*-band magnitude and* $^{0.1}(g-r)$ *colour for both redshift surveys. The contributions from blue and red galaxies are indicated by dashed and dotted lines, respectively. Note the good agreement between SDSS and SAM-RS. Panels in the third row show histograms of morphological parameters. In the case of the SDSS, we plot the distribution of the concentration parameter c, defined as the ratio of the radii containing 90 and 50 percent of the petrosian flux. In the case of the SAM-RS, we plot the distribution of the bulge-to-total mass ratio* B/T *instead. Although these can not be compared directly, in general a more concentrated galaxy (higher c) will also have a larger* B/T*. Again, the contributions from red and blue galaxies are indicated. Finally, the fourth row of panels shows the colour-*

One of the relative novelties of this SAM is the inclusion of 'radio mode' feedback from AGN that lie at the center of a halo with a static corona of hot gas. As shown in C06, this feedback mode suppresses the cooling flow in massive haloes at relatively late times, which in turn yields luminosities, colours and stellar ages for massive galaxies in better agreement with observations. In particular, the inclusion of the radio-mode AGN feedback can explain the exponential cut-off at the bright end of the galaxy luminosity function, and the fact that the most massive galaxies are red and consist of old stellar populations (see De Lucia et al. 2006 for details). The model also predicts star formation histories, cold gas mass fractions and metallicities that are all in good agreement with observations. The model even predicts a Tully-Fisher zero-point that matches the data, as long as the rotation velocity of a disk galaxy is equal to the maximum circular velocity of the dark matter halo (however, see Dutton et al. 2007 for the unorthodox implications of this assumption).

Since the halo masses M assigned to our SDSS galaxy groups are obtained by matching the abundances to the halo mass function, these are to be interpreted as the masses inside a radius with an overdensity of 180. As shown by Jenkins et al. (2001), for this definition of halo mass the analytical halo mass function of Sheth, Mo & Tormen (2001) used here is in good agreement with the halo mass function obtained from numerical simulations. The halo masses in the C06 catalogue, however, are defined as the masses inside a radius with a mean density that is 200 times the critical density, which we denote by M_{200}. In order to convert M_{200} to M, we assume that dark matter haloes follow a NFW density distribution (Navarro, Frenk & White 1997). Using the relation between halo mass and halo concentration of Eke, Navarro & Steinmetz (2001), we find that the relation between M and M_{200} is well fit by

$$\frac{M_{200}}{M} = 0.745 - 0.0006\ [\log(M_{200}) - 7.0]^{2.45}\ . \tag{3.2}$$

In what follows, we only consider the galaxies with $M_r \leq -16.72$, which reflects the magnitude completeness limit of the SAM, yielding a total of approximately 9 million model galaxies. The main information used in this work are the r band and g band magnitudes of these galaxies, and the mass M of the halo in which they reside. For comparison with the SDSS, we also compute the g and r-band magnitudes k-corrected to $z = 0.1$, using

$$^{0.1}g = g + 0.3113 + 0.4620\ (g - r - 0.6102) \tag{3.3}$$

and

$$^{0.1}r = g - 0.4075 - 0.8577\ (g - r - 0.6102) \tag{3.4}$$

(Blanton et al. 2003b)[2].

As we will see below, despite the AGN feedback the SAM still contains a significant number of very bright and blue galaxies that are not present in the SDSS. As mentioned in C06, these are mainly ULIRG-type starbursts for which the dust treatment of the model is inadequate; with a more proper dust model, these galaxies would be much more extincted, making them both fainter and redder. In order to suppress the impact of these galaxies on our SAM-SDSS comparison we remove all galaxies with $(g - r) < 0$ from both the SAM

[2]These filter transformations are taken from a manuscript in preparation by Michael Blanton and Sam Roweis, available at http://cosmo.nyu.edu/blanton/kcorrect

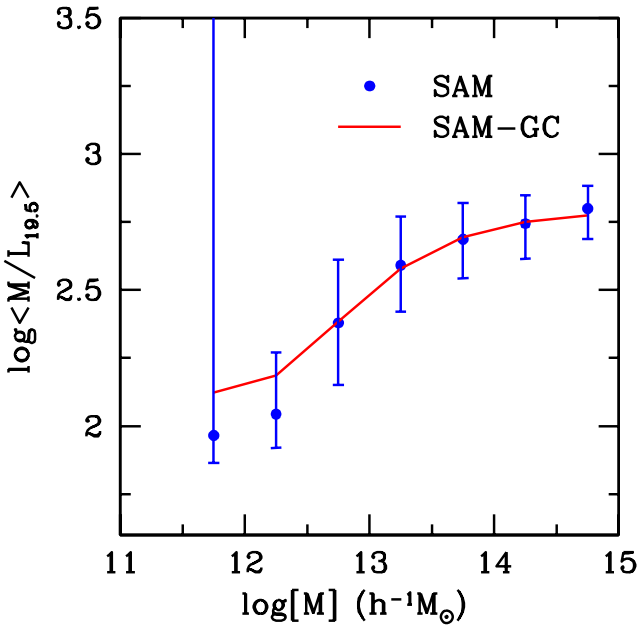

Figure 3.2: *The average mass-to-light ratio, $\langle M/L_{19.5}\rangle$ as a function of halo (group) mass. Here $L_{19.5}$ is the total luminosity of all galaxies in a halo with ${}^{0.1}M_r - 5\log h \leq -19.5$. Filled circles with errorbars (indicating the 68 % confidence level) show the results obtained from the SAM directly, using the original halo masses and halo membership. The solid line shows the $\langle M/L_{19.5}\rangle$ as obtained from the SAM group catalogue, and is thus based on the assigned group masses and the assigned group memberships. The agreement with the true $\langle M/L_{19.5}\rangle$ is excellent, indicating that our group finder allows an accurate recovery of the average relation between mass and light.*

and the SDSS. In the case of the SAM this only affects 0.5 percent of all galaxies, while in the case of the SDSS, this fraction is completely negligible.

We split the SAM model galaxies into 'red' and 'blue' subsamples using the same magnitude dependent colour-cut as for the SDSS, given by equation (3.1). In addition, we discriminate between 'central' galaxies, defined as the galaxy in a halo that is closest to the halo center, and 'satellite' galaxies. This differs from the definition used for the group catalogues, where the central galaxy is defined as the brightest group member. However, 97.5 percent of all central galaxies in the SAM are also the brightest galaxy in their halo, virtually independent of halo mass. We have verified that defining central galaxies in the SAM as the brightest halo members instead does not have a significant impact on any of our results.

3.4.1 Constructing a SAM redshift survey

In order to be able to compare the SAM to the SDSS results we need to mimic the construction of a galaxy redshift survey. We do so using the following steps. First, we construct a large virtual universe by replicating the periodic simulation box in a stack of $2 \times 2 \times 2$ boxes. This is required in order to be able to probe out to sufficiently high redshifts. Next we compute the redshift and apparent magnitude of each galaxy as seen by a virtual observer located in a corner of this virtual universe (who can thus see $\pi/2$

steradian of 'sky'). We mimic the selection criteria of the SDSS discussed in Section 3.3.1 by only selecting those galaxies with $0.01 < z < 0.2$ and with $r < 17.77$. This leaves us with a grand total of 428,013 model galaxies. In what follows, we refer to this sample as the "SAM redshift survey" (hereafter SAM-RS).

Fig. 3.1 compares a number of statistics of these galaxies with those from the SDSS. The upper panels plot the distribution of absolute magnitudes, ${}^{0.1}M_r$, and their contribution due to red (dotted curves) and blue (dashed curves) galaxies. The agreement is very satisfactory, consistent with the fact that the SAM matches the observed luminosity functions (see C06). The second row of panels indicate the color distributions. Once again, the agreement is reasonable, although the bimodality in the SAM-RS seems somewhat more pronounced than in the SDSS, with a somewhat narrower 'red peak'. Nevertheless, with blue fractions of 48 and 46 percent in the SDSS and SAM-RS, respectively, the overall agreement is very satisfactory.

In the third row of panels, we 'compare' two different morphology indicators. For the SDSS galaxies we plot the distribution of the concentration c, defined as the ratio between the radii that contain 90 and 50 percent of the Petrosian flux. For the SAM model galaxies, we plot the distribution of the bulge-to-total (B/T) stellar mass ratio instead. Typically, a galaxy with a large B/T will also have a high concentration parameter. For both c and B/T there is a very significant overlap of red and blue galaxies. Therefore, our split in red and blue galaxies does not necessarily correspond to a morphological split in early and late-type galaxies, respectively, even though both are clearly correlated (see Fig. 1 in paper I).

Finally, the lower panels of Fig. 3.1 show scatter plots of the color-magnitude relations. The solid line corresponds to the bimodality scale given by equation (3.1). Again, there is reasonable overall agreement between the SAM-RS and the SDSS, although there are more galaxies with very blue colours in the SAM-RS, especially at the bright end. Recall that galaxies with $(g-r) < 0$ have already been excluded from these plots. As mentioned before, these bright, blue galaxies would appear significantly fainter and redder with proper dust modeling. Another apparent discrepancy concerns the red sequence, which at the bright end appears significantly tighter for the SAM than for the SDSS, which is also apparent from the histograms in the second row of panels.

To summarize, despite some small discrepancies, the global, statistical properties of the SAM model galaxies are in good agreement with the SDSS. However, this does not mean that the SAM also predicts the correct statistics *as a function of halo mass*. This is clearly a much tighter constraint for the model, and, as we argued in Section 3.2, may provide useful insights regarding the halo-mass dependence of various physical processes.

3.4.2 Construction of the SAM group catalogue

The main goal of this work is to compare the fractions of red and blue galaxies as a function of both halo mass and luminosity in the SAM with those obtained from our SDSS group catalogue. In principle we could do so by comparing our SDSS group results directly with the SAM. However, our group finder, and in particular the algorithm used to assign the masses, is not perfect. Hence, it is unclear whether any discrepancy between SDSS group catalogue and SAM reflects an artefact of the group finder, or whether there is a true difference in the halo occupation statistics of SDSS and SAM. To circumvent this problem, we use the SAM-RS described above to construct a "SAM group catalogue" (hereafter

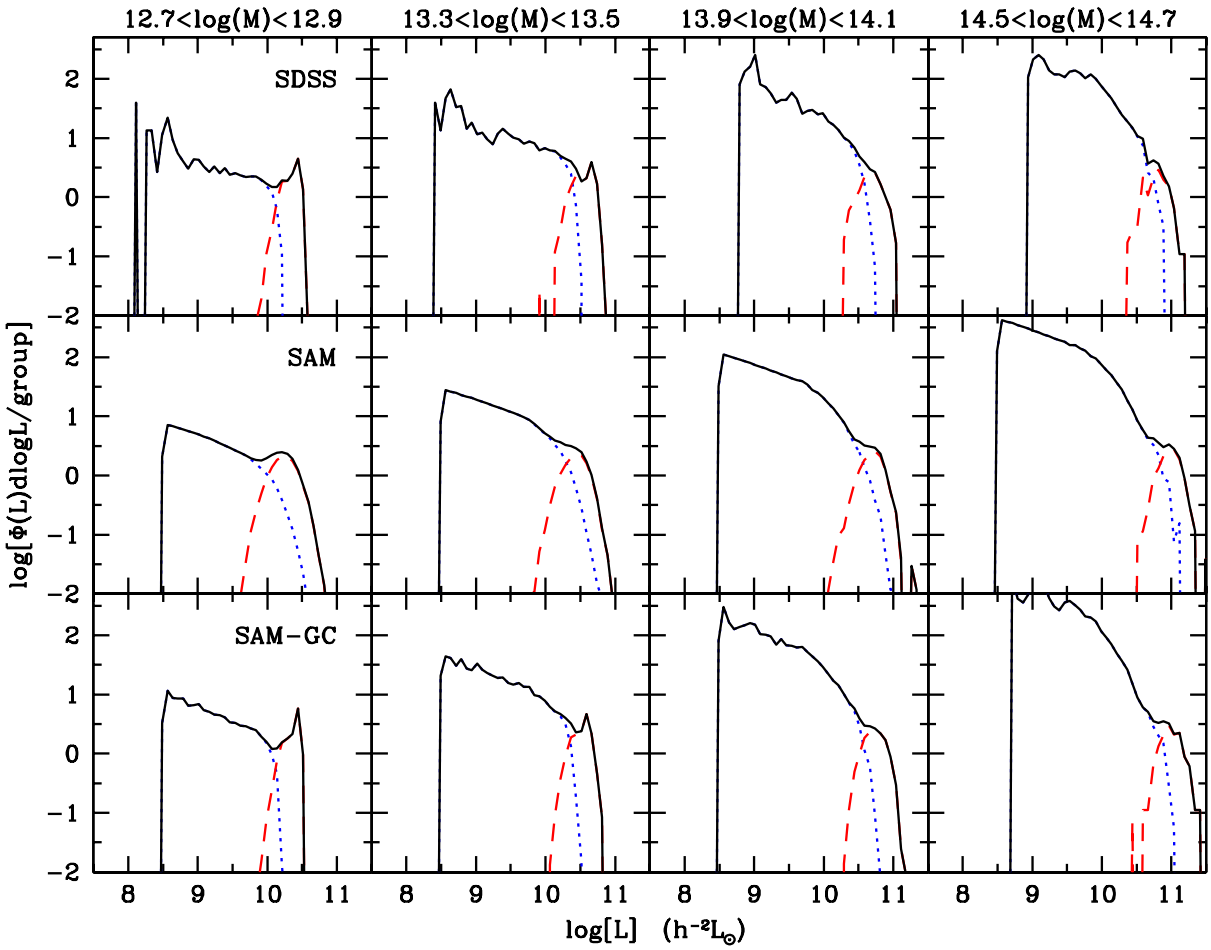

Figure 3.3: *The conditional luminosity function obtained from the SDSS group catalogue (upper panel) from the SAM directly, using true halo masses and true halo members (middle panel) and from the SAM group catalogue, using assigned group masses and assigned memberships (lower panels). Results are shown for four different mass bins (masses in* $h^{-1}\,\mathrm{M}_{\odot}$*), as indicated at the top of each column. Luminosities are in the* $^{0.1}r$*-band. The dotted (blue) line marks the contribution from the satellite galaxies, the dashed (red) line the contribution from the central galaxies.*

SAM-GC), using exactly the same group finder and mass assignment algorithm as for the SDSS. By comparing this SAM-GC with the SDSS group catalogue we significantly reduce the impact of possible inaccuracies related to the group finder, making the comparison more fair.

Application of our group finder to the SAM-RS described above yields 98,130 groups with an assigned mass, which host a total of 206,076 galaxies. This amounts to an average of 2.10 members per group, which is significantly higher than for the SDSS, where the groups with an assigned mass have on average 1.73 members. However, the SDSS is not complete; in fact, the average completeness of our SDSS sample is 0.88, which largely explains the difference in the mean number of members per group. Another reason for this discrepancy is that, as we will see, massive haloes in the SAM contain too many faint satellites compared to the SDSS.

The fraction of blue galaxies in the SAM-GC is only 29 percent. Comparing this to the fraction of 46 percent of blue galaxies in the SAM-RS indicates that a red galaxy is much more likely to be associated with a group than a blue galaxy. At first sight this seems a logical consequence of the fact that (i) our group catalogue is limited to relatively massive haloes with $M \gtrsim 5 \times 10^{11} h^{-1}\,\mathrm{M}_\odot$ and (ii) low mass haloes are more likely to host blue galaxies, see e.g. paper 1. However, the application of the group finder to the SDSS only reduces the fraction of blue galaxies from 48 percent to 41 percent. This reduction is much less severe than for the SAM. This is the first indication that the SAM and SDSS do not agree well when it comes down to details regarding the distribution of red and blue galaxies (see Section 3.5.2 below).

Since the SAM contains the full halo occupation information, we can check whether our group finder has assigned the correct galaxies to the same group, and whether the assigned mass is in agreement with the true halo mass. We have performed a large number of tests to investigate how well the group finder allows us to recover the true relations between galaxies and their dark matter haloes. Several of these tests have been described in detail in Yang et al. (2005a,b), and show that the average occupation statistic of dark matter haloes are accurately recovered. However, higher-order moments of the occupation statistics, such as the scatter around a mean relation, are typically severely underestimated by the group catalogue, due to the fact that we assume a one-to-one relation between halo mass and halo luminosity (with zero scatter) when assigning masses to our groups. As an illustration of the accuracy of our group finder, Fig. 3.2 plots the average mass-to-light ratio of the dark matter haloes in the SAM (symbols with errorbars). Here M is the halo mass defined according to equation (3.2), and L is the total luminosity in the ${}^{0.1}r$ band of all galaxies in that halo with ${}^{0.1}M_r - 5\log h \leq -19.5$. The solid line in Fig. 3.2 shows the average mass-to-light ratios obtained from the SAM-GC, which agree extremely well with the true $\langle M/L\rangle_M$. This demonstrates that our group finder can accurately recover the average relation between mass and light.

In what follows, whenever we present any result obtained from the SAM-GC, we will also present the same results extracted directly from the SAM (using the true halo masses and the true halo memberships). A comparison among these results safeguards against potential problems with the group finder.

3.5 Galaxy Ecology

3.5.1 Conditional Luminosity Functions

We start our SAM-SDSS comparison by focusing on the conditional luminosity function (CLF), $\Phi(L|M)$, which specifies the average number of galaxies of luminosity L that reside in a halo of mass M (Yang, Mo & van den Bosch 2003; van den Bosch, Yang & Mo 2003). The upper panels of Fig. 3.3 show the CLFs obtained from the SDSS group catalogue. Results are shown for four different mass bins, as indicated at the top of each column. Note that these masses are the assigned group masses. The dotted (blue) and dashed (red) lines indicate the contributions from the satellite and central galaxies, respectively. The distribution of central galaxies is well approximated by a log-normal distribution, consistent with previous findings (Zheng et al. 2005; Yang et al. 2005b). The panels in the middle row of Fig. 3.3 show the CLFs obtained directly from the SAM; here the masses are the true halo masses, and the true halo members are used to construct the CLFs. The overall agreement with the CLFs extracted from the SDSS group catalogue is very satisfactory, although the width of the CLF for central galaxies is significantly broader in the SAM than in the SDSS. To allow for a more meaningful comparison, the lower panels of Fig. 3.3 plot the CLFs obtained from the SAM-GC. The first thing to notice is that the width of the CLFs of the central galaxies are now in much better agreement with the SDSS; apparently, the group finder artificially 'narrows' the scatter in the relation between halo mass and the luminosity of the central galaxy. This simply owes to the fact that we use the group luminosity to determine the group mass. Other than that, the agreement between the CLFs obtained from the SAM-GC, and those extracted directly from the SAM is very good, indicating that our group finder allows an accurate recovery of the true $\Phi(L|M)$ (see also tests in Yang et al. 2005b).

Except for the highest mass bin, the CLFs extracted from the SDSS and the SAM group catalogues are in good agreement with each other, indicating that the SAM not only fits the galaxy luminosity function, but it even does so as function of halo mass. However, at the massive end the SAM predicts significantly more relatively faint galaxies in massive haloes then observed. In the highest mass bin shown, the SAM overpredicts the number of faint satellites with $L = 3 \times 10^9 h^{-2}\,\mathrm{L}_\odot$ by a factor ~ 2. Since these are virtually all red, early-type galaxies (see below), this suggests that the SAM overpredicts the number density of faint, red galaxies. Indeed, as already shown in C06, the SAM overpredicts the luminosity function of red galaxies at the faint end. The analysis here suggests that this largely owes to an overabundance of satellite galaxies in massive haloes with $M \gtrsim 3 \times 10^{14} h^{-1}\,\mathrm{M}_\odot$.

We emphasize that this discrepancy is not due to the fact that we have ignored fiber collisions in the SDSS. Since the spectroscopic fibers of the SDSS have a minimum angular separation of $55''$, the spectroscopic catalogue suffers from an incompleteness on small angular scales. This will impact on the multiplicity function of the groups in our catalogue. However, as shown by Berlind et al. (2006), the effect is relatively small, typically reducing the multiplicity of groups by ~ 10 percent, which is negligible compared to the factor 2 eluded to above.

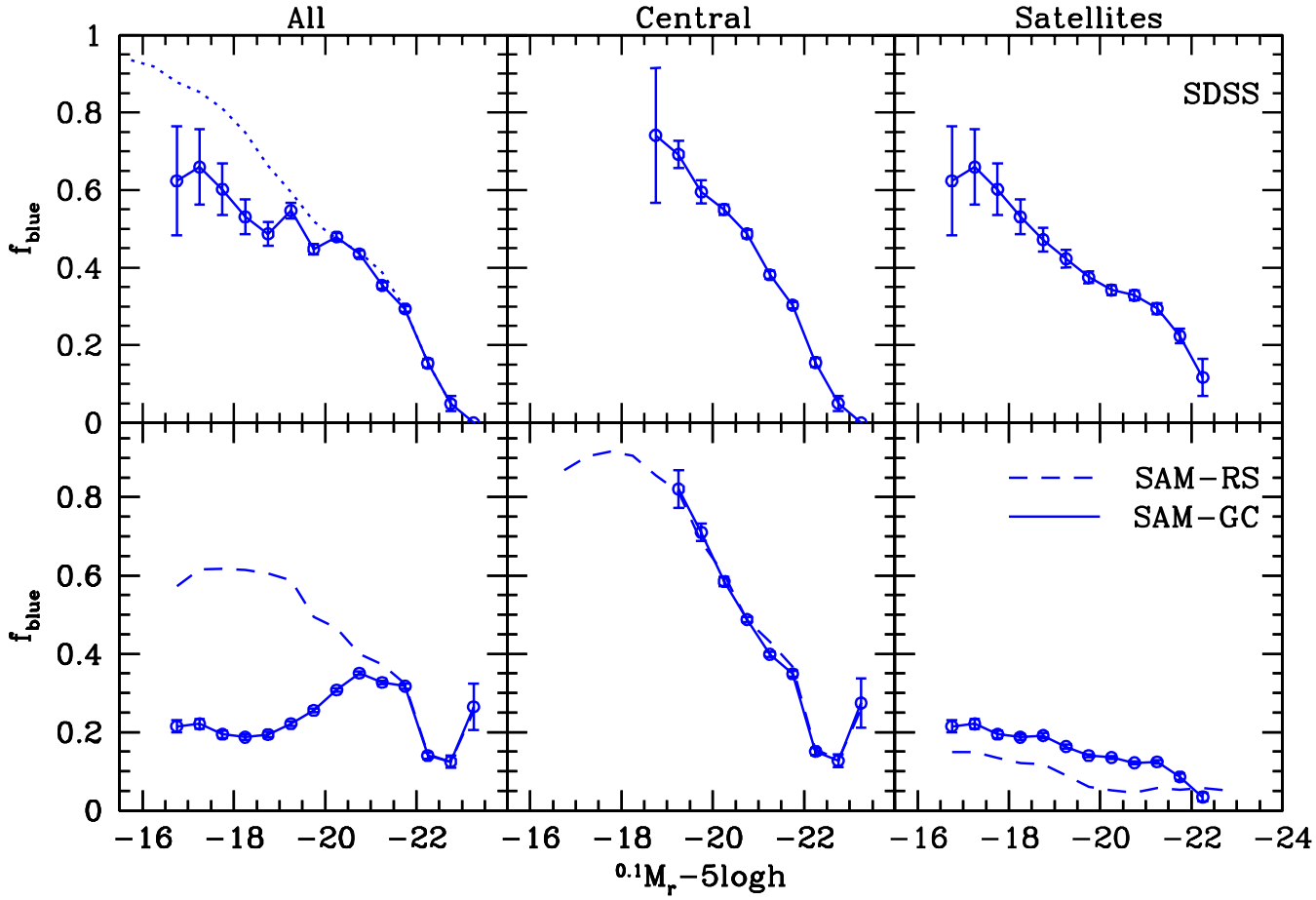

Figure 3.4: *The luminosity dependence of blue galaxy fractions. From left to right, the panels show the blue fractions of all galaxies (centrals plus satellites), central galaxies, and satellite galaxies. The top panels show the results from the SDSS group catalogue (open circles with Poissonian errorbars). The dotted line in the top-left panel shows the results obtained from the full SDSS, including those galaxies that were not assigned to a galaxy group by the group finder. The bottom panels show the results from the SAM of C06. Results are shown for both the SAM-RS (dashed lines) and the SAM-GC (open circles with Poissonian errorbars). See Section 3.5.2 for a detailed discussion.*

3.5.2 Blue fraction as Function of Luminosity

The dotted line in the upper-left panel of Fig. 3.4 shows the fraction of blue galaxies, $f_{\rm blue}$, in the SDSS as a function of luminosity. Here all 184,425 galaxies in our SDSS sample defined in Section 3.3.1 are used. As is well known, the fraction of blue galaxies decreases drastically with increasing luminosity, dropping from ~ 95 percent at ${}^{0.1}M_r - 5\log h = -16$ to $\lesssim 5$ percent for galaxies with ${}^{0.1}M_r - 5\log h < -22.5$. The dashed line in the lower-left panel shows the blue fraction for the 428,013 model galaxies in the SAM-RS. Although this blue fraction also reveals an overall decrease with increasing luminosity, there are two marked differences with respect to the SDSS. First of all, at the bright end there is a sudden upturn in $f_{\rm blue}$; galaxies with ${}^{0.1}M_r - 5\log h \simeq -23$ have a blue fraction of $\sim 26 \pm 6$ percent, compared to zero percent in the SDSS (note though that there are only 8 SDSS galaxies in this luminosity bin). As already mentioned in Section 3.4, these bright blue galaxies in the SAM are ULIRGs for which the dust modeling is inadequate (cf. lower panels of Fig. 3.1). The second discrepancy between SAM-RS and SDSS is more important; at the faint end the blue fraction in the SAM-RS never exceeds 62 percent, and is therewith much lower than the blue fraction of faint SDSS galaxies. Consistent with what we inferred above from the CLFs, this indicates that the SAM severely overpredicts the fraction of faint, red galaxies.

To investigate whether this mainly concerns central galaxies, satellite galaxies, or both, we now resort to the group catalogues extracted from the SDSS and SAM. The open circles with errorbars, connected by solid lines, indicate the blue fractions of galaxies that make it into the group catalogue. Comparing these for the SDSS to those obtained from the full sample (dotted lines), we see that the blue fraction has become somewhat lower at the faint end. We can understand this by looking at the blue fractions of central galaxies (upper middle panel) and satellite galaxies (upper right panel). This shows that both blue fractions decrease with increasing luminosity, but that the luminosity dependence is more pronounced for the centrals. Since the galaxies that do *not* make it into the group catalogue are mainly isolated, and thus central, galaxies that live in haloes below the mass limit of the group catalogue, these are mainly blue. This explains why the fraction of faint blue galaxies is lower in the group catalogue than in the full redshift catalogue.

In the SAM, the group selection also causes a drop of the blue fraction of faint galaxies, but of a much larger amplitude. In fact, the fraction of 'group' galaxies with $-16 > M_{b_J} - 5\log h > -18$ is ~ 20 percent in the SAM, compared to ~ 60 percent in the SDSS. The reason for this discrepancy is largely due to the satellite galaxies: as shown in the lower right-hand panel, the blue fraction of satellite galaxies in the SAM is much too low, especially at the faint end. In the case of the central galaxies (middle panels), the agreement between SAM and SDSS is much better, especially for centrals with $M_{b_J} - 5\log h \simeq -21$. However, at the faint and bright ends, the SAM significantly overpredicts the blue fractions by ~ 15 and ~ 25 percent, respectively.

The dashed lines in the lower middle and lower right-hand panels show the blue fractions of centrals and satellites of *all* galaxies in the SAM-RS (including those that are not in the group catalogue). This shows that the group finder very accurately recovers the blue fraction of central galaxies, but slightly overpredicts that of satellites. This owes to the interlopers (group members that do not actually belong to the same halo), which tend to be isolated, central galaxies in low mass haloes, and which are thus preferentially blue. The contamination, however, is sufficiently small that it does not significantly affect any

of our results.

In summary, although the SAM matches the overall blue fraction of galaxies almost exactly (see Section 3.4.1), when split according to luminosity or according to centrals and satellites, there are very significant differences between SAM and SDSS. The SAM overpredicts the blue fraction of central galaxies at both the bright and the faint end of the distribution, and dramatically underpredicts the blue fraction of (faint) satellite galaxies. In particular, the SAM predicts that virtually all ($\gtrsim 85\%$) satellite galaxies are red, whereas the SDSS indicates that the fraction of red satellites decreases from ~ 90 percent at ${}^{0.1}M_r = -22 + 5\log h$ to ~ 40 percent at ${}^{0.1}M_r = -17 + 5\log h$. This suggests shortcomings for the star formation truncation mechanisms in the SAM: apparently the treatment of strangulation is too efficient, while the model for AGN feedback is not efficient enough (see Section 3.6 for a more detailed discussion).

3.5.3 Blue Fraction as Function of Halo Mass

We now turn to the mass dependence of $f_{\rm blue}$. We split the SDSS and SAM group catalogues in six logarithmic mass bins and determine how the blue fractions in each of these bins depend on luminosity. For each bin in mass and luminosity, the blue fraction is defined as the total number of blue galaxies in that bin, divided by the total number of galaxies in that bin (i.e., we do not average the blue fraction over individual groups or haloes).

The results for the SDSS group catalogue are shown in the upper panels of Fig. 3.5 and are listed in tabular form in Appendix A. The upper left-hand panel shows the result for all galaxies (centrals plus satellites). In each mass bin, the blue fraction decreases with increasing luminosity, but only very mildly. In fact, over the magnitude range $-19 \gtrsim {}^{0.1}M_r - 5\log h \gtrsim -21.5$ the luminosity dependence is remarkably weak, for all six mass bins. At fixed luminosity, however, there is a clear mass dependence, with the blue fraction decreasing with increasing halo mass. Over the range $10^{12}h^{-1}\,{\rm M}_\odot \lesssim M \lesssim 10^{15}h^{-1}\,{\rm M}_\odot$, the blue fraction changes by ~ 30 percent, at all luminosities. This indicates that the colour of a galaxy is more strongly determined by the mass of the halo in which it resides than by its own luminosity (cf. Yang et al. 2005b; paper I). Consequently, the strong luminosity dependence of $f_{\rm blue}$ seen in Fig. 3.4 is mainly a reflection of the fact that more luminous galaxies typically reside in more massive haloes. Note that some earlier work (e.g. Balogh et al. 2004, Tanaka et al. 2004) has found no correlation between galaxy properties and halo velocity dispersion. However, as shown in paper I this is most likely due to the smaller sample size and the fact that using velocity dispersion as a mass estimator tends to smear out the mass dependence.

The upper middle panel shows the blue fractions of central galaxies. Note that at a given halo mass, there is only a relatively small dynamic range of luminosities over which we can measure $f_{\rm blue}(L)$. Nevertheless, at a given halo mass there is a clear indication that the blue fraction decreases with increasing luminosity. At the same time, at a given luminosity the blue fraction also decreases with increasing halo mass. Finally, the upper right-hand panel shows the results for the satellite galaxies in the SDSS group catalogue, which look similar to those for the full sample of galaxies shown in the upper left-hand panel.

The middle and lower rows of panels in Fig. 3.5 show the results obtained from the SAM-RS and SAM-GC, respectively. In the former no group finder has been applied, and

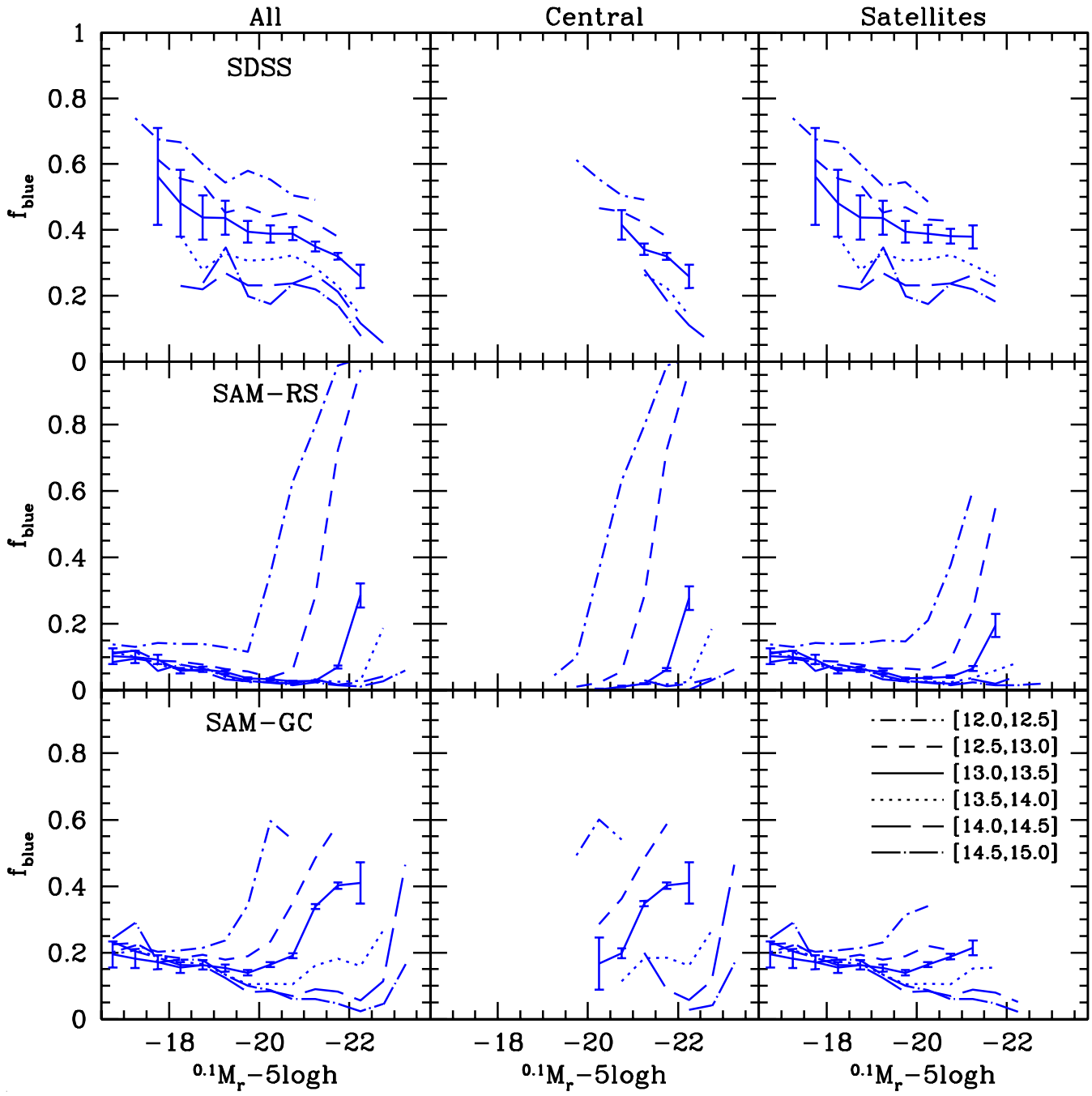

Figure 3.5: *Blue galaxy fractions as a function of absolute magnitude in the* $^{0.1}r$*-band. Results are shown for all galaxies (left-hand panels), central galaxies (middle panels) and satellite galaxies (right-hand panels), and for 6 different mass bins as indicated (the values in square brackets indicate the range of* $\log(M/h^{-1}\,\mathrm{M}_\odot)$*). Results are only shown for mass-luminosity bins that contain at least 50 galaxies in total, and for clarity (Poissonian) errorbars are only shown for one mass bin. From top to bottom, results are shown for the SDSS group catalogue, the SAM redshift survey (SAM-RS), and the SAM group catalogue (SAM-GC). Note the poor agreement between SDSS and SAM-GC, indicating that the SAM is not correctly treating the physics responsible for determining whether a galaxy is red or blue. See Section 3.5.3 for a detailed discussion.*

the mass binning is according to the true halo masses of the galaxies. A comparison with the results obtained from the SAM group catalogue is therefore indicative of the accuracy with which our group finder allows a recovery of the true underlying $f_{\rm blue}(L,M)$. A number of differences are clearly apparent, which mainly owe to the impact of interlopers and, more importantly, to errors in the assigned group masses. Since the true $f_{\rm blue}(L,M)$ has extremely steep gradients in both L and M, even small errors in any of these quantities can have a significant impact on the blue fraction obtained from the group catalogue. This mainly causes errors in the *absolute* values of $f_{\rm blue}(L,M)$. However, the *relative* relations of $f_{\rm blue}(L|M)$ and $f_{\rm blue}(M|L)$ are well recovered. Note that the blue fraction of central galaxies with ${}^{0.1}M_r - 5\log h = -19.5$ is less than 10 percent for all mass bins shown. Yet, as can be seen from Fig.4, the blue fraction of central galaxies in the group catalogue with that luminosity is ~ 80 percent. This indicates that virtually all blue centrals with ${}^{0.1}M_r - 5\log h \leq -19.5$ reside in haloes with $M < 10^{12}h^{-1}\,{\rm M}_\odot$.

Comparing the $f_{\rm blue}(L,M)$ obtained from the SAM-GC with those obtained from the SDSS, one notices immediately that they have very little in common. Probably the most dramatic difference between the SDSS and the SAM-GC concerns the blue fraction of satellite galaxies (shown in the panels on the right hand side), which is much too low in the SAM-GC, especially for faint galaxies and for low mass haloes. A comparison with the SAM-RS results shows that this discrepancy can not be attributed to artefacts of the group finder. In addition, the SAM-GC predicts that the blue fraction of central galaxies increases with increasing luminosity, opposite to what is seen in the SDSS (middle panels). This effect is most severe for haloes with masses $M < 10^{13}h^{-1}\,{\rm M}_\odot$. These two problems conspire to produce a blue fraction of the full galaxy population (centrals and satellites) in the SAM-GC which is very different from the SDSS (left hand panels), both quantitatively (mainly because of the too low number of blue satellites) and qualititatively (mainly because of the reversed relation between luminosity and the blue fraction of central galaxies).

We are thus led to conclude that although the SAM reproduces the overall blue fraction (when integrated over all galaxies), when it comes to $f_{\rm blue}(L,M)$, there are dramatic differences between model and data. Note that the SAM of C06 fits the overall luminosity function and even yields CLFs, i.e., luminosity functions as function of halo mass, whose shapes are in remarkably good agreement with the SDSS data. This suggests that one of the main problems for the SAM is the treatment of the physics responsible for determining whether a galaxy is red or blue. This includes the star formation truncation mechanisms, such as strangulation and AGN feedback, but also the treatment of dust extinction. In the next section we present a more detailed discussion of the possible implications.

3.6 Discussion

The above analysis of the fractions of blue galaxies as function of halo mass and luminosity has revealed several problems for the SAM of C06. In the following we discuss the possible implications for galaxy formation models.

3.6.1 Tidal Stripping

The first problem concerns the abundance of satellite galaxies. As shown in Section 3.5.1, the SAM overpredicts the number of faint satellite galaxies in massive haloes by up to

a factor ~ 2. Most likely, this indicates that the luminosity evolution of the satellites is not properly accounted for. Satellite galaxies can become fainter due to star formation truncation followed by passive evolution, or due to tidal stripping of their stellar mass. Since most of the satellite galaxies in the SAM are already red, they can not become much fainter than they already are for their given stellar mass. In other words, there is little to gain from adding physical processes that may speed up the star formation truncation, such as ram pressure stripping. In fact, this will only increase the fraction of red satellites, which is already much too large. The most plausible explanation for the overabundance of satellite galaxies is the neglect of tidal stripping. It is well known that the tides in massive haloes can easily strip satellite galaxies and their dark matter haloes of large fractions of their mass. This is supported by the detection of intracluster light (e.g., Bernstein et al. 1995; Gonzalez et al. 2000) due to a diffuse population of intergalactic stars. Most likely, these stars, which contribute around 10 percent of the total cluster light (Zibetti et al. 2005), have been tidally stripped from satellite galaxies.

Formalisms to describe tidal stripping in the presence of dynamical friction in a background potential have been developed by, among others, Taylor & Babul (2001, 2004) and Zentner & Bullock (2003). As shown in Benson et al. (2002), including such a formalism in semi-analytical models significantly reduces the abundance of satellite galaxies. Furthermore, since tidal stripping predominantly affects satellites with small pericentric radii, which are typically redder (blue galaxies have only recently been accreted by the halo, and have not yet experienced much dynamical friction), tidal stripping may also reduce the red fraction of satellites and thus help towards solving the problem with the red fractions of satellites being too large.

3.6.2 Strangulation

The second problem for the SAM of C06 is that the fraction of blue satellite galaxies is much too low, especially for faint galaxies and in low mass haloes. This suggests that 'strangulation', as incorporated in the SAM, is much too efficient. In virtually all semi-analytical models, strangulation is included and modeled in the same way: as soon as a galaxy becomes a satellite galaxy, its hot gas reservoir is 'stripped' (i.e., the hot gas that belonged to the satellite galaxy is added to the hot gas reservoir of the central galaxy). Consequently, after a delay time in which the new satellite galaxy consumes (part of) its cold gas, its star formation is truncated. The results presented here suggest that this formulation is too crude, as it predicts a blue satellite fraction that is much too low[3]. In particular, strangulation is modeled without any explicit halo mass dependence, which explains why the blue fraction of satellite galaxies in the SAM is virtually independent of halo mass. In the SDSS, however, the blue satellite fraction decreases with increasing halo mass, suggesting a clear mass scaling of the strangulation efficiency. The physical mechanisms thought to be responsible for the removal of the satellite's hot gas reservoir are tides and ram pressure stripping. The latter requires that the parent halo has a sufficiently dense hot corona. Since this requirement is more likely to be fulfilled for more massive haloes, which in general have a larger fraction of hot gas, one actually expects that the strangulation efficiency increases with increasing halo mass. Indeed, using numerical simulations, Bekki et al. (2002) find that strangulation is significantly more effective in

[3]Note that the SAM of C06, as most other SAMS, does not even account for ram pressure stripping, which will only shorten the truncation time, thus decreasing the blue satellite fraction.

massive galaxy clusters than in lower mass groups. It remains to be seen whether a simple scaling along these lines can bring the red and blue fractions of satellite galaxies in SAMs in better agreement with the SDSS data presented here.

Interestingly, in a comparison of semi-analytical models and hydrodynamical SPH simulations of galaxy formation, Zheng et al. (2005) have shown that the later predicts that haloes with $10^{12}\,\mathrm{M}_\odot \lesssim M \lesssim 10^{13}\,\mathrm{M}_\odot$ have a significantly higher fraction of young satellites (similar to the blue satellites discussed here) than SAMs, in much better agreement with the SDSS results presented here (see their Fig. 4). Similarly, Cattaneo et al. (2007) find that their semi-analytic model produces too few blue satellite galaxies compared to their SPH simulation. Since these SPH simulations follow the actual hydrodynamical processes leading to strangulation, this indeed suggests that a more realistic treatment of strangulation in the SAMs may solve the problem with the colors of satellite galaxies. SPH simulations such as those described in Zheng et al. (2005) and Cattaneo et al. (2007) may prove useful in calibrating such a new and improved strangulation model.

3.6.3 Dust Extinction and AGN Feedback

The SAM also has problems with the blue fractions of central galaxies, which are too high, especially at the bright and faint ends. In addition, for a given halo mass, the blue fraction of central galaxies increases with luminosity, contrary to what is seen in the SDSS. Which aspect(s) of the semi-analytical model are responsible for these problems is not entirely clear. They can indicate a problem with the modeling of dust extinction, a problem with the treatment of AGN feedback, or both. The former is almost certainly responsible for the overproduction of bright and blue centrals. As already discussed in C06, this population of galaxies is reminiscent of the ULIRG population, for which the oversimplified treatment of the dust extinction is certainly inadequate: real starburst are likely to be accompanied by additional extinction which would make these galaxies both fainter and redder. This would help to suppress the strong increase of f_{blue} with increasing luminosity, though it remains to be seen whether it can result in a blue fraction that decreases with increasing luminosity, as observed. Furthermore, in order to suppress the impact of these starbursting model galaxies on the comparison presented here, we already removed all galaxies with $(g-r)<0$ from the SAM. Despite this, however, the SAM still significantly overpredicts the fraction of blue centrals with ${}^{0.1}M_r - 5\log h \simeq -23$. Although improper dust modeling is likely to be the cause for this discrepancy, it remains to be seen whether this can also explain the overprediction (by ~ 15 percent) of the blue fraction of *faint* centrals.

Alternatively, the blue fractions of central galaxies may be modified by changing the AGN feedback description. As discussed in the introduction, it is still largely unknown how AGN impact on their surroundings, and thus feed back on the process of galaxy formation. It should therefore not come as a surprise if the parameterization of C06 is not entirely correct or complete. The purpose of this work, however, is not to find an improved formulation of AGN feedback. Rather, we have presented data, in the form of blue galaxy fractions as function of both halo mass and luminosity, which we believe to be useful in discriminating between different AGN feedback models. Future SAMs can test and/or calibrate their particular parameterizations against these data.

3.7 Conclusions

It has become clear that a successful reproduction of the galaxy luminosity function, and of the bimodality in the galaxy distribution, requires a mechanism that can truncate the star formation in massive galaxies at relatively late epochs. At the same time, the fact that red, passive galaxies preferentially reside in overdense regions, such as clusters and groups of galaxies, suggests that star formation truncation acts preferentially in massive haloes. Current models consider two such truncation mechanisms: strangulation, which acts on satellite galaxies, and AGN feedback, which predominantly affects central galaxies.

Typically, galaxy formation models are tuned to reproduce the *global* properties of the galaxy distribution, such as the luminosity function and the total fraction of blue and red galaxies. However, even when two models predict exactly the same global statistics, their statistics as function of halo mass may be very different. The latter is clearly more constraining for the model, and furthermore, holds important information regarding the mass-dependence of the various physical mechanisms associated with galaxy formation. In particular, since star formation truncation causes a galaxy to become red, the relative fractions of red and blue galaxies as a function of halo mass holds important clues regarding the halo mass dependence of the efficiencies of AGN feedback and strangulation.

To provide a test-bed for models of galaxy formation, we have used a galaxy group catalogue extracted from the SDSS for which we have computed the fraction of blue and red galaxies as function of both galaxy luminosity and group (halo) mass. To illustrate the potential constraining power of this data we have compared these fractions to those in the semi-analytical model for galaxy formation of Croton et al. (2006), which includes both 'radio mode' AGN feedback and strangulation. To allow for a fair comparison between the SDSS group catalogue and the SAM, not influenced by potential inaccuracies associated with the group finder (i.e., interlopers, incompleteness, errors in assigned group mass), we have applied the same group finder over a mock redshift survey constructed from the SAM. The $f_{\rm blue}(L,M)$ obtained from this SAM group catalogue is in fair agreement with the true $f_{\rm blue}(L,M)$ obtained directly from the SAM, indicating that our group finder allows a reliable recovery of the blue fraction as a function of both galaxy luminosity and halo mass. Although interlopers and errors in the group masses may cause some errors in the absolute values of $f_{\rm blue}(L,M)$, the relative scalings of $f_{\rm blue}(L|M)$ and $f_{\rm blue}(M|L)$ are well recovered.

Although the SAM fits the overall luminosity function, reproduces the overall color distribution of the SDSS galaxies, and even predicts a conditional luminosity function whose shape is in excellent agreement with the data, its prediction of $f_{\rm blue}(L,M)$ is in poor agreement with the SDSS data. In particular, we have identified four problems:

1. In massive haloes the abundance of faint satellite galaxies is too high by up to a factor ~ 2.

2. The fraction of blue satellite galaxies is much too low, especially for faint galaxies and in low mass haloes.

3. The fraction of blue central galaxies is too high, especially at the bright and faint ends.

4. For a given halo mass the blue fraction of central galaxies increases with luminosity, contrary to what is seen in the SDSS.

The first of these problems is likely to owe to the fact that the SAM does not model the tidal stripping of the stellar mass of the satellite galaxies as they orbit the parent halo. As shown in Benson et al. (2002), inclusion of this effect significantly reduces the abundance of satellite galaxies at a fixed luminosity. The second problem is most likely due to an oversimplification of the treatment of strangulation. In the SAM, strangulation occurs instantaneously, independent of halo mass. However, based on the SDSS data, we have argued that the strangulation efficiency has to scale with halo mass, such that more massive haloes strangulate their satellites on a shorter time scale. The physical motivation for such a scaling is that the ram pressure stripping of the hot gas reservoir of newly accreted satellites requires the parent halo to have a sufficiently dense corona of hot gas. Since the fraction of hot gas is typically an increasing function of halo mass, this may introduce a mass dependence in the strangulation efficiency as required. Indeed, hydrodynamical SPH simulations, which automatically take this into account, seem to predict blue satellite fractions that are significantly higher than in the semi-analytical models (Zheng et al. 2005, Cattaneo et al. 2007). Finally, the third and fourth problem listed above, both of which concern central galaxies, are likely to reflect shortcomings of the modeling of dust extinction and/or AGN feedback.

In summary, galaxy formation models are often tested and calibrated against global properties of the observed galaxy distribution. Recently, with the inclusion of AGN feedback, numerous studies have claimed success in reproducing these global statistics, even though very different formulations for the various physical processes have been used. In order to discriminate between these models more specific data is required. In this work we have presented the fractions of blue and red galaxies as function of luminosity, halo mass, and separately for central and satellite galaxies. Clearly this data is far more constraining, and thus more challenging, than the global fractions of red and blue galaxies, or the overall luminosity function. We have shown that indeed these data provide valuable new insights regarding the physics of galaxy formation, and we hope that they will provide a useful test-bed for future models of galaxy formation.

3.8 Acknowledgments

We thank Simon D.M. White for valuable comments. FvdB acknowledges useful discussions with Eric Bell, Fabio Fontanot, Xi Kang, Anna Pasquali and Rachel Somerville. SW thanks Christian Thalmann for help with data handling. SW has been partially supported by the Swiss National Science Foundation (SNF). The work described in this chapter has made extensive use of the Sloan Digital Sky Survey (SDSS). In particular, we have used the New York University Value-Added Galaxy Catalogue (http://sdss.physics.nyu.edu/vagc/), and we are grateful to Michael Blanton for his help with this fantastic data set. Funding for the SDSS has been provided by the Alfred P. Sloan Foundation, the Participating Institutions, the National Aeronautics and Space Administration, the National Science Foundation, the U.S. Department of Energy, the Japanese Monbukagakusho, and the Max Planck Society. The SDSS Web site is http://www.sdss.org/. The SDSS is managed by the Astrophysical Research Consortium (ARC) for the Participating Institutions. The Participating Institutions are The University of Chicago, Fermilab, the Institute for Advanced Study, the Japan Participation Group, The Johns Hopkins University, Los Alamos National Laboratory, the Max-Planck-Institute for Astronomy (MPIA), the

Max-Planck-Institute for Astrophysics (MPA), New Mexico State University, University of Pittsburgh, Princeton University, the United States Naval Observatory, and the University of Washington. The Millennium Run simulation used in this paper was carried out by the Virgo Supercomputing Consortium at the Computing Centre of the Max-Planck Society in Garching. Semi-analytic galaxy catalogues from the simulation are publicly available at http://www.mpa-garching.mpg.de/galform/agnpaper.

Chapter 4

Dependence of the Local Reionization History on Halo Mass and Environment: Did Virgo Reionize the Local Group?[1]

The Sun, with all the planets revolving around it, and depending on it, can still ripen a bunch of grapes as though it had nothing else in the Universe to do.

Galileo Galilei

4.1 Abstract

The reionization of the universe has profound effects on the way galaxies form and on their observed properties at later times. Of particular importance is the relative timing of the reionization history of a region and its halo assembly history, which can affect the nature of the first stars formed in that region, the properties and radial distribution of its stellar halo, globular cluster population and its satellite galaxies. We distinguish two basic cases for the reionization of a halo - internal reionization, whereby the stars forming in situ reionize their host galaxy, and external reionization, whereby the progenitor of a galaxy is reionized by external radiation before its own stars are able to form in sufficient numbers. We use a set of large-scale radiative transfer and structure formation simulations, based on cosmologies derived from both WMAP 1-year and WMAP 3-year data to evaluate the mean reionization redshifts and the probability of internal/external reionization for Local Group-like systems, galaxies in the field and central cD galaxies in clusters. We find that these probabilities are strongly dependent on the underlying cosmology and the efficiency of photon production, but also on the halo mass. There is a rapid transition between predominantly external and predominantly internal reionization at a mass scale of $\sim 10^{12} M_{\odot}$ (corresponding roughly to L* galaxies), with haloes less massive than this

[1]This chapter has been accepted for publication in MNRAS (astro-ph/0705.0530)

being reionized preferentially from distant sources. We provide a fit for the reionization redshift as a function of halo mass, which could be helpful to parameterize reionization in semi-analytical models of galaxy formation on cosmological scales. We find no statistical correlation between the reionization history of field galaxies and their environment.

4.2 Introduction

The lack of Gunn-Peterson troughs in the spectra of distant galaxies and QSO's show that the universe has been almost completely ionized ever since redshift $z \sim 6$. This reionization was a consequence of the ionizing radiation emitted by the first galaxies, which started forming at $z > 20$ through the gravitational growth of the primordial density fluctuations. The recent 3-year results from the WMAP satellite (Spergel et al. 2007) indicated that reionization was well-advanced by $z \sim 10$ and was thus fairly extended in time. Reionization had some profound implications on star and galaxy formation. First, stars forming in a reionized medium of low metallicity are probably considerably less massive than stars forming in a neutral medium of low metallicity (e.g. Johnson & Bromm 2006) and follow a different evolutionary path. Second, the formation of low-mass galaxies is suppressed in the presence of an ionizing background. The shallow gravitational wells of the small haloes cannot hold onto their gas if the halo virial temperature is below $T_{\rm vir} \sim 10^4$ K (Dekel & Silk 1986; Shapiro et al. 2004; Iliev, Shaprio & Raga 2005b) the gas accretion rate decreases, and the cooling time of the gas increases, thereby suppressing further star formation (Efstathiou 1992; Thoul & Weinberg 1996; Navarro & Steinmetz 1997; Bullock et al. 2000; Dijkstra et al. 2004). Therefore, reionization is a promising candidate for reconciling the discrepancy between the number of observed low luminosity satellite galaxies around the Local Group and the CDM simulation predictions, often referred to as the 'missing satellite problem' (Klypin et al. 1999; Moore et al. 1999; Tully et al. 2002. Third, reionization may have truncated the formation of the blue, old globular clusters that are still observed today (Santos 2003; Moore et al. 2006. Since massive galaxies will be reionized considerably before reionization is completed in the entire IGM, it is interesting to ask when and how a galaxy of a given mass, located in a given environment, will be reionized.

Generically, there are two ways in which a galaxy can be reionized. The process could be driven by the radiation emanating from its own stars forming in situ ('internal reionization') or the galaxy or its progenitors could be overrun by the global ionization fronts created by objects which collapsed earlier ('external reionization'). The second scenario is expected to occur e.g. for low mass satellites that have been close to large galaxies like the Milky Way since before reionization, while the first scenario should be typical for very massive galaxies in the central regions of clusters. It is less clear what scenario should be expected for intermediate-mass galaxies. For example, a field galaxy which resides close to a massive cluster could have been reionized by the radiation coming from the proto-cluster before the galaxy itself formed. The concept of a non-uniform, density-dependent reionization redshift has been introduced by Barkana & loeb (2004). They point out that external reionization may become important in underdense regions and voids, thus causing the relatively low number of dwarf galaxies in these regions.

In this work we study the reionization history of haloes and its dependence on the halo mass and environment. To this end, we explore data from series of large-scale structure

Table 4.1: Overview of the three different codes and the resolutions used in our WMAP3 simulation (WMAP1 is similar). Note that the spatial resolution in PMFAST is better by at least an order of magnitude as far as the position of halo centers are concerned. In the PKDGRAV simulation, the spatial resolution is not clearly defined and was assumed to be equal to the force resolution.

	code	mass res.	spatial res.
high res	PMFAST	$2 \times 10^7\ h^{-1}\mathrm{M}_\odot$	$\sim 30\ h^{-1}$kpc
low res	PKDGRAV	$9.96 \times 10^8\ h^{-1}\mathrm{M}_\odot$	$\sim 10\ h^{-1}$kpc
RT	C^2-ray	-	$\sim 0.5\ h^{-1}$Mpc

formation and radiative transfer simulations of cosmic reionization. We re-simulate the same initial conditions at lower resolution which allows for tagging of the particles and thus for following the detailed merger and accretion history of haloes from the reionization epoch to the present. This allows us to identify the progenitors of massive cluster galaxies, field galaxies and Local Group-like systems and simultaneously follow both their reionization history and their mass growth history.

In this work, we will use two different flat ΛCDM cosmologies, the first with parameters $(\Omega_m, \Omega_\Lambda, \Omega_b, h, \sigma_8, n) = (0.27, 0.73, 0.044, 0.7, 0.9, 1)$ (Spergel et al. 2003, hereafter WMAP1) and $(\Omega_m, \Omega_\Lambda, \Omega_b, h, \sigma_8, n) = (0.24, 0.76, 0.042, 0.73, 0.74, 0.95)$ (Spergel et al. 2007, hereafter WMAP3. Here Ω_m, Ω_Λ, and Ω_b are the total matter, vacuum, and baryonic densities in units of the critical density, h is the Hubble constant in units of 100 $\mathrm{km\,s^{-1}Mpc^{-1}}$, σ_8 is the standard deviation of linear density fluctuations at present on the scale of $8h^{-1}$Mpc, and n is the index of the primordial power spectrum.

This chapter is organized as follows: In § 4.3 we summarize our simulations. In § 4.4 we present our techniques used to select field haloes and follow the reionization histories of individual haloes. In § 4.5 we present our results for the reionization histories of field galaxies, cD galaxies in the centers of galaxy clusters and Local Group-like objects. In § 4.6 and § 4.7 we discuss potential caveats and discuss the implications of external vs. internal reionization on the observable galaxy characteristics. Finally, in § 4.8, we give a summary of our results.

4.3 Simulations

Our simulations follow the evolution of a comoving simulation volume of $(100\,h^{-1}\mathrm{Mpc})^3$. Our basic methodology and simulation parameters are described in detail in Iliev et al. (2006b); Mellema et al. (2006b); Iliev et al. (2007). Here we provide just a brief summary, in addition to a detailed discussion of the elements which are first presented in this work. See Table 4.3 for listing of the codes used in this work and their effective mass and spatial resolutions.

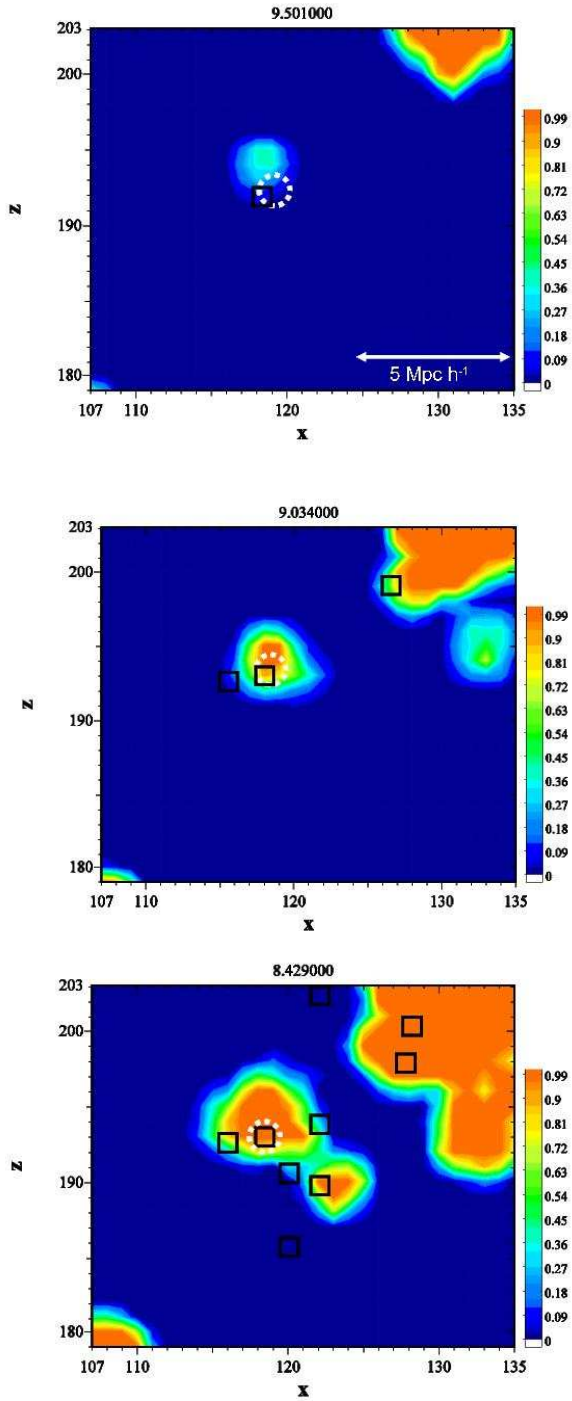

Figure 4.1: *Reionization colour plot, showing an example of internal reionization. Redshifts are denoted on the top of the plots. The reionization status of the gas is shown in colours, dark blue showing completely neutral gas, orange completely reionized gas. Black rectangles denote the position of identified haloes, the white dashed circle denotes the position of the LG progenitor, identified by its densest particles. The ionization state of the gas was identified in a slice with a thickness of one cell of the simulation outputs at different redshifts, with the position of the slice centered around the Local Group progenitor in consideration. Identified haloes are shown if they are within a box of volume* 20^3 *cells centered around the Local Group progenitor (i.e. can be up to 10 cells offset from the slice shown in the pictures).*

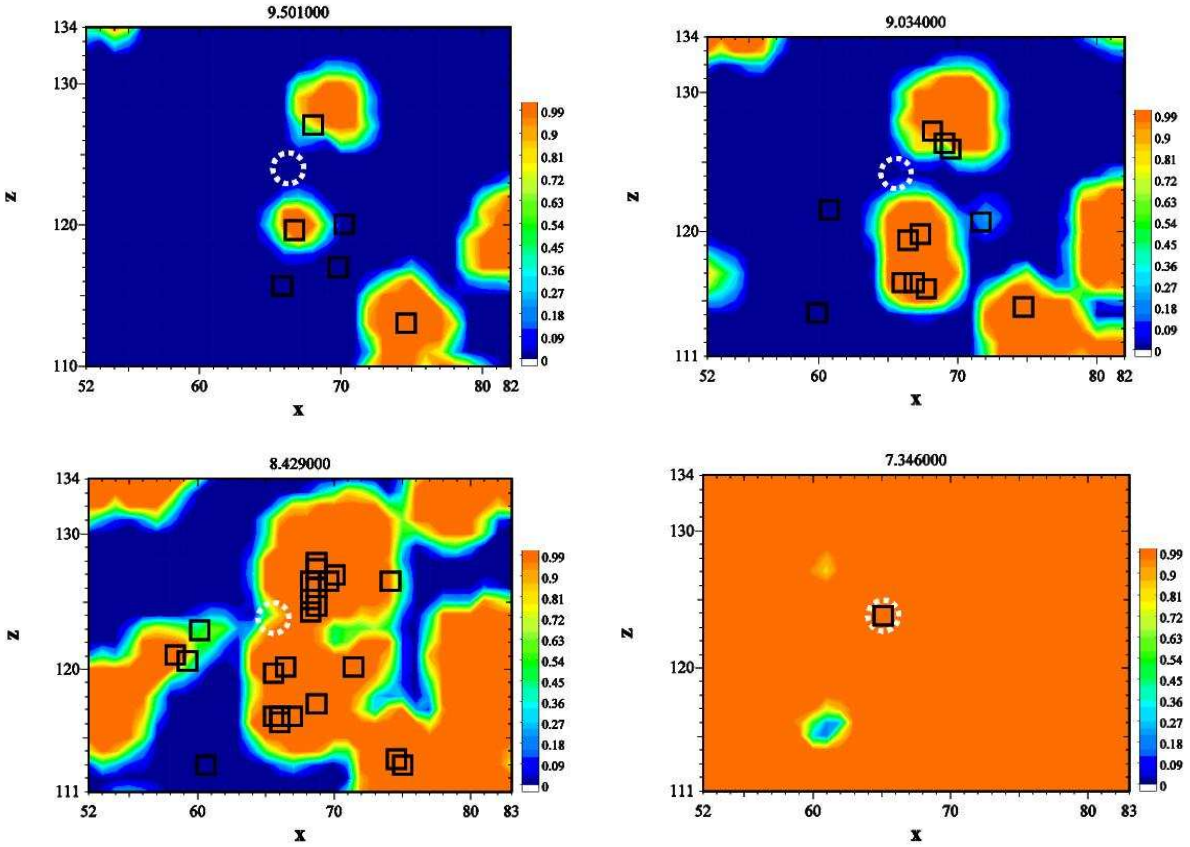

Figure 4.2: *Reionization colour plot, showing an example of external reionization. Symbols/Colours have the same meaning as in Figure 4.1. At z=7.346, the number of haloes is so large that we do not show them anymore in the plot.*

4.3.1 Structure Formation Simulations

We start by performing a very large dark matter only simulation of early structure formation, with $1624^3 \approx 4.3$ billion particles and 3248^3 grid cells[1] using the code PMFAST (Merz et al. 2005). This allows reliable identification (with 100 particles or more per halo) of all haloes with masses $\sim 2 \times 10^9\ h^{-1}\mathrm{M}_\odot$ or larger. We compile and save the halo catalogues, in up to 100 time slices starting from high redshift ($z \sim 30$) to the observed end of reionization at $z \sim 6$. In what follows, we will refer to this simulation as HR (high-resolution) simulation. This HR-simulation and in particular the halo catalogues based on it are used as the framework for our radiative transfer (RT) simulation which will be explained in detail in section 4.3.2. In order to maximize the mass resolution, the dark matter particles are not labelled in the HR simulation, which does not allow us to identify the progenitors of any given structure at $z = 0$. We resolved this problem by re-simulating the same initial conditions at lower resolution (called LR simulation hereafter) which allows for tagging of the particles. This enables us to identify the progenitors of haloes at z=0 and to simultaneously follow their reionization and mass growth histories. To obtain the LR simulation, the original HR PMFAST initial conditions (with 1624^3 particles) were generated again using the same random seeds. They were then coarsened to 406^3 particles by averaging the properties (positions and velocity components) of every 4^3 neighboring particles. We evolved these coarsened initial conditions from $z = 100$ to $z = 0$ using PKDGRAV, a fast parallel tree code written by Joachim Stadel and Tom Quinn (Stadel 2001).

4.3.2 The Radiative Transfer Simulations

We proceed by applying our radiative transfer code to the HR-simulation described above. Since radiative transfer simulations at the full grid size of our N-body simulations are still impractical, we follow the radiative transfer on coarser grids, of sizes 203^3. All identified haloes are assumed to be sources of ionizing radiation and each is assigned a photon emissivity proportional to its total mass, M, according to

$$\dot{N}_\gamma = f_\gamma \frac{M\Omega_b}{\mu m_p t_s \Omega_0}, \tag{4.1}$$

where t_s is the source lifetime, m_p is the proton mass, μ is the mean molecular weight and f_γ is a photon production efficiency which includes the number of photons produced per stellar atom, the star formation efficiency (i.e. what fraction of the baryons are converted into stars) and the escape fraction (i.e. how many of the produced ionizing photons escape the haloes and are available to ionize the IGM). Since we do include in the halo catalogue only haloes defined by more than 100 particles, this criterion introduces a minimum mass for haloes in order to act as ionizing sources. For our choice of the simulation parameters this corresponds to a mass threshold of $M_{th} = 2.5 \times 10^9\ h^{-1}\mathrm{M}_\odot$ (WMAP1) and $M_{th} = 2.2 \times 10^9\ h^{-1}\mathrm{M}_\odot$ (WMAP3). Note that this mass corresponds roughly to the halo mass above which a galaxy forming in it is largely unaffected by reionization (see Iliev et al. 2007 for discussions and references).

The radiative transfer is followed using our fast and accurate ray-tracing photoionization and non-equilibrium chemistry code C^2-Ray (Mellema et al. 2006). The code has

[1] $3248 = N_{nodes} \times (512 - 2 \times 24)$, where $N_{nodes} = 7$ (with 4 processors each), 512 cells is the Fourier transform size and 24 cells is the buffer zone needed for correct force matching on each side of the cube.

been tested in detail for correctness and accuracy against available analytical solutions and a number of other cosmological radiative transfer codes (Mellema et al. 2006a; Iliev et al. 2006a. The radiation is traced from every source on the grid to every cell using short-characteristic ray-tracing. The runs and notation are the same as the ones presented in Iliev et al. (2006b), Mellema et al. (2006b), Iliev et al. (2007). These include simulations with both WMAP1 and WMAP3 background cosmology. The runs for a given cosmology share the same underlying N-body simulation (but with different random realizations for WMAP1 and WMAP3), and each adopts different assumptions about the source efficiencies and the sub-grid level of gas density fluctuations. In part of the simulations, a sub-grid gas clumping is included, $C(z) = \langle n^2 \rangle / \langle n \rangle^2$, which evolves with redshift according to

$$C_{\rm subgrid}(z) = 27.466 e^{-0.114z+0.001328\,z^2}. \tag{4.2}$$

in WMAP1 cosmology and as

$$C_{\rm sub-grid}(z) = 26.2917 e^{-0.1822z+0.003505\,z^2}. \tag{4.3}$$

for WMAP3 cosmology. These fits were obtained from another set of two high-resolution PMFAST N-body simulation, with box sizes $(3.5\,{\rm h}^{-1}$ Mpc$)^3$ and a computational mesh and number of particles of 3248^3 and 1624^3, respectively. The inclusion of gas clumping results in a slower propagation of the reionization fronts and a delay of the final overlap.

In what follows, we will concentrate on three cases, two 'extreme' models and an intermediate one. The extreme cases (in terms of $z_{\rm ov}$, the redshift at which the final overlap is reached), are the following: WMAP1-f2000 (WMAP1, $f_\gamma = 2000$, no sub-grid gas clumping) and WMAP3-f250C (WMAP3, $f_\gamma = 250$, with sub-grid gas clumping). These two simulations should roughly bracket the allowed range in cosmological and reionization parameters. Among all of our radiative transfer simulations, the WMAP1-f2000 simulation has the earliest redshift of overlap, $z_{\rm ov}$=11.3, while simulation WMAP3-f250C has the latest overlap, $z_{\rm ov} \sim 6.5$. We add a simulation in between those two cases: WMAP1-f250C (WMAP1, $f_\gamma = 250$, with sub-grid gas clumping), resulting in $z_{\rm ov}$=8.2. This allows us to study the effect of changing only the cosmology or changing only the reionizing photon production efficiency. The lower efficiency of $f_\gamma = 250$ appears more realistic at present, and the corresponding cases match the late end of reionization at $z \sim 7$ well. We note that the delayed structure formation due to the lower power spectrum normalization, tilt and lower matter density in the favoured WMAP3 cosmology naturally predicts the lower integrated Thomson scattering optical depth the same measurements found, and thus do not seem to require a lower reionizing photon production efficiency (Alvarez et al. 2006, but see also Haiman & Bryan 2006; Shull & Venkatesan 2007).

For the WMAP1 simulations, transmissive boundary conditions on the ray-tracing were used. As a consequence, haloes close to the boundaries of our computational volume will be somewhat less affected by external radiation, particularly towards the end of reionization. Thus, in order to be conservative, we do not include in our analysis any haloes that are within 10 h^{-1}Mpc from the simulation boundary. The WMAP3 simulation utilized periodic boundary conditions, which allows for all haloes to be used in our analysis.

4.4 Methods

4.4.1 Matching the HR and LR Simulations

In order to investigate the reionization and formation history of a given halo, we first identify it at z=0 in our LR simulation, using a Spherical Overdensity Halo Finder (see Macciò et al. 2007 for a detailed description). We then track the particles of the halo in consideration back to higher redshift in the LR simulation and match them to the HR simulation in order to analyze its formation and reionization history. This can only be done if the density distribution in the HR and LR simulation agree well; since two quite different methods and resolutions are used for them, this merits checking and evaluating the closeness of the match between the two. If they match well, the location of the haloes which can be identified in the LR simulation should be similar to the location of the most massive haloes in the HR simulation (where the total number of identified haloes at any redshift is much higher than in the LR simulation). As a test, we identify for each halo in the LR simulation which is found by our Spherical Overdensity Halo Finder the nearest halo in the HR simulation which has a similar mass (within a factor of 2). At z=6 in the WMAP3 simulation, we find that the median distance between the haloes in the two catalogues is 0.3 Mpc h^{-1}, with a similar result for the WMAP1 simulation. Since this distance is below the grid size of the RT code, we consider this reasonable agreement for our current purposes. However, for around 3 percent of all cases, no nearby halo with similar mass is identified. This is not surprising given the fact that we use two different halo finders and have a large difference in resolution. Note that the median distance and the number of unmatched haloes decreases with increasing redshift. This reflects the fact that the DM distribution in the HR and LR simulation becomes more similar at high z, since the effects of different force resolution, etc., are diminished. As all of our comparisons between LR and HR simulations are done at times when the universe is not yet completely reionized, i.e. $z > 6$, we consider the median distance and the fraction of unmatched haloes quoted above an upper limit.

In what follows, we will explain in more detail how the formation and the reionization history of a given $z = 0$ halo is investigated. We mark the particles that will end up in a given halo at $z = 0$ and track them back to simulation outputs at higher redshifts. At any redshift, we identify the center of the halo progenitor as the densest particle (smoothing over the 32 closest neighbours) in the marked set and measure the fraction of reionized gas in the central cell and the 26 neighbouring cells, using the radiative transfer grid consisting of 203^3 cells. In this way, an offset of one radiative transfer (RT) cell (corresponding to $\sim 0.5h^{-1}$Mpc) in each dimension is allowed between the center of reionization in the HR-simulation, and the location of the densest particle in the LR-simulation. If the ionized fraction in any of those cells is higher than a threshold value of $x_{\rm th} = 0.7$, we define the halo as reionized and the corresponding reionization redshift z_r is set equal to the current output redshift. The particular value of $x_{\rm th}$ has a negligible impact on the final results thanks to the sharp transition across the ionization fronts (see Fig. 4.1 and 4.2).

Next we check at which redshift the most massive progenitor of the halo in consideration first reaches a halo mass of M_{th} (as defined in § 4.3.1), and define this as redshift of formation, z_f. To do this, we again trace back the halo progenitor particles and identify the densest particle at each redshift. Again allowing for an offset of one cell, we consider a halo as formed if it is identified by our halo finder based on the HR simulation. Only

for less than 2 percent of all haloes, no formation redshift could be identified. They were removed from the sample.

Since ionizing radiation in the ray tracing simulation can, by definition, only be produced by haloes that have been identified, this allows us to clearly separate internally reionized haloes from externally reionized ones. If $z_r > z_f$ ($z_r \leq z_f$), the halo has been reionized externally (internally). For illustrative purposes, in Figures 4.1 and 4.2 we show the evolution of the ionization fronts around an internally and an externally reionized Local Group-like object, respectively.

Our method can occasionally fail if the halo progenitor under consideration has a very large extent (i.e. is larger than two cells) and has two dense centers. If one of those is identified as densest particle by our smoothing algorithm, while the other is recognized by the high-resolution halo finder, external reionization will be always assumed. Eye inspection indicates that this happens in less than roughly 10% percent of all cases we have identified as external reionization. On the other hand, if the reionization and the formation of a halo occur in-between two timesteps, we always assume internal reionization. Although external reionization is also possible it is unlikely. We did not find a way to solve these two issues, but we expect that their impact on our results should be modest, since these effects will both only occur for a small fraction of our haloes.

4.4.2 Sample Selection

We have identified dark matter haloes at z=0 in our LR simulation using our Spherical Overdensity Halo Finder. From this halo catalogue we selected three sets of objects for further consideration: 1) field haloes, 2) central objects of massive clusters, likely to correspond to central cD galaxies and 3) Local Group-like systems. As a subset of the field haloes, we also selected a sample of haloes likely to host an L* galaxy.

The sample sets of such systems were chosen as follows. The field halo samples consist of all the haloes with masses between $1.8 \times 10^{11}\ h^{-1}\mathrm{M}_{\odot}$ and $3.7 \times 10^{13}\ h^{-1}\mathrm{M}_{\odot}$ that have been found by the Spherical Overdensity Halo Finder in both simulations. Such haloes are always isolated in the sense that they are not subhaloes in a larger group or cluster. In the WMAP1-f2000 and the WMAP1-f250C simulation, haloes with distances closer than 10 h^{-1} Mpc from the edges of the simulation box were removed from the sample. In this way, we have identified 9683 haloes in the WMAP3-f250C simulation, and 7346 haloes in the WMAP1-f2000/WMAP1-f250C simulations. A sample of haloes likely to host an L* galaxy was chosen as follows. According to Madgewick et al. (2002), L* - galaxies have a b_J-luminosity of $1.1 \times 10^{10}\ h^{-1}\ \mathrm{L}_{\odot}$. A central or isolated L* galaxy is therefore most likely to be found in a halo with $\log(M)$=12.2 $[\,h^{-1}\mathrm{M}_{\odot}]$ in a WMAP3, and in a halo with mass $\log(M)$=12.3 $[\,h^{-1}\mathrm{M}_{\odot}]$ in a WMAP1 cosmology, following the relation between L_{cen} and halo mass in van den Bosch et al. (2007). The difference in the two cosmologies is mainly due to the different halo clustering properties. We select for our L* galaxy sample haloes with mass $\log(M)$=12.1-12.3 $[\,h^{-1}\mathrm{M}_{\odot}]$ for the simulation based on WMAP3, and with $\log(M)$=12.2-12.4 $[\,h^{-1}\mathrm{M}_{\odot}]$ for the simulations based on WMAP1. We find 437 such haloes in the two simulations based on the WMAP1 cosmology, and 575 haloes in the WMAP3-f250C simulation.

The second set of haloes consists of the central objects in the 20 most massive galaxy clusters in each simulation. These massive objects are likely to correspond to central cluster cD galaxies. Finally, the third halo sample consists of all Local Group-like systems

Table 4.2: *Summary of the results. Listed are the mean redshift of formation, z_f, the mean starting redshift of the halo reionization, z_r, and the mean redshift at which 70 percent of the final halo mass is reionized, $z_{70\%}$, the fraction of objects reionized externally, $f_{\rm ext}$, the average time interval between formation and reionization, $\Delta t \equiv t_f - t_r$ (in Myr), and $\Delta t*$, which is the same time difference in units of the Hubble time when 50 % of the mass in the universe is ionized, for all of our simulations, as labelled. If Δt is negative, haloes are on average reionized before formation.*

	z_f	z_r	$z_{70\%}$	$f_{\rm ext}$	Δt	Δt^*
WMAP1-f2000						
field haloes	10.8	13.4	13.1	0.79	-114	-0.237
L* halo sample	12.6	13.6	12.85	0.62	-36	-0.075
central cDs	16.7	15.5	14.1	0.0	26	0.055
LG sample	12.8	13.3	12.9	0.44	-21	-0.044
WMAP1-f250C						
field haloes	11.0	11.7	10.4	0.4	-33	-0.053
L* halo sample	12.6	12.4	10.9	0.17	8	0.013
central cDs	16.7	15.5	11.8	0.0	26	0.042
LG sample	12.8	12.4	10.8	0.1	13	0.021
WMAP3-f250C						
field haloes	8.2	8.9	8.2	0.56	-60	-0.062
L* halo sample	9.3	9.4	8.6	0.27	-9	-0.009
central cDs	13.0	12.6	9.6	0.0	15	0.016
LG sample	9.1	9.2	8.3	0.24	-8	-0.008

in our volume. These are identified as binary systems of dark matter haloes satisfying the following criteria (see Macciò, Governato & Horellou 2005 for details):

1. The mass of each of the two haloes is between 4×10^{11} and $5 \times 10^{12}\ h^{-1}{\rm M}_\odot$.
2. The distance between the two haloes is below 700 h^{-1} kpc.
3. The two haloes are moving towards each other.
4. There is no massive neighbour with a mass above 5×10^{11} closer than 2.1 h^{-1} Mpc.

4.5 Results

4.5.1 Reionization Histories of Galaxies of Different Mass and Environment

On average, reionization *predates* formation for typical field haloes in all three simulation cases that we have considered. We compare the redshift of formation, z_f, the starting redshift of the halo reionization, z_r, and the redshift at which 70 percent of the final halo mass is reionized, $z_{70\%}$, for all our halo samples (field haloes, haloes likely to host an L* galaxy, haloes likely to host a cD galaxy, LG like haloes) in Table 4.5.1. We note

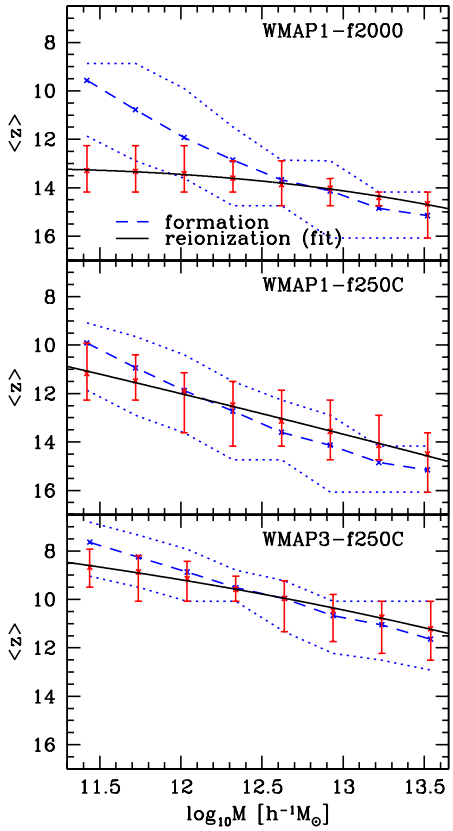

Figure 4.3: *The average formation and reionization redshift (calculated converting redshift to lookback time and back) as a function of the halo mass for the WMAP1-f2000 (top panel), the WMAP1-f250C(middle panel) and the WMAP3-f250C (bottom panel) simulation. Errorbars/dotted lines denote the 68 percent confidence level. The black solid line is a fit to the average redshift of reionization, as explained in the text. Note that formation redshift here means the redshift at which* $M > M_{th}$.

that by definition $z_r > z_{70\%}$, and especially for massive haloes these redshifts could differ significantly since the material that will end up in the final halo is generally spread out over a very large region in space, and therefore a fairly long time could pass from start to finish of the reionization of that halo's material. As mentioned before, z_f is the redshift at which the largest progenitor of the halo reaches M_{th}.

We find that external reionization occurs for roughly 80% of all field haloes in the WMAP1-f2000 simulation, for 40 % in the WMAP1-f250C simulation and for $\sim$ 55% in the WMAP3-f250C simulation. Apparently, our "intermediate case" with a redshift of overlap in between the two other cases, has the lowest number of externally reionized haloes. This is caused by an interplay of two different effects. First, the higher the reionizing photon production, the more effective is a halo in reionizing its surroundings. If f_γ=2000, each halo quickly reionizes a large volume, containing a mass $\sim$ 2000 times the halo mass, as recombinations are not very important. This explains the very high fraction of external reionization in the WMAP1-f2000 case, which indicates that in this

case, few early collapsing haloes are responsible for most of the reionization of the matter in the universe. The influence of the cosmological framework is more complicated. As pointed out by Alvarez et al. (2006), structure formation is delayed by a factor of ~ 1.4 in $(1+z)$ in a WMAP3 cosmology compared to a WMAP1 cosmology. This means that structure formation becomes more extended in time in a WMAP3 cosmology, i.e. the time of formation of low and high mass haloes are further apart. In order for external reionization to occur, the radiation of an early collapsing halo has to reach other haloes before they have started to form. This window in time will be shorter in a WMAP1 cosmology than a WMAP3 cosmology, which explains the lower external fraction. This means that for a WMAP3 cosmology and a higher reionizing photon production efficiency, the external fraction would be even above 80 %.

Another important outcome of our analysis is that differences in formation time cannot be directly translated into a difference in reionization time (cfr. Table 4.5.1). Due to the contribution of external reionization, field galaxies "catch up" with central cD galaxies when it comes to reionization. The time elapsed between formation and reionization (Δt) depends both on the cosmological model and on the reionization parameters. In the early-reionization scenario WMAP1-f2000, Δt for field haloes and LG-like objects is always negative and maximal in absolute value, which means that these objects form a fairly long time after they have been reionized. Field haloes are reionized on average noticeably earlier in WMAP1-f2000 model than in the extended reionization scenarios. This is to be expected considering the much faster and earlier reionization in this case, allowing for significantly fewer field haloes to form before reionization. Some L* haloes in the WMAP1-f2000 simulation also do not manage to reach a mass of M_{th} before their reionization. Thus the coeval formation and reionization of L* haloes observed in the other two simulation cases is broken for early reionization. WMAP1-f250C and WMAP3-f250C share the same reionization parameterization. Thus, differences in Δt are due to the different cosmological models. The characteristic time scale for structure formation is roughly the current Hubble time, $t_H(z)$. So, in an attempt to scale-out the cosmological dependence of Δt, we divided it by the Hubble time $t_{H,50\%}$ when the ionized fraction (in mass) is 50% to obtain $\Delta t^*=\Delta t/t_{H,50\%}$. Comparing the extended reionization scenarios, WMAP1-f250C and WMAP3-f250C, we see that Δt^* is very similar for all objects.

Haloes likely to host massive cD galaxies in centers of clusters are always internally reionized in all the different simulations. This reflects the strong inside-out nature of reionization. Reionization always starts from the highest density peaks, inside which cD haloes reside, and thus these are reionized early, regardless of the details of the reionization parameters and the background cosmology.

In summary, the timing of reionization compared to formation for L* and field haloes is sensitive to the reionization parameters (ionizing efficiency of the sources and gas clumping) and rather insensitive to the background cosmology, while in contrast the reionization history of central cD galaxies is largely independent of either the reionization parameters, or the cosmology.

In Fig. 4.3, we show the mean values of z_r and z_f as a function of the halo mass at $z = 0$. Averages are calculated by converting redshift to lookback time, averaging and converting the result again back to redshift. The reionization redshift as a function of halo mass at z=0 can be fitted by a simple polynomial:

$$\langle z_r \rangle = ax + bx^2 + cx^3 \tag{4.4}$$

Table 4.3: Fitting parameters for $\langle z_r \rangle$ (M), with $\langle z_r \rangle = ax+bx^2+cx^3$, where x=log($M/M_\odot$)

	a	b	c
WMAP1-f2000	5.07902	-0.598801	0.0223759
WMAP3-f250C	0.186979	0.0785205	-0.00104072
WMAP3-f250C	1.59182	-0.166783	0.00807599

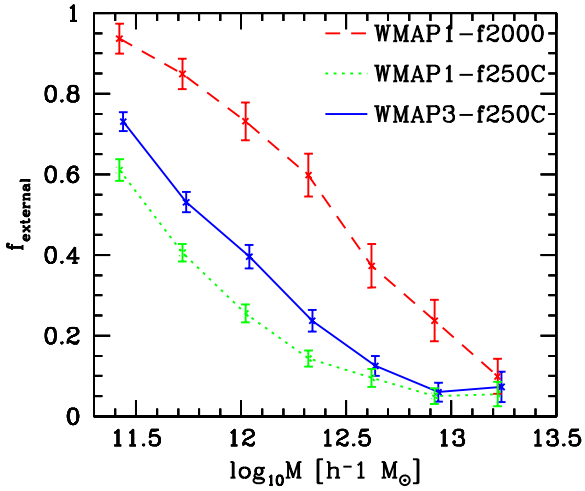

Figure 4.4: *The fraction of externally ionized haloes as a function of halo mass respectively for the three simulations considered.*

where x=log($M/M_\odot$), expressed without h^{-1}. We list the relevant values for a, b, c in Table 4.5.1.

There are clear trends for the redshift of formation and reionization as a function of halo mass. For lower mass haloes, reionization typically happens prior to their formation (external reionization), but for higher mass haloes, formation tends to predate reionization (internal reionization). As mentioned above, Alvarez et al. (2006) found that structure formation is delayed by a factor of 1.4 in (1+z) in a WMAP3 cosmology. We roughly find a similar change in the average formation time of a halo, comparing WMAP1 and WMAP3 cosmologies. The 68 percent confidence level around average formation redshift is considerably larger for a WMAP1 cosmology than for a WMAP3 cosmology at low masses. However, this simply reflects the fact that a similar interval in time corresponds to a much larger interval in redshift at higher redshifts. Measured in lookback time, the scatter around the average formation redshift is very similar in the two cosmologies and even slightly higher for WMAP3 at low masses.

In Fig. 4.4, we show the fraction of externally reionized haloes as a function of halo mass. It is apparent that the probability of external reionization is strongly dependent on mass, mainly because the formation redshift and the mass of a halo are correlated, and haloes which form later have a higher probability of being externally reionized. We note that even if on average a halo forms after it vicinity has been reionized, the fraction of externally reionized haloes can still be rather low. The reason for this is that for many

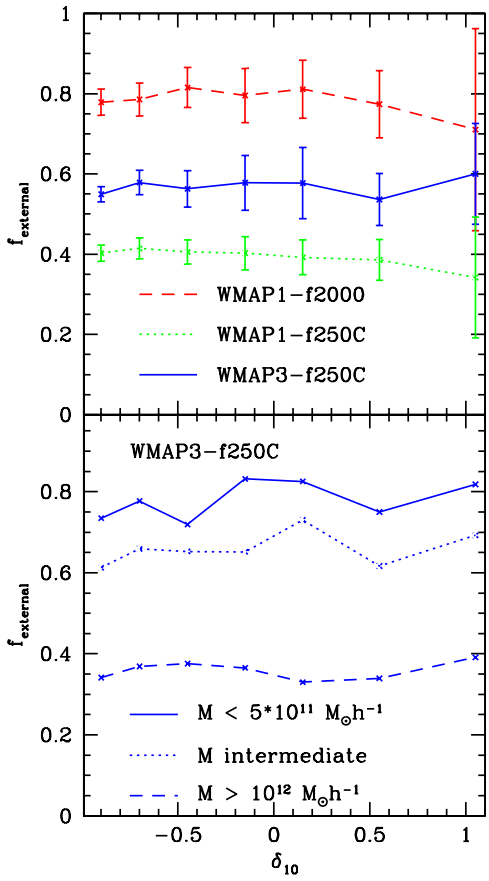

Figure 4.5: *Top Panel: The fraction of externally ionized haloes as a function of the overdensity by measuring only the mass in collapsed haloes with masses above* 5×10^{12}. *The overdensity is calculated with respect to the mean matter density in the simulation box. Results for all three simulations are shown. Errorbars denote the 1-*σ *error. Bottom Panel: Same as shown top panel, for the WMAP3-f250C simulation only, but for three different bins regarding the mass of the halo in consideration. The way the surrounding overdensity is measured remains unchanged. For clarity, no errorbars are shown.*

internally reionized haloes, the redshift of formation and the redshift of reionization are the same or at least very close. Thus, even a relatively small fraction of externally reionized haloes can shift the mean reionization redshift so that it predates the formation redshift.

Generally, one might expect that the probability of external reionization of a field galaxy could also depend upon the local overdensity around it, since the latter is closely related to the abundance of sources of ionizing radiation near the field galaxy in consideration. In Fig. 4.5 (upper panel) we plot the fraction of externally reionized field haloes as a function of the surrounding overdensity in collapsed haloes with mass $M > 5 \times 10^{12} h^{-1} \mathrm{M}_{\odot}$ at $z = 0$. The overdensity is measured within a sphere of radius 10 h^{-1}Mpc centered on the halo in consideration, does not include this central halo, and is measured relative to the average density of the simulation box. Contrary to what one might expect, there is no clear trend.

This result persists if we change the mass limit on the surrounding collapsed haloes,

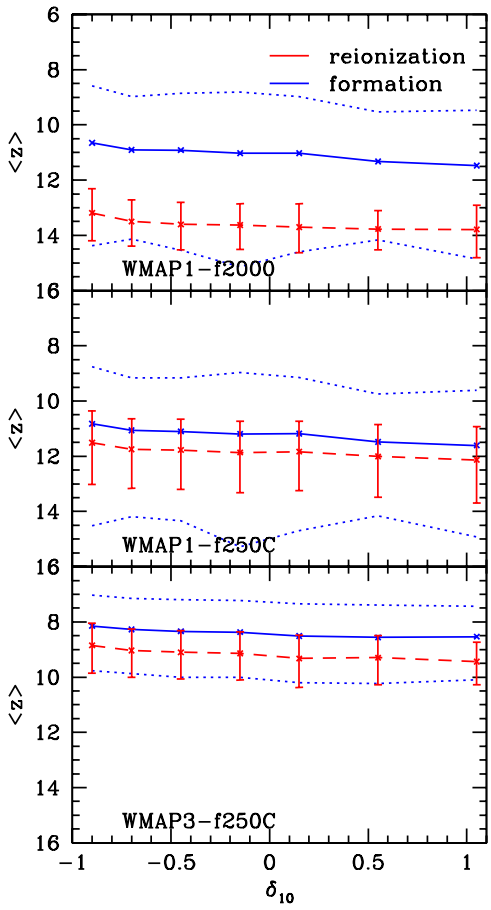

Figure 4.6: *The average formation and reionization redshift (calculated converting redshift to lookback time and back) as a function of the overdensity measured only for the mass in collapsed haloes with masses above 5* $\times 10^{12}$*, for the WMAP1-f2000 (top panel), WMAP1-f250C and the WMAP3-f250C (bottom panel) simulation. Dotted lines/errorbars denote the 1-*σ *error.*

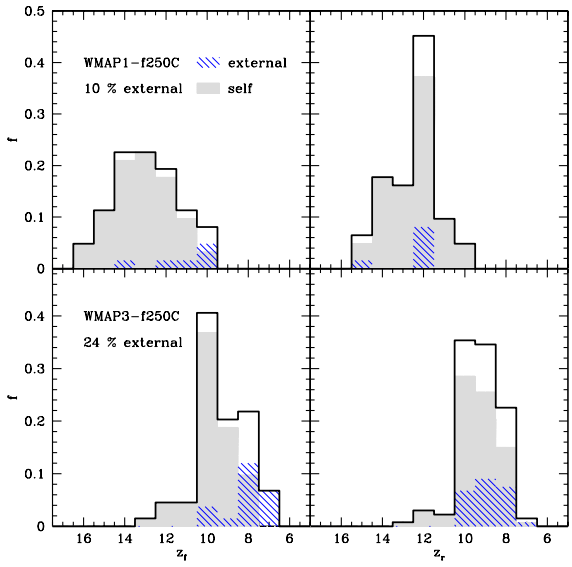

Figure 4.7: *Comparison between formation redshift (z_f) and reionization redshift (z_r) for LGs that are externally (diagonal texture) and internally (grey area) reionized. Results are shown for the WMAP1-f250C and the WMAP3-f250C simulation. Again, z_f is defined as the redshift where the mass of the halo exceeds M_{th}.*

or the radius of the sphere. In Fig. 4.5, bottom panel, we show for the example of the WMAP3-f250C simulation that the constant behaviour of the externally reionized halo fraction also persists if we divide the halo sample into different mass bins. As evident in Fig. 4.6, the reason for the constant behaviour of the external fraction with halo mass is that not only the reionization, but also the formation of a halo occurs at slightly lower redshifts in under-dense regions, since the local "clock" of structure formation is slower in voids. Therefore, we conclude that the environment of haloes does not change the way in which they are reionized, at least if the dark matter halo is isolated. For cluster and group galaxies being part of a larger dark matter halo, this statement might not be correct anymore. Satellite galaxies in massive clusters that are close to the center cD galaxy will most probably be reionized by the time when 70 percent of the dark matter mass surrounding the central cD galaxy itself is reionized. This is clearly earlier than the typical redshift where galaxies in the field are reionized. However, the difference is probably less dramatic than the difference in formation redshift. One could speculate that this means that galaxies in clusters are reionized internally more often than galaxies in the field. We have found this to be the case at least for the resolvable subhaloes in clusters, which we have identified with our subhalo finder SKID (Stadel 2001). However, since they are not a fair tracer of the subhalo population, we do not discuss our results in detail.

4.5.2 The Reionization History of the Local Group

In this section, we study the reionization history of Local Group like objects. As binary systems, Local Group like objects might be expected to have a different average formation and reionization history than typical field galaxies. Our Local Group of galaxies

also provides the most detailed set of observational data for testing the consequences of reionization on subsequent galaxy formation.We apply the same definitions of internal and external reionization we described above to our LG candidate sample. For WMAP3-f250C we find that 24% (32 out of 133 LGs) are externally reionized. For WMAP1-f250C, the probability of external reionization is only $\sim$ 10% (6 out of 62 LG). As for L* and field galaxies, WMAP1-f2000 shows the highest fraction of external reionized LGs: 44% (27 out of 62). In Fig. 4.7, we show the distribution of the reionization and formation redshifts of LG candidates for the two simulations with the lower reionization efficiency: WMAP1-f250C and WMAP3-f250C. As in Fig. 4.3 at the lower mass end, it is evident that the scatter in formation redshift is larger than the scatter in reionization redshift. This is caused by the contribution of external reionization.

To summarize, the probability for LG-like objects to be externally reionized is lower than the corresponding probability for low-mass field galaxies, which can be as high as 60-80%. Compared to typical L* galaxies, LG-like systems form slightly earlier, get reionized slightly earlier and are somewhat less likely to be externally reionized than L* galaxies.

4.6 Potential Caveats

All of our simulations resolve only haloes with masses above $M_{th} \sim 2 \times 10^9 M_\odot$ and these are the only sources which contribute to the reionization of the universe in this set of simulations. However, in hierarchical structure formation scenarios the smallest haloes form first and merge up. Thus it is expected that the first sites of star formation were "minihaloes" with a mass roughly between 10^4 and 10^8 $h^{-1}\mathrm{M}_\odot$. By definition the minihaloes have virial temperatures below 10^4 K, where the radiative gas cooling through hydrogen and helium atomic lines is not efficient. Thus, these haloes have to rely on the much less efficient molecular line cooling for their star formation. However, the hydrogen molecules are easily destroyed by radiative feedback (e.g. Haiman, Abel & Rees 2000) and thus it is generally expected that most minihaloes were 'sterilized' and in most cases did not form stars (e.g. Shapiro et al. 2004; Iliev et al. 2005b, and references therein). Haloes with a mass between 10^8 and $10^9 M_\odot$, on the other hand, which are also not resolved in our simulations, are able to cool efficiently and may actually be an important source of ionizing radiation. Iliev et al. (2007) have performed a number of smaller-scale high-resolution simulations of reionization, with a simulation volume $(35\,\mathrm{h}^{-1}\mathrm{Mpc})^3$, which include radiation from these smaller haloes. The most important effect is that reionization starts much earlier than without those sources. However, due to Jeans-mass filtering in the ionized regions and the strong clustering of haloes around the density peaks, the majority of these low-mass haloes are suppressed throughout most of the reionization process and hence their effect is mostly limited to the early stages of reionization and the progress of reionization is delayed. The time of overlap and the large-scale geometry of reionization are both largely dominated by the high-mass haloes and thus are not strongly affected by the absence of low-mass haloes in the simulations.

Could the inclusion of low-mass haloes and minihaloes significantly modify our results? A halo with a mass of $10^8 M_\odot$ can reionize a mass between $2.5 \times 10^{10} - 2.5 \times 10^{11} M_\odot$ (somewhat decreased once recombinations are accounted for) during its lifetime of $\sim$20 Myr (before star formation shuts off again due to feedback, and recombinations set in, decreasing the reionized fraction further). Thus, in order to reionize a (proto-)halo with a mass

around $10^{12} M_{\odot}$, several $10^{8} M_{\odot}$ haloes ought to have formed at very similar times within the region considered. They should also have been spaced far enough apart so that the halo forming first does not suppress star formation in the other haloes. If this were the case, this group of $\sim 10^{8} M_{\odot}$ haloes would most probably quickly merge, forming a halo with a mass above $10^{9} M_{\odot}$, which would be resolved in our simulations. Moreover, regions which contain only $10^{8} - 10^{9} M_{\odot}$ haloes, but not any of the more massive ones tend to be near the boundaries of the ionized regions, and are thus quickly overrun by the expanding I-fronts. Furthermore, both low-mass atomically-cooling haloes and minihaloes are strongly clustered around the density peaks, which are the first regions to be reionized, as we have shown. Therefore the vast majority of these small haloes would be affected by Jeans-mass filtering. As a consequence, haloes forming after their vicinity is ionized would not be able to accrete gas, while haloes that have formed before their region became ionized would either not accrete more gas and thus have their star formation shut off (in the case of low-mass sources), or would be photoevaporated (in the case of minihaloes).

For all these reasons, we expect that neither haloes with masses between $10^{8} - 10^{9} M_{\odot}$, nor minihaloes would change our average reionization redshifts significantly and hence would not modify our results for the external/internal reionization fractions. Once future cosmological simulations become large enough to allow resolving low-mass haloes in a large volume, it would be interesting to verify if our assertions here are correct and evaluate the level of this effect precisely.

Furthermore, the reionization parameters, photon production efficiencies and small-scale gas clumping (and to lesser level, also the background cosmology) are still quite uncertain. We have addressed this by comparing three reionization scenarios which roughly bracket the expected range of reionization histories, from the very early reionization given by f2000_WMAP1 (high-efficiency sources, no sub-grid clumping, WMAP1 cosmology), to the late overlap, extended reionization scenarios, f250C_WMAP1 and f250C_WMAP3 (low-efficiency sources, sub-grid clumping, WMAP1 or WMAP3 cosmology). Most of the reasonable reionization scenarios which satisfy the current observational constraints should fall between these cases. Further improvement would require better, more detailed observational data which would constrain the reionization scenarios (and thus the reionization parameters) better.

4.7 Implications of External vs. Internal Reionization regarding Galaxy Properties

Reionization can affect the properties of galaxies in many ways, and the relative timing of reionization across the mass scales will leave distinct observable signatures.

- The mode of galaxy formation may be fundamentally different between haloes less massive and more massive than $10^{12} M_{\odot}$. Late forming haloes that are externally ionized will have hotter, more extended and smoother gas distributions. The gas accretion into the galaxy will proceed differently, perhaps providing an explanation for the red-blue galaxy sequence, bulgeless disks, lower-baryon fractions in less massive galaxies, etc.

- Early star formation will be affected, since stars forming in ionized gas may have different properties than stars forming in neutral gas. According to Johnson &

Bromm (2006), Pop II.5 could have formed from primordial gas that is strongly ionized since the free-electron-catalyzed formation of molecules enables enhanced gas cooling. Similarly, Nagakura & Omukai (2005) predict the formation of low mass stars in ionized gas with very low metallicity. External reionization provides an alternative pathway to Pop II.5 star formation.

- The abundance of Galactic satellites has been reconciled with observational data using the idea that reionization suppresses the formation of late forming haloes - only the rare peaks that collapse before reionization can cool gas to form stars. If the gas in a late-forming galaxy is externally reionized it may suppress the formation of some or even all of its satellite population.

- The radial distribution of old stars in the Galactic Halo might reflect the rarity of the density peaks in which they formed at the epoch of reionization (Diemand, Madau & Moore 2005, Moore et al. 2006). If stars form only in the rarest peaks, then their final distribution can be highly concentrated with a radial profile as steep as r^{-4}. Thus, externally reionized galaxies may be expected to have steeper diffuse stellar halo profiles.

- Similar to the old stellar halo, globular cluster formation may be truncated at reionization, altering the relative abundances and radial distributions of the old blue population in galaxies of different masses and environments. Rhode et al. (2005) found that the number of old blue GCs per galaxy stellar mass increases with increasing mass for cluster ellipticals, while it seems to be constant for spiral galaxies in the field. They suggest that the reason for this is that more massive elliptical galaxies assemble earlier and have more time to form blue GC before reionization, assuming that reionization happens at a fixed point in time. Although we find that reionization will occur considerably earlier in massive elliptical galaxies than for low-mass field galaxies, their redshift of formation is shifted even more strongly, as they are usually internally reionized. Thus it is indeed the case that typically more time elapses between the formation and reionization of massive cluster ellipticals than for field galaxies.

We conclude that it may already be possible to discriminate between galaxies that have been reionized internally or externally using one or more of the above characteristics. This will be an interesting new and complementary way to probe the history of reionization in the Universe and its effect on galaxy formation.

4.8 Summary and Discussion

The reionization history of a given galaxy is strongly dependent on its mass due to the correlation between galaxy mass and formation redshift. Higher mass haloes on average form earlier and are also reionized earlier. The lower the mass of a halo, the more important does external reionization (i.e. reionization emanating from sources outside the halo) become. The effect of the large-scale environment on the reionization history, on the other hand, is negligible for field haloes. By using a simple polynomial fit, we can parameterize the average reionization redshift of a galaxy as a function of halo mass for three different

combinations of cosmology and reionizing photon production efficiency. Typical L* galaxies and LG like systems are reaching reionization considerably before the final overlap, at a redshift where roughly half of the universe is reionized. Very massive, elliptical galaxies in clusters are reionized even earlier and are always internally-reionized. Our prescription for the reionization redshift as a function of galaxy mass might be of use for semi-analytical models of galaxy formation. Normally, these models assume a fixed, fairly low redshift of reionization of around $z \sim 7$ (e.g. Croton et al. 2006), from which the baryon fraction in a low mass haloes can be calculated, given redshift and halo mass (Gnedin 2000, Kravtson et al. 2004). Using our fitting formulae, one could utilize a more realistic reionization redshifts in semi-analytical models by introducing a dependence on the mass of the halo in which a given subhalo ends up. This may help alleviate the problem of the overproduction of satellite galaxies in massive clusters in semi-analytical models (Weinmann et al. 2006).

We suggest that whether a galaxy experiences internal or external reionization might affect its properties considerably. Externally reionized haloes could experience different gas accretion: could have a different first generation of stars (i.e. Pop II.5 instead of Pop III); may host a lower number of satellite galaxies and blue globular clusters; and could have steeper diffuse stellar halo profiles.

Acknowledgments

Part of the N-body simulations have been performed on the zBox2 supercomputer at the University of Zurich (http://www-theorie.physik.unizh.ch/~dpotter/zbox2/). We thank D. Potter and J. Stadel for building and maintaining the zBox2. We also thank F. van den Bosch and M. Volonteri for useful discussion and an anonymous referee for comments which helped us improve this work. SW has been partially supported by the Swiss National Science Foundation (SNF).

Chapter 5

Concluding Remarks

Consistency is the last refuge of the unimaginative.

Oscar Wilde

5.1 What have we learned?

The most important scientific results of my thesis are the following:

- It is indeed useful to describe galaxy environment in terms of the halo mass in which a given galaxy resides, and we have found a nice and smooth dependence of galaxy type fractions on halo mass. This relation still lacks complete theoretical explanation, but may help to discriminate between different models explaining galaxy evolution as a function of environment. For example, our results indicate that processes inhibiting star formation can not only be occurring in massive clusters, but are already at work in poor groups.

- Although it sometimes seems that we have all the necessary ingredients to roughly explain galaxy evolution and formation on large scales using semi-analytical models, this is in fact not yet the case. For example, as we have shown in Chapter 3 of this thesis, the fraction of red satellites is much too high in semi-analytical models considered state-of-the-art at present. In the meantime, this result has been confirmed by other studies (e.g. Coil et al. 2007). The overproduction of red satellites may be a small problem which can easily corrected; but due to the complexity of the semi-analytical model this correction could cause another problem.

- We have found that reionization, which is invoked to explain many different observations like the missing satellite problem, the abundance of blue globular clusters etc., is likely to occur at quite different times for galaxies of different masses and therefore at different stages in their own formation process. This is expected to introduce correlations between galaxy mass and different observables that are suggested to be linked to reionization.

Galaxies are crucially dependent on their cold gas supply. So many mechanisms have been suggested that might heat up or expel the gas from the galaxies that it even seems surprising that most galaxies are still able to form stars. Thus, it is likely that some of the proposed mechanisms are less efficient than predicted or even not occurring at all. Maybe in some years only a few of the proposed mechanisms will have survived, which would make things clearer and easier to model. In the ideal case, we would be left with one mechanism that becomes effective above a certain stellar mass, one that only affects satellites and one that inhibits star formation in small galaxies. Maybe we will even only be left with one main process which is triggered in a different way for the three cases listed above. "Hot" vs. "cold" accretion seems to be a promising candidate which could simplify our picture of galaxy evolution.

5.2 Outstanding Issues and Future Projects

5.2.1 Estimating the Efficiency of Strangulation

As mentioned above, a large number of mechanisms have been suggested which could truncate star formation in galaxies and/or induce morphological transformation, and it is important to investigate those processes in detail. The process I find most interesting at the moment is strangulation, which is likely to be important, but probably overestimated in semi-analytical models. In order for the surrounding hot halo gas around a galaxy to be removed, the ram pressure has to be higher than the gravitational pressure. To get a first rough estimate of the efficiency of strangulation, we have made the following calculation. The gravitational pressure as a function of the radius r of the gas halo of the infalling galaxy is equal to the thermal pressure, which can be approximated by:

$$P_{\rm thermal}(r) = \frac{GM\rho_{\rm gas}(r)}{3 \cdot r_{200}} \tag{5.1}$$

if one assumes the gas to have a constant temperature, which is equal to the virial temperature (Mori & Burkert 2000). G is the gravitational constant, M the mass of the dark matter halo of the infalling galaxy, $\rho_{\rm gas}$ is the density of the gas, assuming that it traces the dark matter, and r_{200} is the radius at which the density of the enclosed mass is 200 times the critical density of the universe. On the other hand, the ram pressure as a function of the radius of the host halo is characterized by

$$P_{\rm ram}(R) = \rho_{\rm gas,host}(R) \cdot v^2 \tag{5.2}$$

where v is the velocity of the infalling halo. Using these simple equations, we investigate the case of a small galaxy residing in a halo with mass $10^{11} M_{\odot}$, a gas fraction of 1% and a central concentration of 16, which falls into a small galaxy group in a halo with mass $10^{12} M_{\odot}$, a gas fraction of 1% and a central concentration of 10. We assume that the galaxy is falling in with a velocity of 100 km/s. In such a case, one would assume that strangulation is minimal, due to the low fraction of gas in the parent halo, its small mass and the low infall velocity. However, even if we assume that the closest approach to the center of the larger halo is only at $0.4 \cdot R_{200}$, the small halo will have its surrounding gas halo stripped down to $0.15 \cdot r_{200}$. This is even without the influence of supernova feedback, which tends to make the gas halo less bound, and the consumption of gas by

star formation. Therefore, it seems that strangulation is efficient even in small groups, which is in agreement with the findings of Hester 2006 and Kawata & Mulchaey 2007. The latter find that efficient removal for a hot gas halo around a galaxy in a $3 \cdot 10^{11} M_{\odot}$ halo is occurring within 1 Gyr when it falls into a halo with a mass of $7 \cdot 10^{12} M_{\odot}$. So why are many satellites in the real world still blue?

What is not taken into account in the semi-analytical model is the following:

- A large fraction of groups and clusters (30 – 50% according to Rasmussen et al. 2006 and references therein) found in the dark matter simulation are actually collapsing for the first time at present. Those systems are not expected to contain a hot intragroup/intracluster medium which could strip galaxies of their hot gas halo. In such systems, the shutdown of star formation will thus be far from complete.

- The timescale of the decline in star formation in semi-analytical models might be too short, since it is assumed that all the gas is stripped immediately, which is not the case. Also, the efficiency with which gas is reheated (which is the efficiency with which cold disk gas is added to the hot gas halo, where it can be stripped) is assumed to be independent of mass (e.g. Croton et al. 2006), which is not the case: in more massive galaxies, gas is ejected into the hot halo far less easily due to the greater gravitational potential well, which may make it possible for the galaxy to retain more gas than expected.

It is at present not clear if changing the details mentioned above would bring model and observations into better agreement.

One should also bear in mind that the surrounding hot halo around star forming galaxies has not been proven to exist — there is only one detection of a hot gas halo around a disk galaxy, which is still quite uncertain (Pedersen et al. 2006). Gas maybe accretes into galaxies in the form of cold clumps along filaments ("cold accretion", e.g. Dekel & Birnboim 2006). It is not clear exactly what the effect of the hot intragoup medium on this form of accretion might be, although it is quite obvious that it would be disturbing it in some way. Detailed modelling of such a process is still outstanding.

5.2.2 Gas Stripping in the LMC

A nearby example of an ongoing interaction between a galaxy and its surrounding medium is the Large Magellanic Cloud. Recent results by Kallivayalil et al. 2006 and Besla et al. 2007 indicate that the LMC has a much higher 3D velocity than previously estimated and is likely on its first orbit around the Milky Way. This makes it even harder for theoretical models to explain the observed stripping of the LMC, which is expected to be the origin of the Magellanic Stream. Previous simulations of the origin of the Magellanic Stream (e.g. Mastropietro et al. 2005b) were thus relying on potentially faulty assumptions of the orbital parameters of the LMC; in addition, as shown by Agertz et al. 2006, the previously used SPH simulations are not able to capture the complexity of gas stripping. Therefore, we plan to revisit the question of the stripping of the LMC in a simulation using AMR and the new orbital parameters. Since we can compare our results to nearby and very detailed observations, we will hopefully be able to test whether or not AMR simulations are able to capture gas stripping of galaxies falling into larger haloes. If this is the case, it will be a natural next step to carry out simulations of galaxies orbitting in clusters and

groups and to estimate the efficiency of strangulation and ram-pressure stripping of the ISM in these cases.

5.2.3 Satellite Galaxies vs. Central Galaxies

In an ongoing project (van den Bosch et al., in prep.) we are examining the difference between satellite and central galaxies in an updated group catalogue based on the SDSS DR4. Our results suggest that the average colour difference between a given satellite and a random central galaxy of the same stellar mass is in fact very small. This seems to be somewhat at odds with the results presented in Chapter 2 of this thesis; the reason for this is that we have used a magnitude-dependent colour cut to distinguish between early- and late-type galaxies which emphasized the difference between central and satellite galaxies. Furthermore, we find that only relatively low-mass galaxies in fact undergo a transformation when changing from being a central galaxy to being a satellite galaxy; galaxies with a high stellar mass ($> 10^{11} M_{\odot}$) are not becoming any redder when they become part of a larger system. Surprisingly, we also find that the transformation efficiency at fixed stellar mass is *independent* of the group mass. This seems to be in contradiction with our finding in Chapter 2 where we have shown that the early type fraction at fixed luminosity is increasing with group mass. However, note there is no one-to-one mapping between luminosity and stellar mass. Satellites in massive haloes may tend to be more massive than satellites in smaller groups and due to their higher mass the probability that they were already red *before* becoming part of a group is enhanced. Since red galaxies tend to be significantly less luminous than blue galaxies, it is likely that the galaxies which we find to be in the same luminosity bin in high and low mass groups are in fact in different stellar mass bins, with the galaxies residing in higher mass groups tending to reside in the high stellar mass bin.

This new findings are in agreement to what we have suspected already in Chapter 2 to be the origin of the enhanced fraction of red galaxies in groups: Strangulation would exactly lead to the trends described above. Strangulation is occurring both in low and high mass groups (e.g. Hester et al. 2006, Kawata & Mulchaey 2007) and it is likely to be more efficient for galaxies with lower stellar mass, since due to the more shallow potential wells supernova feedback can eject gas more easily into the hot halo in such systems.

5.2.4 Isolated Blue Galaxies

According to Maulbetsch et al. (private comm.), it is not clear why isolated, blue galaxies are blue. According to the hierarchical scenario, they should form relatively early. The highly efficient supernova feedback quickly heats up their surrounding hot gas halo and makes cooling very inefficient. This problem is not addressed in current semi-analytical models like for example in the one by Croton et al. 2006, since their lower mass limit is too low. It will thus be interesting to see what problems will be encountered in future semi-analytical models with an increased mass resolution.

5.2.5 The Reionization History of Galaxies in Clusters

In Chapter 4, we have examined the reionization history of isolated galaxies. It is a natural next step to investigate how galaxies in clusters are reionized. Galaxies in clusters form earlier, but also become reionized earlier. Thus, it is not clear a priori if galaxies in clusters

are normally reionized externally or internally. In an ongoing project (Macciò et al., in prep), we plan to investigate this issue. See Fig. 5.1 for an image of one of the clusters which is currently being analyzed.

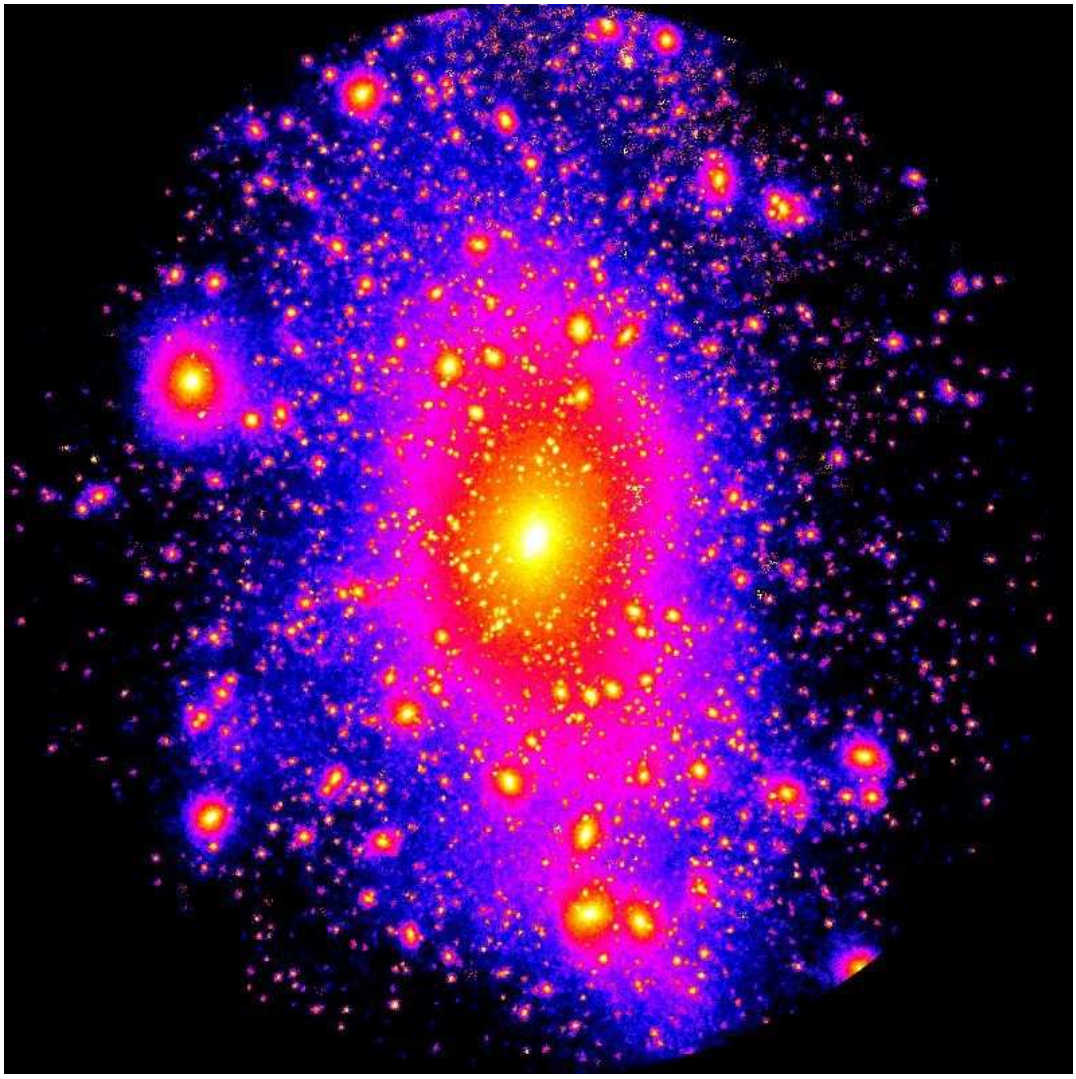

Figure 5.1: *This is one of the clusters for which the detailed reionization history is currently analyzed. It contains 12 million particles within 1.5 Mpc and has a mass of* $1.7 \cdot 10^{14} M_{\odot}$. *There are roughly 400 satellites present within this cluster.*

Bibliography

Abazajian, K. et al, 2004, AJ, 128, 502

Agertz O. et al., to be submitted to MNRAS, astro-ph/0610051

Aguilar L.A., White S.D.M., 1985, ApJ, 295, 374

Alvarez M.A., Shapiro P.R., Ahn K., & Iliev I.T., 2006, ApJL, 644, L101

Baldry I.K., Glazebrook K., Brinkmann J., Ivezić Ž., Lupton R.H., Nichol R.C., Szalay A.S., 2004, ApJ, 600, 681

Baldwin J.A., Phillips M.M., Terlevich R., 1981, PASP, 93, 5

Balogh M.L., Morris S.L., Yee H.K.C., Carlberg R.G., Ellingson E., 1997, ApJ, 488, L75

Balogh M.L., Morris S.L., Yee H.K.C., Carlberg R.G., Ellingson E., 1999, ApJ, 527, 54

Balogh M.L., Navarro J.F., Morris S.L., 2000, ApJ, 540, 113

Balogh M.L., et al., 2004a, MNRAS, 348, 1355

Balogh M.L., Baldry I.K., Nichol R., Miller C., Bower R., Glazebrook K., 2004b, ApJ, 615, L101

Barkana R., & Loeb A. 2004, ApJ, 609, 474

Baugh C.M., 2006, Reports on Progress in Physics, 69, 3101

Beers T.C., Flynn K., Gebhardt K., 1990, AJ, 100, 32

Bekki K., Couch W.J., Shioya Y., 2002, ApJ, 651, 657

Bell E.F., Wolf C., Meisenheimer K., Rix H.-W., Borch A., Dye S. Kleinheinrich M., Wisotzki L., McInthosh D.H., 2004, ApJ, 608, 75

Bell E.F., Zheng Z.X., Papovich C., Borch A., Wolf C., Meisenheimer K., 2007, ApJ, 663, 834

Berlind A.A., Weinberg D.H., Benson A.J., Baugh C.M. Cole S., Davé R., Frenk C. S., Jenkins A., Katz N., Lacey C.G., 2003, ApJ, 593, 1

Berlind A.A., et al., 2006, ApJ, 167,1

Besla, G., Kallivayalil, N., Hernquist, L., Robertson, B., Cox, T. J., van der Marel, R. P.,

& Alcock, C. 2007, preprint, astro-ph/0703196

Benson A.J., Lacey C.G., Baugh C.M., Cole S., Frenk C.S., 2002, MNRAS, 333, 156

Benson A.J., Bower R.G., Frenk C.S., Lacey C.G., Baugh C.M., Cole S., 2003, ApJ, 599, 38

Bernstein G.M., Nichol R.C., Tyson J.A., Ulmer M.P., Wittman D., 1995, AJ, 110 1507

Birnboim, Y., Dekel, A., & Neistein, E. 2007, preprint, astro-ph/0703435

Biviano A., Katgert P., Thomas T., Adami C., 2002, A&A, 387, 8

Blair M., Gilmore G., 1982, PASP, 94, 741

Blanton M. R. et al. , 2001, AJ, 121, 2358

Blanton M. R. et al. , 2003a, ApJ, 592, 819

Blanton M. R. et al. , 2003b, ApJ, 594, 186

Blanton M. R. et al. , 2003c, AJ, 125, 2348

Blanton M.R. et al. , 2005a, AJ, 129, 2562

Blanton M.R., Eisenstein D., Hogg D.W., Schlegel D.J., Brinkman J., 2005b, ApJ, 629, 143

Blanton M.R., Eisenstein D., Hogg D.W., Zehavi I., 2006, ApJ, 645, 977

Blumenthal G.R., Faber S.M., Primack J.R., Rees M.J, 1984, Nature, 311, 517

Bonnell I.A., Bate M.R., Clarke C.J., Pringle J.E., 1997, MNRAS, 285, 201

Boselli A., Gavazzi G., 2006, PASP, 118, 517

Bower R.G., Benson A.J., Malbon R., Helly J.C., Frenk C.S., Baugh C.M., Cole S., Lacey C.G., 2006, 370, 645

Brainerd T.G., Specian M.A., 2003, ApJ, 593, L7

Brinchmann J., Charlot S., White S.D.M, Tremonti C., Kauffmann G., Heckman T., Brinkmann J., 2004, MNRAS, 353, 713

Bryan G., Norman M., 1998, ApJ, 495, 80

Bullock J.S., Kolatt T.S., Sigad Y., Somerville R.S., Kravtsov A.V., Klypin A.A., Primack J.R., Dekel A., 2001, MNRAS, 321, 559

Bullock J.S., Kravtsov A.V., & Weinberg D.H., 2004, ApJ, 539, 517

Byrd G., Valtonen M., 1990, ApJ, 350, 89

Cattaneo A., Dekel A., Devriendt J., Guiderdoni B., Blaizot J., 2006, MNRAS, 370, 1651

Cattaneo A. et al. , 2007, MNRAS, 377, 63

Chung A., van Gorkom J.H., Kenney J.D.P., Vollmer B., 2007, ApJ, 659, 115

Ciotti L., Ostriker J.P., 1997, ApJ, 487, L105

Coil A.L., et al., 2007, submitted to ApJ, preprint, astro-ph/0708.0004

Cole S., Lacey C.G., Baugh C.M., Frenk C.S., 2000, MNRAS, 319, 168

Colless M., The 2dFGRS team, 2001, MNRAS, 328, 1039

Collister A.A., Lahav O., 2005, MNRAS, 361, 415

Conroy C., Wechsler R.H., Kravtsov A.V., 2006, ApJ, 647, 201

Cooper M.C., Newman J.A., Madgwick D.S., Gerke B.F., Yan R., Davis M., 2005, ApJ, 634, 833

Cooper M.C. et al., 2007, preprint (astro-ph/0706.4089)

Cooray A., Sheth R., 2002, Phys. Rep. 372, 1

Cooray A., 2005, MNRAS, 363, 337

Cooray A., Milosavljević M., 2005, ApJ, 627, L89

Cowie, L.L., Songalia A., Hu E.M., Cohen J.G., 1996, AJ, 112, 839

Cowie L.L., Songalia A., 1977, Nature, 266, 501

Croton D.J., et al., 2005, MNRAS, 356, 1155

Croton D.J., et al., 2006, MNRAS, 356, 11

Cucciati O., et al., 2006, A&A, 458, 39

Davies R.L, Efstathiou G., Fall S.M., Illingworth G., Schechter P.L., 1983, ApJ, 266, 41

Dekel A., Silk J., 1986, ApJ, 303, 39

Dekel, A., & Birnboim, Y. 2006, MNRAS, 368, 2

Dekel, A., & Birnboim, Y. 2007, preprint, astro-ph/0707.1214

De Lucia G., Springel V., White S.D.M, Croton D., Kauffmann G., 2006, MNRAS, 366, 499

De Lucia G., to appear in ASP Conference Series (Proceedings of the "Cosmic Frontiers" conference), preprint, astro-ph/0611350

De Propris R., et al., 2004, MNRAS, 351, 125D

Diaferio A., Kauffmann G., Balogh M.L, White S.D.M, Schade D., Ellingson E., 2001, MNRAS, 323

Diemand J., Madau P., & Moore, B. 2005, MNRAS, 364, 367

Dijkstra M., Haiman Z., Rees M.J., & Weinberg D.H., 2004, ApJ, 601, 666

Domínguez M.J., Muriel H., Lambas D.G., 2001, AJ, 121, 1266

Domínguez M.J., Zandivarez A.A., Martínez H.J., Merchán M.E., Muriel H., Lambas D.G., 2002, ApJ, 335, 825

Dressler A., 1980, ApJ, 236, 351

Dutton A.A., van den Bosch F.C., Dekel A., Courteau S., 2007, ApJ, 654, 27

Ebeling H., Voges W., Böhringer H., 1994, ApJ, 436, 44

Efstathiou G., 1992, MNRAS, 256, 43

Eggen O.J., Lynden-Bell D., Sandage A.R., 1962, AJ, 136, 748

Eke V.R.& The 2dFGS team, 2004a, MNRAS, 348, 866

Eke V.R.& The 2dFGS team, 2004b, MNRAS, 355, 769

El-Zant A., Kim W.-T., & Kamionkowski M. 2004, MNRAS, 354, 169

Evrard A.E., Silk J., Szalay A.S., 1990, ApJ, 365, 13

Faber S.M., et al., 2005, preprint (astro-ph/0506044)

Fabian A.C et al, 2003, MNRAS, 344, L43

Fukugita M., Ichikawa T., Gunn J.E., Doi M., Shimasaku K., Schneider D.P., 1996, AJ, 111, 1748

Gao L., White S.D.M., Jenkins A., Stoehr F., Springel V., 2004, MNRAS, 355, 819

Gao L., Springel V., White S.D.M., 2005, MNRAS, 363, 66

Gao L., White S.D.M, 2007, MNRAS, 377L, 5

Geller M.J., Huchra J.P., 1983, ApJS, 47, 139

Gerke B.F. et al., 2005, ApJ, 625, 6

Ghigna S., Moore B., Governato F., Lake G., Quinn T., Stadel J., 1998, MNRAS, 300, 146

Girardi M., Rigoni E., Mardirossian F., Mezzetti M., 2003, A&A, 406, 403G

Gnedin N.Y. 2000, ApJ, 542, 535

Gómez P.L., et al., 2003, ApJ, 584, 210

Gonzales A.H., Zabludoff A.I., Zaritsky D., Dalcanton J.J., 2000, ApJ, 536, 561

Goto T., Yamauchi C., Fujita Y., Okamura S., Sekiguchi M., Smail I., Bernardi M., Gomez P.L., 2003, MNRAS, 346, 601

Goto T., Masafumi Y., Tanaka M., Okamura S., 2004, MNRAS, 348, 515

Goto T., 2005, MNRAS, 356, L6

Granato G.L., De Zotti G., Silva L., Bressan A., Danese L., 2004, MNRAS, 600, 580

Guth A.H, Physical Review D, 1981, 23, 347

Gunn J.E., Gott J.R., 1972, ApJ, 176, 1

Haiman Z., Abel T., & Rees M.J. 2000, ApJ, 534, 11

Haiman Z. & Bryan G.L. 2006, ApJ, 650, 7

Hashimoto Z., Oemler A., Lin H., Tucker D.L., 1998, ApJ, 499, 589

Hashimoto Z., Oemler A., 1999, ApJ, 510, 609

Heavens A., Panter B., Jimenez R., Dunlop J., 2004, Nature, 428, 625

Hester J.A. 2006, ApJ, 647, 910

Hickson P., Ninkov Z., Huchra J., Mamon G., 1984, in Clusters and Groups of Galaxies, eds. F. Mardirossian, G. Giuricin, M. Mezzetti, Reidel, Dordrecht, Holland, p. 367

Hogg D.W., et al., 2003, ApJ, 585, L5

Hogg D.W., et al., 2004, ApJ, 601, L29

Hopkins P.F., Hernquist L., Cox T.J., Di Matteo T., Robertson B., Springel V., 2006, ApJS, 163, 1

Hoyle F., Rojas R.R., Vogeley M.S., Brinkmann J., 2005, ApJ, 620, 618

Huchra J.P., Geller M.J., 1982, ApJ, 257, 423

Iliev I.T., Scannapieco E., & Shapiro P.R., 2005a, ApJ, 624, 491

Iliev I.T., Shapiro P.R., & Raga A.C, 2005b, MNRAS, 361, 405

Iliev I.T., et al. 2006a, MNRAS, 371, 1057

Iliev I.T., Mellema G., Pen U.-L., Merz H., Shapiro P.R., & Alvarez M.A., 2006b, MNRAS, 369, 1625

Iliev I.T., Mellema G., Shapiro P.R., & Pen U.L., 2007, MNRAS, 376, 534

Jenkins A., Frenk C.S., White S.D.M., Colberg J.M. Cole S., Evrard A.E., Couchman H.M.P., Yoshida N., 2001, MNRAS, 321, 372

Jing Y.P., Suto, Y., 2002, ApJ, 574, 538

Johnson J.L. & Bromm V. 2006, MNRAS, 366, 247

Kallivayalil, N., van der Marel, R. P., & Alcock, C. 2006, ApJ, 652, 1213

Kang X., Jing Y.P, Mo H.J., Börner G., 2005, ApJ, 631, 21

Kauffmann G., White S.D.M, Guiderdoni B., 1993, MNRAS, 264, 201

Kauffmann G., Charlot S., 1998, MNRAS, 294, 705

Kauffmann G., et al. , 2003, MNRAS, 341, 33

Kauffmann G., White S.D.M, Heckman T.M., Ménard B., Brinchmann J., Charlot S., Tremonti C., Brinkmann J., 2004, MNRAS, 353, 713

Kawata, D., & Mulchaey, J. S. 2007, preprint, astro-ph/0707.3814

Kelm B., Focardi P., Sorrentino G., 2005, A&A, 442, 117

Kepner J., Fan X., Bahcall N., Gunn J., Lupton R., Xu G., 1999, ApJ, 517, 78

Kereš, D., Katz, N., Weinberg, D. H., & Davé, R. 2005, MNRAS, 363, 2

Khochfar S. & Ostriker J.P., 2007, submitted to ApJ, astro-ph/0704.2418

Kim R.J.S. et al, 2002, AJ, 123, 20

Klypin A., Kravtsov A.V., Valenzuela O., & Prada F., 1999, ApJ, 609, 482

Kochanek C.S., White M., Huchra J., Macri L., Jarrett T.H., Schneider S.E., Mader J., 2003, ApJ, 585, 161

Kodama T., Bower R.G., 2001, MNRAS, 321, 18

Kodama T., et al., 2004, MNRAS, 350, 1005

Koester B.P., et al. 2007, ApJ, 660, 239

Koopmann R. A., Kenney D. P., 2004, MNRAS, 613, 866

Kravtsov A.V., Gnedin O.Y., & Klypin A.A., 2004, ApJ, 522, 82

Krumholz M.R., McKee C.F., Klein R.I., 2005, Nature, 7066, 332

Kuehn F., Ryden B.S., 2005, ApJ, 634, 1032

Larson R.B., 1974, MNRAS, 169, 229

Larson R.B., Tinsley B.M., Caldwell C.N., 1980, ApJ, 237, 692

Lemson G. & Kauffmann G., 1999, MNRAS, 302, 111

Levy L., Rose J.A., van Gorkom J.H., Chaboyer B., 2007, AJ, 133, 1104

Lewis I, et al., 2002, MNRAS, 334, 673

Li, Z., Wang, Q. D., Hameed, S., 2007, MNRAS, 376, 960

Loveday J., Peterson B.A., Efstathiou G., Maddox S.J., 1992, A&A, 390, 338

Macciò A.V., Dutton A.A., van den Bosch F.C., Moore B., Potter D., & Stadel J. 2007, MNRAS, 378, 55

Macciò A.V., Governato F., & Horellou C., 2005, MNRAS, 359, 941

Madgwick D.S. & the 2dFGRS team, 2002, MNRAS, 333, 133

Madau P. et al., 1996, MNRAS, 283, 1388

Magliocchetti M. & Porciani C., 2003, MNRAS, 345, 186

Martínez H.J., Zandivarez A., Domínguez M., Merchán M.E., Lambas D.G., 2002, MNRAS, 333, L31

Marzke R.O., da Costa L.N., 1997, AJ, 113, 185

Marzke R.O., da Costa L.N., Pellegrini P.S., Willmer C.N.A., Geller M.J., 1998, ApJ, 503, 617

Mastropietro, C., Moore, B., Mayer, L., Debattista, V. P., Piffaretti, R., Stadel, J., 2005a, MNRAS, 364, 607

Mastropietro, C., Moore, B., Mayer, L., Wadsley, J., Stadel, J., 2005b, MNRAS, 363, 509

Maulbetsch C. et al., 2007, ApJ, 654, 53

McKay T.A., et al, ApJ, 2002, 571, L85

McNamara B.R., Nulsen P.E.J., Wise M.W., Rafferty D.A., Carilli C., Sarazin C.L., Blanton E.L., 2005, Nature, 433, 45

Melbourne J., Koo D.C., & Le Floc'h E., 2005, ApJ, 632, L65

Mellema G., Iliev I.T., Alvarez M.A., & Shapiro P.R., 2006a, New Astronomy, 11, 374

Mellema G., Iliev I.T., Pen U.-L., & Shaprio P.R. 2006b, MNRAS, 372, 679

Menci N., Fontana A., Giallongo E., Salimbeni S., 2005, ApJ, 632, 49

Merchán M., Zandivarez A., 2002, MNRAS, 335, 216

Merz H., Pen U.L., & Trac H., 2005, New Astronomy, 10, 393

Mihos J.C., Hernquist L., 1996, ApJ, 464, 641

Miller L. 1986, MNRAS, 220, 713

Mo H.J., White S.D.M., 1996, MNRAS, 282, 347

Mo H.J., Mao S., White S.D.M., 1998, MNRAS, 295, 319

Mo H.J., Yang X., van den Bosch, F.C., Jing Y.P., 2004, MNRAS, 349, 205

Mo H.J., Yang X., van den Bosch, F.C., Katz N., 2005, MNRAS, 363, 1155

Mori, M., & Burkert, A. 2000, ApJ, 538, 559

Moore B., Katz N., Lake G., Dressler A., Oemler A., 1996, Nature, 379, 613

Moore B., Lake G., Quinn T., Stadel J., 1999, MNRAS, 304, 465

Moore B., Ghigna S., Governato F., Lake G., Quinn T., Stadel J., & Tozzi P., 1999, ApJ, 524, L19

Moore B., Diemand J., Madau P., Zemp M., & Stadel J., 2006, MNRAS, 368, 563

Naab T. & Ostriker J.P, 2007, submitted to MNRAS, astro-ph/0702535

Nagakura T., & Omukai K. 2005, MNRAS, 364, 1378

Navarro J.F., Frenk C.S., White S.D.M, 1997, ApJ, 490, 493

Navarro J.F.& Steinmetz M., 1997, ApJ, 478, 13

Neistein E., van den Bosch F.C., Dekel A., 2006, MNRAS, 372, 933

Noeske K.G., et al., 2007, ApJ, 660, 47

Norberg P., et al., 2002, MNRAS, 332, 827

Nulsen P.E.J., 1982, MNRAS, 189, 1007

Nusser A., Silk J., Babul A., 2006, MNRAS, 373, 739

Oemler A., 1974, ApJ, 194, 1

Okamoto T., Nagashima M., 2001, ApJ, 547, 109

Osmond J.P.F., Ponman T. J., 2004, MNRAS, 350, 1511

Peacock, J., "Cosmological Physics", 1999, Cambridge University Press

Pedersen, K., Rasmussen J., Sommer-Larsen J., Toft S., Benson A.J., Bower R.G., 2006, NewA, 11, 465

Poggianti B.M., Smail I., Dressler A., Couch W.J., Barger A.J., Butcher H., Ellis R.S., Oemler A.J., 1999, ApJ, 518, 576

Postman M. Geller M.J., 1984, ApJ, 281, 95

Postman M. et al, 1996, AJ, 111, 615

Prada F., Vivitska M., Klypin A., Holtzman J.A., Schlegel D.J., Grebel E.K., Rix, H.-W., Brinkmann J., McKay T.A., Csabai I., 2003, ApJ, 598, 260

Ramella M., Giuricin G., Mardirossian F., Mezzetti M., 1987, A&A, 188, 1

Ramella M., Geller M.J., Huchra J.P., 1989, ApJ,344, 57

Rasmussen J., Ponman T. J., Mulchaey J.S., Miles T.A., Raychaudhury S., 2006, MNRAS, 373, 653

Rees M.J., Ostriker J.P., 1977, MNRAS, 179, 541

Rhode K.L., Zepf S.E., & Santos M.R., 2005, ApJL, 630, L21

Santos M.R. 2003, in Extragalactic Globular Cluster Systems, ed. M.Kissler-Patig, 348-+

Scannapieco E., Silk J., Bouwens R., 2005, ApJ, 635, L13

Schlegel D.J., Finkbeiner D.P., Davis M., 1998, ApJ, 500, 525

Shapiro P.R., Iliev I.T. & Raga A.C. 2004, MNRAS348, 753

Shectman S.A., Schechter P.L., Oemler A., Tucker D.L., Kirshner R.P., Lin H., 1996, ApJ, 470, 172

Sheth R.K., Mo H.J., Tormen G., 2001, MNRAS, 323, 1

Shull M., & Venkatesan A., 2007, astro-ph/0702323

Sijacki D., Springel V., 2006, MNRAS, 366, 397

Silk, J., 1977, ApJ, 1977, 211, 638

Skibba R.A., Sheth R.K., Martino M.C., submitted to MNRAS, preprint, astro-ph/0707.3218

Spitzer L.Jr., 1958, ApJ, 127, 17

Spergel D.N. et al. 2003, ApJS, 148, 175

Spergel D.N. et al. 2007, ApJS, 170, 377

Springel V., White S.D.M., Tormen G., Kauffmann G., 2001, MNRAS, 328, 726

Springel V., Di Matteo T., Hernquist L., 2005a, MNRAS, 361, 776

Springel V., White S.D.M, Jenkins A. et al, 2005b, Nature, 435, 629

Stadel J.G. 2001, PhD thesis, University of Washington

Stoughton C., et al., 2002, AJ, 123, 485

Strateva I., et al., 2001, ApJ, 122, 1861

Tabor G., Binney J., 1993, MNRAS, 263, 323

Tanaka M., Goto T., Okamura S., Shimasaku K., Brinkman J., 2004, AJ, 128, 2677

Tanaka M., Kodama T., Arimoto N., Okamura S., Umetsu K., Shimasaku K., Tanaka I., Yamada T., 2005, MNRAS, 362, 268

Tanaka M., Hoshi T., Kodama T., Kashikawa N., 2007, accepted for publication in MNRAS, astro-ph/0706.0783

Taylor J.E., Babul A., 2001, ApJ, 559, 716

Taylor J.E., Babul A., 2004, MNRAS, 348, 811

Thomas D., Maraston C., Bender R., de Oliveira C.M., 2005, ApJ, 621, 673

Toft, S., Rasmussen, J., Sommer-Larsen, J., Pedersen, K., 2002, MNRAS, 335, 799

Toomre A., Toomre J., 1972, ApJ, 178, 623

Thoul A.A. & Weinberg D.H. 1996, ApJ, 465, 608

Tran K.-V., Simard L., Zabludoff A.I., Mulchaey J.S., 2001, ApJ, 549, 172

Tucker D.L., et al., 2000, ApJS, 130, 237

Tully R.B., Somerville R.S., Trentham N., & Verheijen M.A.W, 2001, ApJ, 569, 573

van den Bosch F.C., Lewis G.F., Lake G., Stadel J., 1999, ApJ, 515, 50

van den Bosch F.C., Yang X., Mo H.J., 2003, MNRAS, 340, 771

van den Bosch F.C., Norberg P., Mo H.J., Yang X.H., 2004, MNRAS, 352, 1302

van den Bosch F.C., Yang X.H., Mo H.J, Norberg P., 2005a, MNRAS, 356, 1233

van den Bosch F.C., Weinmann S.M., Yang X.H., Mo H.J, Li C., Jing Y.P., 2005b, MNRAS, 361, 1203

van den Bosch F.C., Tormen G., Giocoli C., 2005c, MNRAS, 359, 1029

van den Bosch F.C., et al. 2007, MNRAS, 376, 841

Wang H.Y., Mo H.J., Jing Y.P., 2007, MNRAS, 375, 726

Wechsler R.H., Zentner A.R., Bullock J.S., Kravtsov A.V., Allgood B., 2006, 625, 71

Weiner B.J., et al., 2005, ApJ, 620, 595

Weinmann S.M., van den Bosch F.C., Yang X., Mo H.J, 2006, MNRAS, 366, 2 (paper I)

Weinmann S.M., van den Bosch F.C., Yang X., Mo H.J., Croton D.J., Moore B. 2006, MNRAS, 372, 1161

Weinmann S.M., Macciò A.V., Iliev I.T., Mellema G., 2007, accepted for publication in MNRAS, astro-ph/0705.0530

Wetzel A.R., Cohn J.D., White M., Holz D.E., Warren M.S., 2007, ApJ, 656, 139

White S.D.M., Rees M.J., 1978, MNRAS, 183, 341

White M. & Kochanek C.S., 2002, ApJ, 574, 24

White S.D.M., Frenk C.S., 1991, ApJ, 379, 52

Whitmore B.C., 1995, Groups of Galaixes, ASP Conference Series, Vol. 70, 41

Whitmore B.C., Gilmore D.M., Jones C., 1993, ApJ, 407, 489

Wilman D.J., et al., 2005, MNRAS, 358, 88

Wirth A., 1983, AJ, 274, 541

Yang X., Mo H.J., van den Bosch F.C., 2003, MNRAS, 339, 1057

Yang X., Mo H.J., van den Bosch F.C., Jing Y.P., 2005a, MNRAS, 356, 1293 (YMBJ)

Yang X., Mo H.J., van den Bosch F.C., Jing Y.P., 2005b, MNRAS, 357, 608

Yang X., Mo H.J., Jing Y.P., van den Bosch F.C., 2005c, MNRAS, 358, 217

Yang X, Mo H.J., van den Bosch F.C., Weinmann S.M., Li C., Jing Y.P., 2005d, MNRAS, 362, 711

York D.G., et al., 2000, AJ, 120, 1579

Zabludoff A.I., Mulchaey J.S., 1998, ApJ, 496, 39

Zabludoff A.I., Mulchaey J.S., 2000, ApJ, 539, 136

Zehavi I., et al, 2005, ApJ, 630, 1

Zentner A.R., Bullock J.S., 2003, ApJ, 598, 49

Zheng Z., et al., 2005, ApJ, 633, 791

Zheng X.Z. et al., 2007, ApJ, 661, 41

Zibetti S., White S.D.M, Schneider D.P., Brinkmann J., 2005, MNRAS, 358, 949

Zucca E., et al., 1997, A&A, 326, 477

Acknowledgements

First of all, I would like to thank my advisor Frank van den Bosch, whose contribution to this work has been enormous. I am extremely grateful for his support, many discussions from which I learned very much, and his advice about my future in science. His energy, enthusiasm and extremely efficient and organized way of working have been a great inspiration for me. Next, I would like to thank my other advisor, Ben Moore, who has been so kind to give me the opportunity to continue my thesis in Zurich at the Institute of Theoretical Physics, for his scientific input and useful discussions.

Many other people have contributed to the work presented in this thesis. All my research about the SDSS would never have been possible without the wonderful work of Xiaohu Yang, Houjun Mo and Frank on group catalogues, into which much previous research has gone and from which I have profited a lot. I would like to thank them very much. Special thanks go to Andrea Macciò for patiently explaining me how to run simulations, halo finders and conversions and for his large contribution to Chapter 4. Other people who have greatly contributed to this thesis with their research are Darren Croton, Ilian Iliev and Garrelt Mellema. I am very impressed with the complex semi-analytical model that Darren has built, and also with the complicated radiative transfer simulation of Garrelt and Ilian. Thank you all very much for answering my questions and explaining your work.

I would like to thank Savvas Koushiappas from whom I have learned much about the "hard, yet so glamorous life of a physicist" and who has helped me to stay motivated in the first year of my PhD. Many thanks also to Tobias Goerdt for extensive discussions about whether or not to give up science and become software engineers, and many other topics, and for his help with simulations and dynamical friction. Thanks to everybody at ETH and at the university who has helped me how to use different software, discussed with me about physics and other things. From the people I met at ETH I would like to especially thank Anna Pasquali, Peder Norberg, Kim-Vy Tran, Cristiano Porciani, Thorsten Lisker, Aaron Dutton, Padelis Papadopoulos and Sebastiano Cantalupo. Many thanks to Joachim Stadel, Tobias Kaufmann, Marcel Zemp and Oscar Agertz for helping me with simulation projects which are still underway, for their friendliness and many nice discussions. Many people contributed to the pleasant atmosphere at our Institute, such as Elena D'Onghia, Uli Haisch, Christian Kurz, Alejandro Daleo, Beat Tödtli or Tobias Huber. Thanks to all of you. Many thanks to Roland Bernet, Doug Potter and Peter Englmaier for computer support, and to the administrative staff of ETH and university. Thanks to Stephen Marsden, Marina Battaglia, René Holzreuter and Paolo Grigis from the Downtown Astronomy Institute and to Athman Boukhaoua for trying to teach me how to play D&D.

Many thanks for support and encouragement to my sister Karin, Bettina Reinhardt, Mélanie Pitteloud, Katharina Glatt and especially to my parents, Heinrich and Christine, who are always ready to help me. Many thanks to Annette Pestalozzi who contributed much to the success of this thesis. Finally, I thank Christian Thalmann for help with talks, posters, for editing the writing in this thesis, scientific discussion, for support, encouragement and for calming me down when something went wrong: You have made me happier than I thought I would ever be.

Chapter 6

Appendix

6.1 The Group Finding Algorithm

The group finder, used in Section 2.4 to construct our SDSS group catalogue uses some virial properties of dark matter haloes. Throughout this paper we define dark matter haloes as virialized structures with a mean over-density of 180 and a NFW (Navarro, Frenk & White 1997) density distribution:

$$\rho(r) = \frac{\bar{\delta}\bar{\rho}}{(r/r_{\rm s})(1+r/r_{\rm s})^2} \tag{6.1}$$

Here r_s is a characteristic radius, $\bar{\rho}$ is the average density of the Universe, and $\bar{\delta}$ is a dimensionless amplitude which can be expressed in terms of the halo concentration parameter $c = r_{180}/r_s$ as

$$\bar{\delta} = \frac{180}{3}\,\frac{c^3}{\ln(1+c) - c/(1+c)}, \tag{6.2}$$

with r_{180} the radius within which the halo has an average over-density of 180. We use the relation given by Bullock et al. (2001) to compute c as function of halo mass, properly converted to our definition of halo mass.

Our group finder consists of the following steps:

Step 1: We combine two different methods to identify the centers of potential groups. First we use the traditional FOF algorithm to assign galaxies to groups. Since we are working in redshift space, we separately define linking lengths along the line of sight (ℓ_z) and in the transverse direction (ℓ_p). Since the purpose here is only to identify the group centers, we use relatively small linking lengths: $\ell_z = 0.3$ and $\ell_p = 0.05$, both in units of the mean separation of galaxies. Note that for an apparent magnitude limited survey the mean separation of galaxies is a function of redshift, which we take into account. The geometrical, luminosity weighted, centers of all FOF groups thus identified with two galaxies or more are considered as centers of potential groups. Next, from all galaxies not yet linked together by these FOF groups, we select bright, relatively isolated galaxies which we also associate with the centers of potential groups. Following an approach similar to McKay et al. (2002), Prada et al. (2003) and Brainerd & Specian (2003), we identify a galaxy as 'central', and thus as the center of a potential group, when it is the brightest galaxy in a cylinder of radius $1\,h^{-1}$Mpc and a velocity depth of $500\,{\rm km\,s^{-1}}$.

Step 2: We estimate the luminosity of a selected potential group using

$$L_{\rm group} = \sum_i \frac{L_i}{c_i} \tag{6.3}$$

Here L_i is the ${}^{0.1}r$-band luminosity of the $i^{\rm th}$ galaxy in the group and c_i is the SDSS survey-completeness at the corresponding location. The *total* group luminosity is approximated by

$$L_{\rm total} = L_{\rm group} \frac{\int_0^\infty \Phi(L)\, L\, dL}{\int_{L_{\rm lim}}^\infty \Phi(L)\, L\, dL}\,, \tag{6.4}$$

where $L_{\rm lim}$ is the minimum luminosity of a galaxy that can be observed at the redshift of the group, and $\Phi(L)$ is the galaxy luminosity function in the ${}^{0.1}r$-band, which we model using the Schechter function fit of Blanton et al. (2003a).

Step 3: From $L_{\rm total}$ and a model for the group mass-to-light ratio (see below), we compute an estimate of the halo mass associated with the group in consideration. From this mass estimate we compute the halo radius r_{180}, the virial radius $r_{\rm vir}$[1], and the line-of-sight velocity dispersion σ. For the latter we use

$$\sigma = 428.0\,{\rm km\,s^{-1}} \left(\frac{M_{180}}{10^{14} h^{-1}\,{\rm M}_\odot} \right)^{0.3244} \tag{6.5}$$

This fitting function accurately describes the relation between M_{180} and the mass-weighted one-dimension velocity dispersion (see equation (14) in van den Bosch et al. 2004).

Step 4: Using the sizes, masses, velocity dispersions and centers of the groups thus obtained, we now assign group memberships to all galaxies in the survey. We assume that the phase-space distribution of galaxies follows that of the dark matter particles. In that case the number density contrast of galaxies in redshift space around the group center (which we associate with the center of the dark matter halo) at redshift $z_{\rm group}$ is given by

$$P_M(R, \Delta z) = \frac{H_0}{c} \frac{\Sigma(R)}{\bar\rho} p(\Delta z)\,, \tag{6.6}$$

Here $\Delta z = z - z_{\rm group}$ and $\Sigma(R)$ is the projected surface density of a (spherical) NFW halo:

$$\Sigma(R) = 2\, r_s\, \bar\delta\, \bar\rho\, f(R/r_c)\,, \tag{6.7}$$

with

$$f(x) = \begin{cases} \frac{1}{x^2-1}\left(1 - \frac{\ln\frac{1+\sqrt{1-x^2}}{x}}{\sqrt{1-x^2}}\right) & \text{if } x < 1 \\ \frac{1}{3} & \text{if } x = 1 \\ \frac{1}{x^2-1}\left(1 - \frac{\arctan\sqrt{x^2-1}}{\sqrt{x^2-1}}\right) & \text{if } x > 1 \end{cases}\,. \tag{6.8}$$

The function $p(\Delta z){\rm d}\Delta z$ describes the redshift distribution of galaxies within the halo for which we adopt a Gaussian form

$$p(\Delta z) = \frac{1}{\sqrt{2\pi}} \frac{c}{\sigma(1+z_{\rm group})} \exp\left[\frac{-(c\Delta z)^2}{2\sigma^2(1+z_{\rm group})^2}\right]\,, \tag{6.9}$$

[1]The virial radius is defined as the radius inside of which the average density is $\Delta_{\rm vir}$ times the critical density, with $\Delta_{\rm vir}$ given by Bryan & Norman (1998)

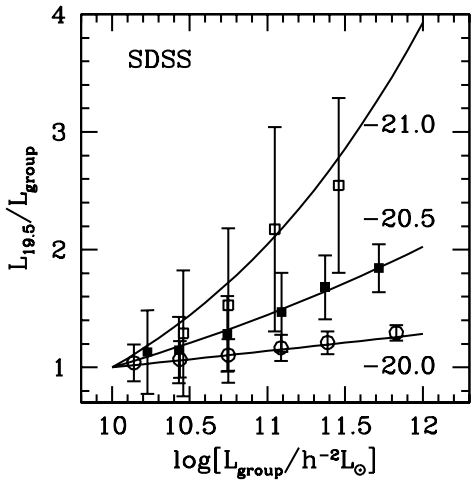

Figure 6.1: The ratio $L_{19.5}/L_{\rm group}$ as a function of $L_{\rm group}$. Here $L_{19.5}$ is the total luminosity of all group galaxies brighter than $M_{r,0.1}$-5log$h$, while $L_{\rm group}$ is defined as the total luminosity of all group galaxies with $M_{r,0.1} \leq$ -20.0 (open circles), -20.5 (filled squares), -21.0(open squares). The errorars indicate 1-σ scatter of the ratios within different group luminosity bins, while the solid lines are our fits to these ratios, used to compute $L_{19.5}$ from an observed $L_{\rm group}$.

where σ is the rest-frame velocity dispersion.

Thus defined, $P_M(R, \Delta z)$ is the three-dimensional density contrast in redshift space. In order to decide whether a galaxy should be assigned to a particular group we proceed as follows. For each galaxy we loop over all groups, and compute the corresponding distance $(R, \Delta z)$ between galaxy and group center. Here R is the projected distance at the redshift of the group. If $P_M(R, \Delta z) \geq B$, with B an appropriately chosen background level (see below), the galaxy is assigned to the group. If a galaxy can be assigned to more than one group, it is only assigned to the group for which $P_M(R, \Delta z)$ has the highest value. Finally, if all members of two groups can be assigned to one group according to the above criterion, the two groups are merged into a single group.

Step 5: Using the group members thus selected we recompute the geometrical, luminosity weighted group center and go back to Step 2, iterating until there is no further change in the memberships of groups. Note that, unlike with the traditional FOF method, this group finder also identifies groups with only one member. The resulting group luminosity function for our catalogue is shown in Fig. 6.3.

The group finding algorithm defined above requires an assumed $M/L_{\rm group}$, possibly as function of halo mass M, and has one free parameter, namely the background level B. In this paper we use $B = 10$, which corresponds roughly to the redshift-space density contrast at the edge of a halo (see YMBJ). As shown in YMBJ, the group catalogue is not very sensitive to the exact value of B used. For $M/L_{\rm group}$ we use the average mass-to-light ratios as function of halo mass obtained by van den Bosch, Yang & Mo (2003; their model D). Since mass-to-light ratio corresponds to the photometric b_J band, we compute $L_{\rm group}$ in both the g and r band (k-corrected to $z = 0$), which we convert to the b_J band using $b_J = g + 0.155 + 0.15238 * (g - r)$ (Fukugita et al. 1996; Blair & Gilmore 1982). Detailed tests in YMBJ have shown that the completeness and contamination levels of our group

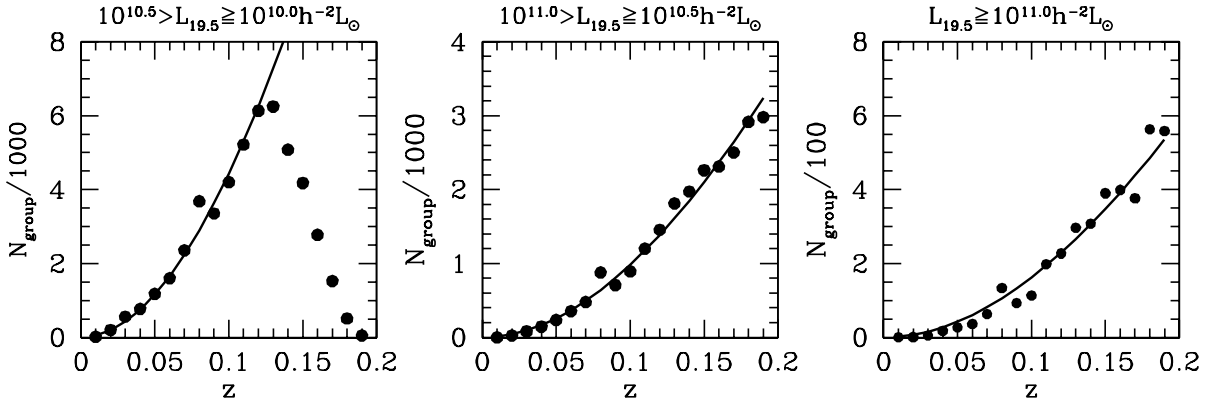

Figure 6.2: The redshift distributions of galaxy groups for three different bins in $L_{19.5}$ (as indicated). The solid dots correspond to the number counts of groups in the SDSS and the solid lines indicate the expected value for a constant group number density.

catalogue are extremely insensitive to the exact values of M/L assumed. We have verified that very significant changes in this assumption have no significant effect of any of the results presented in this paper. This is easy to understand; even if our estimate for M/L is wrong by a factor of 3, the implied radius and velocity dispersion, used in the membership determination, are only off by 44 percent.

As discussed in Section 2.4.2, the final group mass is determined from the group luminosity, $L_{19.5}$, defined as the luminosity of all group members with ${}^{0.1}M_r \leq -19.5 + 5\log h$. For groups with $z > 0.09$, not all these members make it into the flux limited SDSS, and a correction for the missing members is required. For that we use the relation between $L_{\rm group}$ and $L_{19.5}$ determined from the groups with $z < 0.09$. These relations are shown in Fig. 6.1.

Fig. 6.2 shows the number of identified groups as a function of redshift for three different bins in $L_{19.5}$. In the left-hand panel, corresponding to the lowest luminosity bin, it can be seen how the number of identified groups starts to differ from the expected value (solid line, corresponding to a number density that is constant with redshift) at $z \approx 0.12$. This signals an incompleteness which we correct for by not assigning a mass to the groups in this luminosity range with $z > 0.12$ (i.e., these groups are removed from the sample). For more luminous groups, the number of identified groups agrees remarkably well with the constant number density expectation up to the maximum redshift of the sample. This success is partly a result of the fact that our group finder can also identify systems that contain only one or two galaxies (see YMBJ). Fig. 6.3 plots the $L_{19.5}$ luminosity function of our group catalogue (where the volume for the low luminosity groups is computed only out to $z = 0.12$). Note that this is only complete for groups with $L_{19.5} \geq 10^{10.5}h^{-2}\,{\rm L}_\odot$. For lower luminosity groups the sample is clearly incomplete. These groups have not been considered in this paper.

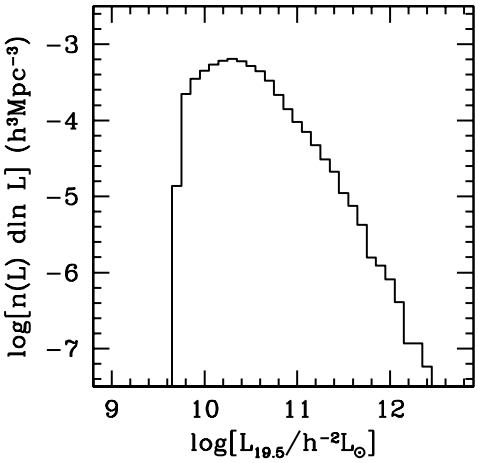

Figure 6.3: The group luminosity function for the flux limited sample.

6.2 Testing the Robustness of our Results with Mock Surveys

In order to address the robustness of our results we construct a mock galaxy redshift survey (hereafter MGRS), which we analyze in exactly the same way as the data described in the previous sections. Even though our data is based on the SDSS, we follow Yang et al. (2005a) and construct a mock version of the 2dFGRS. There are two reasons for this. First of all, we do not yet have accurate models for the conditional luminosity function of SDSS galaxies, which is required for the construction of reliable MGRSs (see below). Secondly, our mock versions of the 2dFGRS have been well tested and are accurate representations of the actual 2dFGRS (see Yang et al. 2005a; van den Bosch et al. 2005a,b). Since the main purpose of this exercise is to test the methodologies used in this paper, the use of a mock 2dFGRS rather than a mock SDSS should not make a significant difference. If anything, since the SDSS sample used here is somewhat larger than the 2dFGRS, and since the redshift errors are substantially smaller, our results regarding the reliability and robustness of the analysis should be considered conservative.

The MGRS is constructed by populating dark matter haloes with galaxies of different luminosities. The distribution of dark matter haloes is obtained from a set of large N-body simulations (dark matter only) for a ΛCDM 'concordance' cosmology with $\Omega_m = 0.3$, $\Omega_\Lambda = 0.7$, $h = 0.7$ and $\sigma_8 = 0.9$. In this paper we use two simulations with $N = 512^3$ particles each, which are described in more detail in Jing & Suto (2002). The simulations have periodic boundary conditions and box sizes of $L_{\rm box} = 100h^{-1}$ Mpc (hereafter L_{100}) and $L_{\rm box} = 300h^{-1}$ Mpc (hereafter L_{300}). Dark matter haloes are identified using the standard FOF algorithm with a linking length of 0.2 times the mean inter-particle separation.

To populate these dark matter haloes with galaxies of different luminosities and different types, we use the conditional luminosity function (hereafter CLF), $\Phi(L|M)$, which gives the average number of galaxies of luminosity L that resides in a halo of mass M (Yang, Mo & van den Bosch 2003). The sample of galaxies is split in 'early types' and 'late types' using a probability function $P_{\rm late}(L, M)$ (see van den Bosch, Yang & Mo 2003). Details of these models are not important for what follows, but we do point out that these models accurately fit the luminosity functions (Madgwick et al. 2002) and the correlation

lengths as function of luminosity (Norberg et al. 2002) for both galaxy types.

Having populated the various simulation boxes with galaxies we first proceed as follows. In each halo we count the number of early and late type galaxies in a given magnitude range, and compute the average late type fraction as function of halo mass. The results for the L_{300} box are shown, for three different magnitude ranges as indicated, in the upper left-hand panel of Fig. 6.4 (symbols connected by thick lines). The thin, lines are the theoretical predictions corresponding to the input CLF, given by

$$f_{\rm late}(M) = \frac{\int_{L_{\rm min}}^{L_{\rm max}} P_{\rm late}(L,M)\,\Phi(L|M)\,{\rm d}L}{\int_{L_{\rm min}}^{L_{\rm max}} \Phi(L|M)\,{\rm d}L}\,. \tag{6.10}$$

Here $L_{\rm min}$ and $L_{\rm max}$ are the luminosities that correspond to the magnitude limits. Not surprisingly, the late type fractions derived are in excellent agreement with these input values; this figure is just to illustrate that the box contains a sufficient number of haloes so that the Poisson errors are negligibly small.

The lower left-hand panel shows the results obtained when using the estimated halo mass, rather than the true halo mass. Halo masses are estimated using a similar procedure as described in Section 2.4.2: for each halo we determine L_{18}, the total luminosity of all halo galaxies with $M_{b_J} - 5{\rm log}h \leq -18$, and we compute the number density, n_+, of haloes with L_{18} larger than that of the halo considered. Using the halo mass function of Sheth, Mo & Tormen (2001), we determine the corresponding halo mass by finding the mass for which the number density of more massive haloes is equal to n_+. As discussed in Section 2.4.2 this method thus assigns masses based on the L_{18} rank order of the haloes. As is evident from the lower left-hand panel of Fig. 6.4, this method of assigning halo masses results in small, systematic errors in the derived late type fractions for haloes with $M \lesssim 2\times10^{12}h^{-1}\,{\rm M}_\odot$, in the sense that the luminosity-dependence is underestimated. This owes to the fact that the luminosities themselves are used to estimate the halo masses. For more massive haloes, however, the resulting $f_{\rm late}(L,M)$ is virtually indistinguishable from the true relation. This demonstrates that our method of assigning halo masses does not introduce any systematic errors in the mass and/or luminosity dependence of the galaxy types for haloes with $M \gtrsim 2\times10^{12}h^{-1}\,{\rm M}_\odot$. We emphasize that the relation between L_{18} and M in the MGRS has a realistic amount of scatter.

The above test, however, is idealized. In reality we have to select haloes using a group finder applied to a redshift survey. Since the survey suffers from observational biases and peculiar velocity distortions, and since the group finder unavoidably suffers from interlopers and incompleteness effects, a more realistic check of our methodology requires a comparison with a proper MGRS. Using the L_{100} and L_{300} simulation boxes described above we create a large virtual universe. We follow Yang et al. (2005a) and replicate the L_{300} box on a $4\times4\times4$ grid. The central $2\times2\times2$ boxes, are replaced by a stack of $6\times6\times6$ L_{100} boxes, and the virtual observer is placed at the center (see Fig. 11 in Yang et al. 2005a). This stacking geometry circumvents incompleteness problems in the mock survey due to insufficient mass resolution of the L_{300} simulations, and allows us to reach the desired depth of $z_{\rm max} = 0.20$ in all directions. Next we construct a mock 2dFGRS using the following steps (see van den Bosch et al. 2005a for details):

1. We define a (α,δ)-coordinate frame with respect to the virtual observer at the center of the stack of simulation boxes, and remove all galaxies that are not located in the areas equivalent to those of the 2dFGRS.

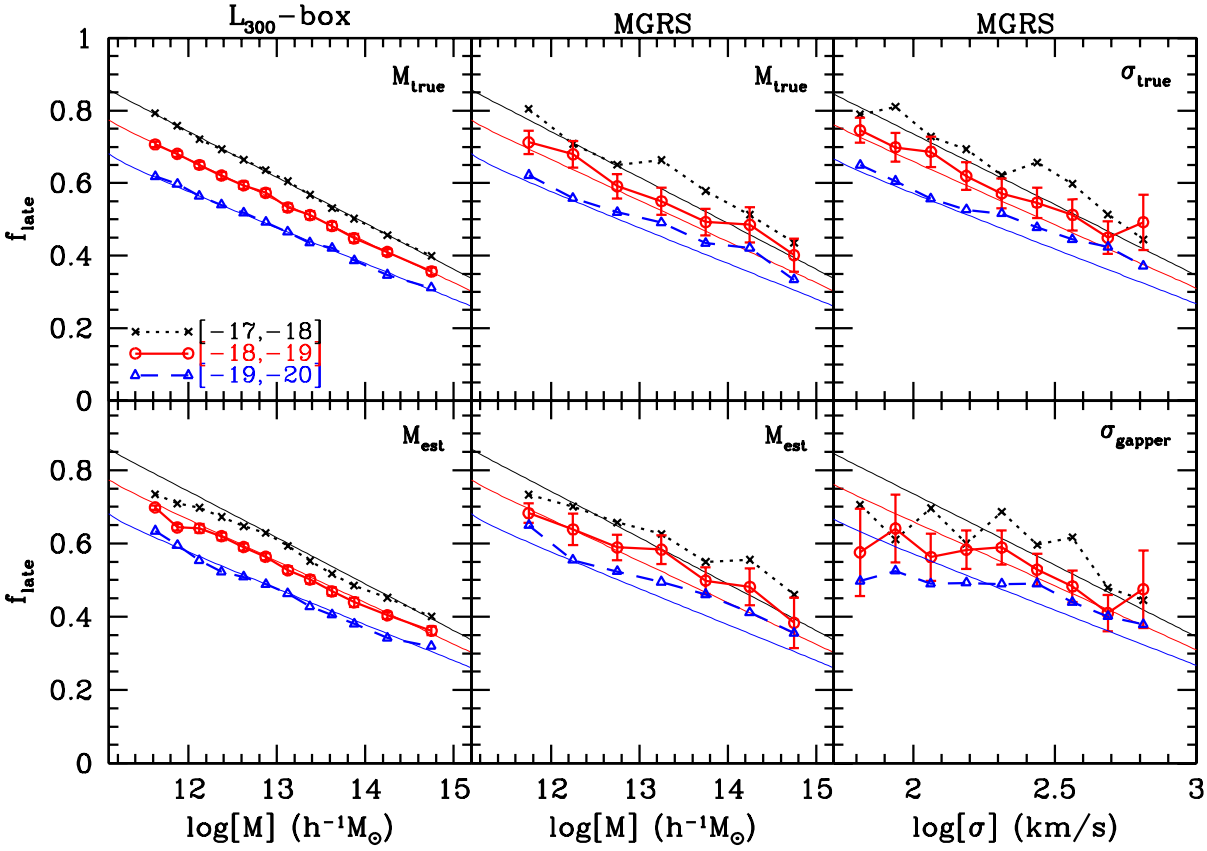

Figure 6.4: Late type fractions as function of halo mass and velocity dispersion. The left-hand panels show the results obtained directly from the L_{300} simulation box, using both the true halo mass ($M_{\rm true}$, upper panel) and the estimated halo mass ($M_{\rm est}$, lower panel). Panels in the middle column show the same, but this time based on a group catalogue extracted from the MGRS. Right-hand panels show the same results but this time as function of velocity dispersion, rather than halo mass. Results are shown for three magnitude-limited samples; the values in square brackets in the upper left-hand panel indicate the range of $M_{b_J} - 5{\rm log}h$ used. The thin lines in each panel correspond to the true underlying fractions as specified by the CLF. For clarity, we only plot (Poissonian) errorbars for the sample with $-18 \geq M_{b_J} - 5{\rm log}h > -19$. See text for a detailed discussion.

2. For each galaxy we compute the apparent magnitude according to its luminosity and distance, to which we add a rms error of 0.15 mag.

3. For each galaxy we compute the redshift as 'seen' by the virtual observer. We take the observational velocity uncertainties into account by adding a random velocity drawn from a Gaussian distribution with dispersion 85 $\mathrm{km\,s^{-1}}$.

4. To take account of the position- and magnitude-dependent completeness of the 2dFGRS, we randomly sample each galaxy using the completeness masks provided by the 2dFGRS team.

5. We also take account of the fiber-collision induced incompleteness as well as the incompleteness due to image blending.

As shown in Yang et al. (2005a) and van den Bosch et al. (2005a), this procedure results in a mock 2dFGRS that accurately mimics all the various incompleteness effects, allowing for a direct, one-to-one comparison with the true 2dFGRS.

Next we apply the YMBJ halo-based group finder to this MGRS, and compute the late type fraction as function of halo mass using both the true halo masses (defined as the true halo mass associated with the brightest group member) and the estimated halo masses (using the L_{18} ranking method described above). The results are shown in the panels in the middle column of Fig. 6.4. Since there are much fewer galaxies/haloes involved than in the case shown in the left-hand panels, and since the group-finder is not perfect, the results are significantly more noisy. Nevertheless, when using the true halo masses, the resulting late type fractions are in good agreement with the input values (eq. [6.10]), except for a small, systematic overestimate at the massive end due to interlopers and incompleteness effects. When the estimated halo masses are used instead, one again notices a small but systematic underestimate of the luminosity dependence of $f_{\rm late}(L,M)$ for haloes with $M \lesssim 2\times10^{12}h^{-1}\,\mathrm{M}_\odot$. For more massive haloes, the results are very comparable to those based on the true halo masses. This indicates that our group finder allows for a fairly accurate determination of $f_{\rm late}(L,M)$. In particular, the method accurately recovers the luminosity dependence. (at least for $M \lesssim 2\times10^{12}h^{-1}\,\mathrm{M}_\odot$). Recall that since the SDSS sample used in this paper is larger than the 2dFGRS, and since the redshift errors in the SDSS are significantly smaller than in the 2dFGRS (resulting in smaller interloper fractions), we may actually expect the SDSS results presented in the previous section to be more robust than the MGRS results shown here.

Finally, the panels on the right-hand side show the late type fractions obtained from the MGRS as function of velocity dispersion. In the upper right-hand panel we plot the fractions as function of the true velocity dispersion, which is the one-dimensional velocity dispersion of the dark matter particles corresponding to the halo that hosts the brightest group galaxy. As expected, these results look very similar to those in the upper panel in the middle column. In the lower right-hand panel, however, we plot $f_{\rm late}$ as function of the velocity dispersion of the group members, measured using the gapper estimator, which is insensitive to outliers (Beers, Flynn & Gebhardt 1990; see YMBJ for our implementation). Only groups with at least three members are taken into account. This time, the dependence of $f_{\rm late}$ on the halo velocity dispersion is much flatter than for the input model. Especially for haloes with $\sigma_{\rm gapper} \lesssim 160\,\mathrm{km\,s^{-1}}$ (corresponding to $M \lesssim 5\times10^{12}h^{-1}\,\mathrm{M}_\odot$), the late type fractions are significantly underestimated. This

Table 6.1: Blue fractions of all galaxies

	$[12, 12.5]$	$[12.5, 13]$	$[13, 13.5]$	$[13.5, 14]$	$[14, 14.5]$	$[14.5, 15]$
$[-17, -17.5]$	0.74 (69)	-	-	-	-	-
$[-17.5, -18]$	0.68 (108)	0.61 (114)	0.56 (80)	-	-	-
$[-18, -18.5]$	0.67 (186)	0.56 (189)	0.48 (133)	0.38 (84)	0.23 (74)	-
$[-18.5, -19]$	0.60 (308)	0.54 (343)	0.44 (265)	0.28 (213)	0.22 (96)	0.24 (67)
$[-19, -19.5]$	0.54 (461)	0.45 (489)	0.44 (449)	0.33 (392)	0.27 (246)	0.35 (98)
$[-19.5, -20]$	0.58 (909)	0.47 (1113)	0.39 (987)	0.30 (878)	0.23 (654)	0.20 (208)
$[-20, -20.5]$	0.55 (9366)	0.44 (1673)	0.39 (1445)	0.31 (1172)	0.23 (771)	0.17 (296)
$[-20.5, -21]$	0.50 (7890)	0.45 (3181)	0.39 (2556)	0.32 (1673)	0.24 (1058)	0.23 (380)
$[-21, -21.5]$	0.49 (61)	0.42 (4752)	0.35 (3657)	0.28 (2164)	0.26 (1068)	0.22 (371)
$[-21.5, -22]$	-	0.38 (956)	0.32 (7327)	0.23 (2231)	0.21 (1001)	0.17 (326)
$[-22, -22.5]$	-	-	0.26 (464)	0.14 (1181)	0.11 (476)	0.08 (143)
$[-22.5, -23]$	-	-	-	-	0.06 (108)	-

Table 6.2: Blue fractions of satellite galaxies

	$[12, 12.5]$	$[12.5, 13]$	$[13, 13.5]$	$[13.5, 14]$	$[14, 14.5]$	$[14.5, 15]$
$[-17, -17.5]$	0.74 (69)	-	-	-	-	-
$[-17.5, -18]$	0.68 (108)	0.61 (114)	0.56 (80)	-	-	-
$[-18, -18.5]$	0.67 (186)	0.56 (189)	0.48 (133)	0.38 (84)	0.23 (74)	-
$[-18.5, -19]$	0.60 (308)	0.54 (343)	0.44 (265)	0.28 (213)	0.22 (96)	0.24 (67)
$[-19, -19.5]$	0.53 (449)	0.45 (489)	0.44 (449)	0.33 (392)	0.27 (246)	0.35 (98)
$[-19.5, -20]$	0.54 (437)	0.47 (1101)	0.39 (987)	0.30 (878)	0.23 (654)	0.20 (208)
$[-20, -20.5]$	0.48 (66)	0.43 (1235)	0.39 (1425)	0.31 (1172)	0.23 (771)	0.17 (296)
$[-20.5, -21]$	-	0.43 (389)	0.38 (2005)	0.32 (1624)	0.24 (1057)	0.23 (380)
$[-21, -21.5]$	-	-	0.38 (810)	0.29 (1568)	0.26 (1000)	0.22 (368)
$[-21.5, -22]$	-	-	-	0.26 (408)	0.23 (621)	0.18 (283)

demonstrates that our mass estimates based on the L_{18}-group ranking are more reliable than those based on the velocity dispersion, especially for low mass haloes.

6.3 Blue Galaxy Fractions in the SDSS

We have included three tables listing the fraction of blue galaxies (as defined in Chapter 3) for all galaxies (6.1), for satellite galaxies (6.2), and for central galaxies (6.3), as obtained from our SDSS group catalogue. Columns correspond to different bins in $\log(M)$, with M in $h^{-1}\,\mathrm{M}_\odot$, as indicated at the top in square brackets. Rows correspond to different magnitude bins ($^{0.1}M_r - 5\log h$), as indicated at the left in square brackets. Each entry lists the blue fraction plus, in brackets, the total number of galaxies (all, satellite or central) in that bin. As in Fig. 3.5, only entries with at least 50 galaxies are indicated.

Table 6.3: Blue fractions of central galaxies

	$[12, 12.5]$	$[12.5, 13]$	$[13, 13.5]$	$[13.5, 14]$	$[14, 14.5]$	$[14.5, 15]$
$[-19.5, -20]$	0.61 (472)	-	-	-	-	-
$[-20, -20.5]$	0.55 (9300)	0.47 (438)	-	-	-	-
$[-20.5, -21]$	0.51 (7890)	0.46 (2792)	0.42 (551)	-	-	-
$[-21, -21.5]$	0.49 (61)	0.42 (4752)	0.34 (2847)	0.26(596)	0.28 (68)	-
$[-21.5, -22]$	-	0.38 (956)	0.32 (7324)	0.22(1823)	0.18 (380)	-
$[-22, -22.5]$	-	-	0.26 (464)	0.14(1178)	0.11 (444)	0.07(95)
$[-22.5, -23]$	-	-	-	-	0.06 (108)	-

CURRICULUM VITAE

Personal data

Name	:	Weinmann
First name	:	Simone M.
Date of birth	:	14/1/1979
Place of origin	:	Herrliberg ZH
Nationality	:	Swiss

Education

9/2005-10/2007:	PhD in Physics, Dr. sc. nat., University of Zurich, Switzerland Title: The Galaxy-Dark Matter Connection Thesis supervisors: Prof. Ben Moore, Dr. Frank C. van den Bosch
9/2004-9/2005:	First Part of PhD at the Swiss Federal Institute of Technology Zurich, Switzerland, Institute for Astrophysics Thesis supervisors: Dr. Frank C. van den Bosch, Prof. Simon J. Lilly
10/1999-05/2004:	M.S. in Physics, Dipl. Phys., Swiss Federal Institute of Technology Zurich, Switzerland Master subjects: Astrophysics, Nuclear Physics ERASMUS exchange: University of Lund Sweden, 09/2002-06/2003 Diploma thesis: The Search for the First Light with the JWST Supervisor: Prof. Simon J. Lilly
6/1999:	Cambridge Certificate of Proficiency in English, Edinburgh UK
8/1992-01/1999:	Matura type B, Kantonsschule ZO, Wetzikon ZH, Switzerland

Teaching experience

10/2005-02/2007:	Teaching assistant, General Mechanics for Physicists University of Zurich, Institute for Theoretical Physics
10/2004-07/2005:	Teaching assistant, Physics for Engineers Swiss Federal Institute of Technology

Languages

German:	Native language
English:	fluent
French:	good
Italian, Swedish:	conversant

LIST OF PUBLICATIONS

Weinmann S.M., Macciò A.V., Iliev I.T., Mellema G., Moore B.
Dependence on the Local Reionization History on Halo Mass and Environment: Did Virgo Reionize the Local Group?
2007, accepted for publication in MNRAS, astro-ph/0705.0530

Weinmann S.M., van den Bosch F.C., Yang X., Mo H.J., Croton D.J., Moore B.
Properties of Galaxy Groups in the SDSS: II. – AGN Feedback and Star Formation Truncation
MNRAS, 2006, 372, 1161

Weinmann S.M., van den Bosch F.C., Yang X., Mo H.J.
Properties of Galaxy Groups in the SDSS: I. – The Dependence of Colour, Star Formation, and Morphology on Halo Mass
MNRAS, 2006, 366, 2

Weinmann S.M., Lilly S.J.
The Number and Observability of Population III Supernovae at High Redshift
ApJ, 2005, 624, 526

Yang X., Mo H.J., van den Bosch F.C., Jing Y.P., Weinmann S.M., Meneghetti M.
Weak Lensing by Galaxies in Groups and Clusters: I. – Theoretical Expectations
MNRAS, 2006, 373, 1159

van den Bosch F.C., Yang X., Mo H.J., Weinmann S.M., Macciò A.V., More S., Cacciato M., Skibba R.
Towards a Concordant Model of Halo Occupation Statistics
MNRAS, 2007, 376, 841

Yang X., van den Bosch F.C., Mo H.J., Mao S., Kang X., Weinmann S.M., Guo Y., Jing Y.P.
The Alignement between the Distribution of Satellites and the Orientation of their Central Galaxy
MNRAS, 2006, 369, 2393

Yang X., Mo H.J., van den Bosch F.C., Weinmann S.M., Li C., Jing Y.P.
The Cross-Correlation between Galaxies and Groups: Probing the Galaxy Distribution in and around Dark Matter Haloes
MNRAS, 2005, 362, 711

van den Bosch F.C., Weinmann S.M., Yang X., Mo H.J., Li C., Jing Y.P.
The Phase-Space Parameters of the Brightest Halo Galaxies
MNRAS, 2006, 361, 1203

Weinmann S.M., van den Bosch F.C., Yang X., Mo H.J.
The Dependence of Galaxy Type on Host Halo Mass
To appear in the proceedings of the XLIst Rencontres de Moriond, astro-ph/0607585